December 1997 • NREL/SR-540-23960 • UC Category: 1504

Urban Airshed Modeling of Air Quality Impacts of Alternative Transportation Fuel Use in Los Angeles and Atlanta

Earth Technology, Inc.
Concord, Massachusetts

NREL Technical Monitors: Paul Bergeron and Michelle Bergin

Needs "MASTER" Stamped.

Alternative Fuels Hotline: 1-800-423-1DOE
Alternative Fuels Data Center World Wide Web Site: http://www.afd

National Renewable Energy Laboratory
1617 Cole Boulevard
Golden, Colorado 80401-3393
A national laboratory of the
U.S. Department of Energy
Managed by the Midwest Research Institute
For the U.S. Department of Energy
Under Contract No. DE-AC36-83CH10093

Prepared under Subcontract Number ACI-7-17013-01
December 1997

Available to DOE and DOE contractors from:
Office of Scientific and Technical Information (OSTI)
P.O. Box 62
Oak Ridge, TN 37831
Prices available by calling (423) 576-8401

Available to the public from:
National Technical Information Service (NTIS)
U.S. Department of Commerce
5285 Port Royal Road
Springfield, VA 22161
(703) 487-4650

TABLE OF CONTENTS

TABLE OF CONTENTS (Concluded)

LIST OF FIGURES

LIST OF FIGURES (Continued)

LIST OF FIGURES (Concluded)

LIST OF TABLES

LIST OF TABLES (Concluded)

List of Acronyms

ACRO	Acrolein - CBM-IV species name for air toxics version
ACET	Acetaldehyde - CBM-IV species name for toxics version
AFV	Alternatively fueled vehicle or alternate fuel vehicle
ALD2	higher aldehydes - Original CBM-IV species name
AQMP	Air Quality Management Plan
ARB	California Air Resources Board
BEIS	Biogenic Emission Information System
BENZ	Benzene - CBM-IV species name for air toxics version
BTU	British thermal unit
BUDI	1,3-butadiene - CBM-IV species name for air toxics version
CBM-IV	Carbon Bond Mechanism, Version IV, a chemical kinetics mechanism used in photochemical models
CH_4	Methane
CNG	Compressed natural gas
CO	Carbon monoxide
CO_2	Carbon dioxide
DNR	Georgia Department of Natural Resources
EMFAC7F	Version for the motor vehicle emission factor model developed by the ARB
ETH	Ethylene - CBM-IV species name
FORM	Formaldehyde - CBM-IV species name
FTP	Federal Test Procedure - the standard driving cycle
GEMAP	Geocoded Emissions Modeling and Projection - an emission processing model used to develop model ready emissions files
GHG	Greenhouse gases
HALD	Higher aldehydes - CBM-IV species name for air toxics version
HNO_3	Nitric acid
IOLE	Internal olefins - CBM-IV species name for air toxics version
IR	Incremental reactivity
LAX	Los Angeles International Airport
LDT	Light-duty truck
LDGV	Light-duty gasoline vehicle
LDV	Light-duty vehicle
LRVP	Low Reid Vapor Pressure Gasoline
LST	Local standard time
MDT	Medium-duty truck
MIR	Maximum incremental reactivity
MOBILE5a	Latest version of the motor vehicle emission factor model developed by the U.S. EPA
MOR	Maximum ozone reactivity
NO	Nitric oxide
NO_2	Nitrogen dioxide
NO_x	Nitrogen oxides, composed of NO and NO_2
NO_y	Total nitrogen oxides
NREL	National Renewable Energy Laboratory
O_3	Ozone

List of Acronyms (Continued)

Off-FTP	As used in this study, operation of a motor vehicle outside the speed and acceleration (load) boundaries of the FTP
OLE	Olefins - CBM-IV species name
PAN	Peroxyacetyl nitrate - CBM-IV species name
PAR	Paraffin - CBM-IV species name
ppb	parts per billion - a unit of concentration
QA	Quality assurance
RFG	Reformulated gasoline
RVP	Reid vapor pressure, a measure of gasoline volatility
SAI	Systems Applications International
SCAQMD	South Coast Air Quality Management District
SIP	State Implementation Plan
TOG	Total organic gas
TOL	Toluene - CBM-IV species name
UAM	Urban Airshed Model - A photochemical grid model
UAM-IV	Version IV of the Urban Airshed Model
ULEV	Ultra low emission vehicle
UNIX	A computer operating system
U.S. DOE	United States Department of Energy
U.S. EPA	United States Environmental Protection Agency
UTM	Universal Transverse Mercator map grid system
VMT	Vehicle miles traveled
VOC	Volatile organic compound
VOC:NO_x	Ratio of volatile organic compound to nitrogen oxides
XYL	Xylene - CBM-IV species name

Summary

This report documents a photochemical modeling study of the potential impacts on air quality of future emissions from alternative fuel vehicles (AFVs). Although the emissions scenarios examined in this study are unlikely to occur in the time frame postulated, they provide a consistent basis on which to evaluate potential air quality impacts associated with future potential use of each fuel. This report is funded under subcontract YCC-05-14072-01 from the National Renewable Energy Laboratory (NREL).

S.1 Project Overview

The main objective of NREL in supporting this study is to determine the relative air quality impact of the use of compressed natural gas (CNG) as an alternative transportation fuel when compared to low Reid vapor pressure (RVP) gasoline and reformulated gasoline (RFG). Table S-1 lists the criteria, air toxic, and greenhouse gas pollutants for which emissions were estimated for the alternative fuel scenarios. Air quality impacts were then estimated by performing photochemical modeling of the alternative fuel scenarios using the Urban Airshed Model Version 6.21 and the Carbon Bond Mechanism Version IV (CBM-IV) (Geary et al., 1988). Using this model, we examined the formation and transport of ozone under alternative fuel strategies for motor vehicle transportation sources for the year 2007. Photochemical modeling was performed for modeling domains in Los Angeles, California, and Atlanta, Georgia.

Table S-1. Criteria, Toxic, and Greenhouse Gas Pollutants for Which Emission Estimates Were Developed for Alternative Fuel Vehicles

Criteria	Toxicities	Greenhouse Gases
Nitrogen oxides (NO_x)	Benzene	Methane (CH_4)
Volatile organic compounds (VOC)	1, 3-Butadiene	Carbon dioxide (CO_2)
Carbon monoxide (CO)	Formaldehyde	Nitrous oxide (N_2O)
	Acetaldehyde	

A project team consisting of Radian Corporation, Earth Technology Corporation, and Mr. James Killus performed this study. Radian was responsible for overall management of the project, emissions estimation and modeling, and preparation of project reports. Earth Technology was responsible for photochemical modeling and analysis of air quality impacts. Mr. Killus modified the chemical mechanisms used in the photochemical modeling to handle explicitly the toxic compounds emitted from AFVs.

S.2 Overview of Methodology

Emissions estimates for the two future-year fuel scenarios, gasoline and CNG, for the two modeling domains, Los Angeles and Atlanta, were based on the most advanced vehicle technology currently available. Advanced CNG vehicles are dedicated to the use of CNG, but are not optimized for use of CNG. Emissions for the future year (2007) baseline scenario were calculated using emission factors for gasoline fueled vehicles from the current emission factor models, MOBILE5a (U.S. EPA 1993) and EMFAC7F (ARB 1994). The gasoline-based fuels are assumed to be California Phase 2 RFG for Los Angeles and conventional reduced Reid vapor pressure (RVP) gasoline for Atlanta. From this future-year

baseline scenario, we developed the future-year CNG scenario which assumes 100% penetration of CNG into the light- and medium-duty vehicle fleet.

After estimating future-year emission factors for vehicle fleets fueled with RFG (Los Angeles) and low RVP (LRVP) gasoline (Atlanta), we developed emission adjustment factors to account for potential average fleet operation outside the bounds of the Federal Test Procedure (FTP) and for the use of CNG as a motor vehicle fuel. For this study, off-FTP operation was defined as vehicle operation outside the speed and load (acceleration) boundaries encompassed by the FTP. Emission adjustment factors for off-FTP operation and for CNG fueled vehicles were developed by Radian from motor vehicle emission test data available from several recent research programs, such as Kelley and Grablicki (1993), and Marshal (1994).

The motor vehicle emissions inputs for UAM-IV for each modeling scenario were calculated using files of hourly, gridded traffic characteristics obtained from the South Coast Air Quality Management District (SCAQMD) and the Georgia Department of Natural Resources (DNR). Emission estimates of the air toxic compounds were obtained directly from the speciation of total organic gas (TOG) emissions into constituent compounds using the Geocoded Emissions Modeling and Projection (GEMAP) System which has been upgraded to the EMS-95 described by Emigh and Wilkinson (1995). For estimating CO_2 emissions, we assumed all fuel carbon was combusted to CO_2. For CH_4 and N_2O emissions, we used three methods to estimate emissions; direct speciation, and application of two alternative sets of emission factors.

To accomplish our modeling objectives, we obtained data files from UAM-IV regulatory ozone modeling episodes developed by SCAQMD and DNR. After evaluating the available episodes, we selected for modeling in this study the 27-28 August 1987 modeling episode for Los Angeles and the 29-31 July 1987 modeling episode for Atlanta. In our modeling, we used the agency methodology and modified model input files only where necessary to address the alternative fuel scenarios. Our goal in modeling was to duplicate the agency regulatory modeling methodology as closely as possible. As part of our analysis of model output, we examined peak 1-hour concentrations of ozone, VOC, NO_x, and air toxicities; 8-hour average ozone concentrations; population exposure to ozone and air toxicities; ozone formation potential of emissions; and reactivity-weighted emissions.

Animation files that include side-by-side comparisons of the emissions and photochemical modeling results are provided as part of the final report. We prepared animations of hourly ozone isopleths and VOC and NO_x emissions tile plots. Individual animations of emissions and ozone concentrations were prepared for both cities for the gasoline and CNG scenarios for 2007. These animations are in a file format suitable for linking to a Web page or viewing with public domain animation software.

S.3 Motor Vehicle Emissions Analysis Results

The available data on motor vehicle emissions reflect both current technology and technology that is expected in the near future. NREL supplied to Radian a database of all motor vehicle emissions test data for alternative fuels and RFG available at NREL at the time of the study. These include exhaust and evaporative emissions data for advanced technology CNG vehicles, as well as data for California RFG vehicles. We also performed a literature search and updated the NREL-supplied data with data from other sources. Of these data, only emissions data that reflect vehicles optimized for RFG or gasoline or dedicated for CNG were used in this study.

After assembling these data, we developed adjustment factors representing the ratio of fleet-average CNG emission factors to low RVP gasoline or RFG emission factors to reflect the use of CNG as the vehicle fuel. In addition, we developed speciation profiles for CNG vehicle exhaust and evaporative emissions.

Our estimates of future-year emissions account for future emission standards and the impact of expected control technology. The emissions adjustment factors account for emissions from vehicles operating under both FTP and off-FTP conditions of speed and load.

Emission adjustment factors were developed from these data for light- and medium-duty gasoline vehicles. The adjustment factors are multiplicative factors that are applied to the MOBILE5a and EMFAC7F emission factors to yield emission factors for CNG-powered vehicles, and to reflect the effects of off-FTP operation. The emission factor models themselves were not modified. The adjustment factors are "fleet-average" values (averaged over vehicle age and operating cycle) by vehicle type (light-duty vehicle, light-duty truck, etc.) and by operating mode (cold start, hot start, etc.). Adjustment factors are applied by vehicle type and emission mode, without regard for variations in other environmental or operating characteristics, such as ambient temperature or speed distribution. Three sets of adjustment factors were developed and applied for this study: off-FTP adjustment factors for gasoline-fueled vehicles (one set of factors applicable to both Atlanta and Los Angeles); gasoline-to-CNG adjustment factors (including off-FTP effects) for Atlanta; and RFG-to-CNG adjustment factors for Los Angeles. Differences in the chemical speciation of the total organic gas (TOG) emissions resulting from CNG rather than gasoline usage were accounted for.

Table S-2 represents our best estimates of composite fleet-average RFG, low RVP gasoline, and CNG emissions factors for 2007 for Los Angeles and Atlanta assuming operation within the bounds of the FTP test procedure. Tables S-3 and S-4 present the adjustment factors applied to estimate exhaust emissions for 2007 for Atlanta and Los Angeles, respectively, that account for the effects of fuel and off-FTP operation by vehicle type and emission mode.

Table S-2. Estimated Light- and Medium-Duty Fleet Composite Average Exhaust Emission Factors for FTP Operation for Year 2007, Average Summer Day (units are grams/mile)

Pollutant	Los Angeles RFG Baseline	Atlanta Low RVP Gasoline Baseline	CNG
TOG	0.27	0.85	0.55
NO_x	0.53	1.1	0.20
CO	3.8	11.0	1.9

Table S-3. Exhaust Emission Adjustment Factors for Atlanta for Year 2007 (off-FTP)

Pollutant	Vehicle Type[a]	Low RVP Gasoline[b]	CNG[b]
TOG	LDGV	1.3	0.75
	LDGT1	1.2	0.69
	LDGT2	1.3	0.62
NO_x	LDGV	2.0	0.29
	LDGT1	1.8	0.27
	LDGT2	1.6	0.30
CO	LDGV	2.7	0.34
	LDGT1	2.2	0.32
	LDGT2	2.4	0.59

[a] Note: LDGV = Light-duty gasoline vehicles
LDGT1 = Light-duty gasoline trucks (0 - 6,000 pounds gross vehicle weight (GVW))
LDGT2 = Light-duty gasoline trucks (6,000 - 8,500 pounds GVW)

[b] To obtain the adjusted exhaust emissions including off-FTP impacts for a given fuel, the baseline emissions estimated using the MOBILE5a emission model are multiplied by the appropriate adjustment factor.

The motor vehicle emissions estimates developed in this study are subject to significant limitations and uncertainties, beyond those associated with emission estimates for conventional gasoline-fueled vehicles. Available test data used to characterize emissions from CNG-fueled vehicles or from off-FTP operation of gasoline-fueled vehicles is quite limited. From the available data, it is not feasible to develop emission factors or adjustment factors that accurately reflect variations in emissions by vehicle type and operating mode. The emissions estimation procedures employed for this study are intended only to characterize the **relative** quantities of composite, fleet-average emissions for different fuel scenarios.

Table S-4. Exhaust Emission Adjustment Factors for Los Angeles for Year 2007 (off-FTP)

Pollutant	Operating Mode	Vehicle Type[a]	RFG[b]	CNG[b]
TOG	Cold Start	LDV	1.3	1.0
		LDT	1.2	1.0
		MDT	1.3	1.0
	Hot Start	LDV	1.3	4.3
		LDT	1.2	4.3
		MDT	1.3	4.3
	Hot Stabilized	LDV	1.3	2.8
		LDT	1.2	2.8
		MDT	1.3	2.8
NO_x	Cold Start	LDV	2.0	1.1
		LDT	1.8	1.1
		MDT	1.6	1.1
	Hot Start	LDV	2.0	0.57
		LDT	1.8	0.57
		MDT	1.6	0.57
	Hot Stabilized	LDV	2.0	0.40
		LDT	1.8	0.40
		MDT	1.6	0.40
CO	Cold Start	LDV	2.7	1.2
		LDT	2.2	1.2
		MDT	2.4	1.2
	Hot Start	LDV	2.7	2.3
		LDT	2.2	2.3
		MDT	2.4	2.3
	Hot Stabilized	LDV	2.7	0.82
		LDT	2.2	0.82
		MDT	2.4	0.82

[a] Note: LDV = Light-duty vehicles
LDT = Light-duty trucks
MDT = Medium-duty trucks

[b] To obtain the adjusted exhaust emissions including off-FTP impacts for a given fuel, the baseline emissions estimated using the EMFAC7F emission model are multiplied by the appropriate adjustment factor.

Estimates of greenhouse gas emissions for 2007 for the gasoline/RFG and CNG scenarios are given in Table S-5. For both areas, the CO_2 emissions for the gasoline scenarios are larger than those for CNG, while CH_4 emissions are smaller. All carbon in the fuels was assumed to be combusted to CO_2. No N_2O is estimated to be emitted from CNG vehicles, while small amounts are emitted from gasoline-fueled vehicles.

Table S-5. Greenhouse Gas Emissions from Light- and Medium-Duty Vehicles for Alternative Fuel Scenarios for 2007 (tons/day)

Area	Modeling Scenario	CO_2	CH_4	N_2O
Los Angeles	RFG	160,000	30	8
	CNG	120,000	200	0
Atlanta	Low RVP Gasoline	67,000	25	15
	CNG	50,000	140	0

Note: All emission estimates are rounded to two or fewer significant figures.

Estimates of air toxic emissions for the two areas and fuel scenarios are given in Table S-6. For each city, the CNG scenario produces lower emissions of all four air toxicities compounds.

Table S-6. Air Toxic Emissions from Light- and Medium-Duty Vehicles for Alternative Fuel Scenarios for 2007 (tons/day)

Area	Fuel Scenario	Benzene	1, 3-Butadiene	Acetaldehyde	Formaldehyde
Los Angeles	RFG	5.7	0.28	0.25	0.80
	CNG	0.03	0.02	0.02	0.15
Atlanta	Low RVP Gasoline	8.2	0.88	0.88	1.9
	CNG	0.02	0.01	0.01	0.11

Note: All emission estimates are rounded to two or fewer significant figures.

S.4 Development of Toxics CBM-IV Chemical Mechanism

The identification of acetaldehyde as a toxic chemical of concern in this project required that the higher aldehyde chemical lumping of the present version of the CBM-IV mechanism be revised to break out acetaldehyde as a separate chemical species. This disaggregation requires significant changes in the CBM-IV mechanism used in UAM-IV version 6.21. Other changes were required to account for the gas phase chemistry of the toxic species benzene and 1, 3-Butadiene.

The highly aggregated version of the Carbon Bond chemical reaction mechanism known as CBM-IV has 10 primary organic species. Three of these species are highly lumped surrogates: paraffins (PAR), olefins

(OLE), and higher aldehydes (ALD2). The complete chemical mechanism has 23 species total and is represented by 86 chemical reactions. In the toxicities enhancement to the CBM-IV mechanism, 23 new reactions have been added. Most significantly, the "higher aldehydes" surrogate (ALD2) has been separated into three species: acetaldehyde (ACET); internal olefins, including cis- and trans-2 butene (IOLE); and the remaining higher aldehydes (HALD).

The toxic species benzene and 1, 3-Butadiene, plus acrolein (a species whose chemistry is linked to 1, 3-Butadiene) were installed as "ghost" state variables, with no feedback to ozone photochemistry. Thus, the emission and decay of those three compounds can be described explicitly, whereas their role in ozone photochemistry is treated within the existing Carbon Bond structural classes already in the model.

The results of testing the toxicities version of the CBM-IV chemical mechanism indicate that:

- Between 5% and 10% less ozone is formed using the toxic CBM-IV mechanism. The modifications lead to reductions in photolysis, changes in radical production resulting from the altered breakdown pathway for aldehydes, and changes in the efficiency of NO to NO_2 conversion by radicals.

- Benzene decays very slowly, so that most emitted benzene is likely to be exported out of the modeling domain. 1, 3-Butadiene reacts very rapidly; significant concentrations of 1, 3-Butadiene are likely to exist only near large source regions.

- The changes in the model chemistry did not make any significant change in either the predicted ambient NO_x concentrations or VOC concentrations.

S.5 Results of Photochemical Modeling

Three modeling emission scenarios were developed for Los Angeles and Atlanta for the future year (2007). The S1 scenario consists of emissions from all sources in the future-year emission inventory except light- and medium-duty gasoline or CNG-fueled vehicles and the fuel marketing and distribution sources supporting these vehicles. This scenario represents the "maximum" emission reduction scenario whereby all light and medium duty gasoline or CNG on-road vehicle emissions are eliminated. This scenario represents the *unaffected sources* whose emissions remain the same, regardless of motor vehicle fuel option.

The gasoline-fueled scenario contains emissions from all light- and medium-duty on-road gasoline vehicles and their associated fuel marketing and distribution emissions, assuming operation on RFG (Los Angeles) or low RVP gasoline (Atlanta), together with the S1 scenario emissions. Likewise, the CNG emissions scenario consisted of all light- and medium-duty vehicles operating on CNG, plus the S1 emissions.

The UAM-IV model output for the three scenarios for the two cities was examined using the following metrics: peak 1-hour and 8-hour surface ozone concentration, cumulative ozone and air toxicities exposures, and sensitivity of predicted ozone production to reactivity-weighted incremental emissions.

For peak 1-hour and 8-hour ozone concentrations, the following results were obtained:

- In Los Angeles, domain-wide emissions of VOC and NO_x were largest for the gasoline-fueled (RFG) scenario. The RFG scenario produced the highest predicted peak 1-hour ozone

concentrations, while the S1 scenario predicted the lowest. This result was true for both days of the two-day simulation.

- For Atlanta, domain-wide NO_x and VOC emissions were highest for the low RVP gasoline scenario. For July 30, the highest peak 1-hour ozone concentration (172 ppb) was predicted for the low RVP gasoline scenario. For July 31, the highest 1-hour ozone concentration (again 172 ppb) was predicted for the S1 scenario.

- For both modeling domains, the spatial pattern of predicted peak 1-hour ozone concentrations for the CNG scenario closely resembles that of the S1 scenario.

- The results for the peak 8-hour average ozone concentrations generally parallel the results for the peak 1-hour ozone concentrations for both cities. For Atlanta, the maximum predicted 8-hour average ozone concentration is 83% of the maximum 1-hour prediction. For Los Angeles, by contrast, the maximum 8-hour prediction is 75% of the maximum 1-hour prediction.

For cumulative population exposure to ozone and toxic compounds, the following results were obtained:

- In Atlanta and Los Angeles, the cumulative exposure to ozone decreased from the S1 scenario for both the gasoline-fueled and CNG scenarios. In Los Angeles, the lowest exposures were predicted for the RFG scenario. The reduction in exposure from the no-vehicle case appears to be due to an increase in titration of ozone by NO emissions from motor vehicles during the course of the entire day, including nighttime hours.

- In Atlanta, the cumulative ozone exposure for the low RVP gasoline scenario is larger than that for the CNG scenario on the first day but is smaller on the second day. This shift in exposure pattern suggests that, meteorology can have a significant influence on estimated ozone exposures.

- The gasoline-fueled scenarios produce the highest emissions and the largest exposures to toxic compounds for both cities.

In terms of reactivity, the following results were obtained:

- Total NO_x and VOC emissions from the gasoline-fueled scenarios are larger than those for the CNG scenario. However, when the mass of ozone formed is normalized by the VOC mass of emissions it was found that less ozone was formed per ton for gasoline fueled vehicles than from the CNG scenario.

- For Atlanta, the net ozone formation was smaller for the low RVP gasoline scenario than the S1 scenario where there were no on-road light duty vehicle emissions.

- The ozone formation potential for only aromatic species were found to be consistently negative. Since the gasoline fueled scenarios have larger mass fractions of aromatics than CNG vehicles, the smaller ozone formation per ton of emission of gasoline fueled vehicles is likely due to the aromatic compounds.

S.6 Conclusions

The principal conclusions from our work are:

1. With the exception of the greenhouse gas methane, CNG fueled vehicles emit less pollutants than gasoline fueled vehicles. CNG vehicles have much lower emission rates of toxic air pollutants, and except for methane, lower emission rates for greenhouse gases. Emission rates for VOC, NO_x and CO are also lower for CNG fueled vehicles.

2. Emissions from RFG and low RVP gasoline fueled vehicles are predicted to promote more incremental ozone formation in the future year (2007) than are emissions from CNG fueled vehicles. The spatial patterns of ozone impacts from the CNG scenarios modeled are closer in appearance to those from scenarios where all light- and medium-duty vehicle emissions have been removed.

3. Cumulative population exposure to toxic air compounds is lower for the CNG scenarios than for the gasoline-fueled scenarios.

4. The modeling results for ozone present a complex picture of the competing processes that contribute to photochemical ozone formation. At night and in the immediate vicinity of NO_x emission sources, ozone titration by NO will reduce predicted ozone concentrations. Farther downwind, the same NO_x emissions can contribute to net ozone formation. Changes in predicted peak ozone concentrations and in ozone exposures, particularly near urban centers, are imperfect metrics for evaluating the impacts of alternative fuel scenarios. As a consequence, a scenario which produces **higher** emissions of ozone precursors may lead to **lower** predicted peak ozone concentrations and ozone exposures for a given city on a given episode day. The results for Atlanta illustrate such counter-intuitive behavior.

5. The directional impacts of alternative motor vehicle fuel strategies on emissions are well understood for most of the pollutants addressed in this study. Important limitations, however, are associated with both the motor vehicle emission factors and the photochemical modeling tools used to quantify emissions and air quality impacts. Further efforts to reduce the uncertainty associated with motor vehicle emission factors and to characterize episode-specific photochemical model performance are needed for a full evaluation of alternative motor vehicle fuel strategies.

6. There is a large amount of uncertainty in the emissions estimates for some greenhouse gases from motor vehicles and in the effects of off-FTP operation on motor vehicle emissions. Consequently, results presented in this study for greenhouse gases and off-FTP effects should be carefully evaluated for usefulness until they are verified in other studies.

1.0 Introduction

This report documents the photochemical modeling study of the potential impacts on air quality of future emissions from alternative fuel vehicles (AFVs). Although the emissions scenarios examined in this study are unlikely to occur in the timeframe postulated, they provide a consistent basis on which to evaluate potential air quality impacts associated with future potential use of each fuel. This report is funded under subcontract YCC-05-14072-01 from the National Renewable Energy Laboratory (NREL).

1.1 Project Overview

The main objective of NREL in supporting this study is to determine the relative air quality impact of the use of compressed natural gas (CNG) as an alternative transportation fuel when compared to low Reid vapor pressure (RVP) gasoline and reformulated gasoline (RFG). Table 1-1 lists the criteria, air toxic, and greenhouse gas pollutants for which emissions were estimated for the alternative fuel scenarios. Air quality impacts were then estimated by performing photochemical modeling of the alternative fuel scenarios using the Urban Airshed Model Version 6.21 with the Carbon Bond Mechanism Version IV (CBIV) (Morris and Myers, 1990). Using this model, we examined the formation and transport of ozone under alternative fuel strategies for motor vehicle transportation sources for the year 2007. Photochemical modeling was performed for modeling domains in Los Angeles, California, and Atlanta, Georgia.

Table 1-1. Criteria, Toxic, and Greenhouse Gas Pollutants for Which Emission Estimates Were Developed for Alternative Fuel Vehicles

Criteria	Toxics	Greenhouse Gases
Nitrogen oxides (NO_x)	Benzene	Methane (CH_4)
Volatile organic compounds (VOC)	1,3-Butadiene	Carbon dioxide (CO_2)
Carbon monoxide (CO)	Formaldehyde	Nitrous oxide (N_2O)
	Acetaldehyde	

A project team consisting of Radian Corporation, Earth Technology Corporation, and Mr. James Killus performed this study. Radian was responsible for overall management of the project, emissions estimation and modeling, and preparation of project reports. Earth Technology was responsible for photochemical modeling and analysis of air quality impacts. Mr. Killus modified the chemical mechanisms used in the photochemical modeling to handle explicitly the toxic compounds emitted from AFVs.

1.2 Overview of Methodology

Emissions estimates for the two future-year fuel scenarios, gasoline and CNG, for the two modeling domains, Los Angeles and Atlanta, were based on the most advanced vehicle technology currently available. Advanced CNG vehicles are dedicated to the use of CNG, but are not optimized for use of CNG. Emissions for the future year (2007) baseline scenario were calculated using emission factors for gasoline fueled vehicles from the current emission factor models, MOBILE5a (U.S. EPA 1993) and EMFAC7F (ARB 1994). The gasoline-based fuels are assumed to be California Phase 2 RFG for Los Angeles and conventional reduced Reid vapor pressure (RVP) gasoline for Atlanta. From this future-year

baseline scenario, we developed the future-year CNG scenario which assumes 100% penetration of CNG into the light- and medium-duty vehicle fleet.

After estimating future-year emission factors for vehicle fleets fueled with RFG (Los Angeles) and low RVP (LRVP) gasoline (Atlanta), we developed emission adjustment factors to account for potential average fleet operation outside the bounds of the Federal Test Procedure (FTP) and for the use of CNG as a motor vehicle fuel. For this study, off-FTP operation was defined as vehicle operation outside the speed and load (acceleration) boundaries encompassed by the FTP. Emission adjustment factors for off-FTP operation and for CNG fueled vehicles were developed by Radian from motor vehicle emission test data available from several recent research programs.

The motor vehicle emissions inputs for UAM-IV for each modeling scenario were calculated using files of hourly, gridded traffic data obtained from the South Coast Air Quality Management District (SCAQMD) and the Georgia Department of Natural Resources (DNR). Emission estimates of the air toxic compounds were obtained directly from the speciation of total organic gas (TOG) emissions into constituent compounds using the Geocoded Emissions Modeling and Projections System (GEMAP). For estimating CO_2 emissions, we assumed all fuel carbon was combusted to CO_2. For CH_4 and N_2O emissions, we used three methods to estimate emissions; direct speciation, and application of two alternative sets of emission factors. Details of the emissions modeling analysis and the estimation of the greenhouse gas and air toxics emissions AFVs are given in Appendix C.

1.3 Overview of Photochemical Modeling Methodology

Over the past five years considerable effort has been devoted to the study of potential air quality impacts of new fuels to be used in automobiles and trucks in the United States (Chang and Rudy 1990), (Pollack et al. 1992), (Russell et al. 1991). This research has been stimulated by provisions of the 1990 Clean Air Act Amendments (CAAA) that set key performance targets for alternative fuels. Major targets are: (1) an eventual 25% reduction of volatile organic compounds (VOCs) and toxics emissions, and (2) no increases in NO_x emissions (Reichhardt 1995). Because of the targets, major air quality considerations have been focused on the impacts of (1) alternative fuel emissions on O_3 formation, and (2) human exposure to toxic compounds.

Comparing the effects of alternative fuels on air quality poses a number of challenges. Many fuels under consideration have potentially conflicting benefits and drawbacks with regard to estimated impacts on human health. For example, a fuel that offers benefits by reducing unhealthy O_3 exposures in heavily populated regions may have the drawback of additional toxic air exposures. Such air quality issues are the major focus of the present study, in which the air quality impacts of AFVs are compared to the impacts of vehicles fueled by low RVP gasoline or RFG.

To accomplish our modeling objectives, we obtained and evaluated UAM-IV regulatory modeling episodes from two urban areas: applications by the SCAQMD for Los Angeles and by the Georgia DNR for Atlanta. After evaluating available episodes, we selected the 27-28 August 1987 modeling episode for Los Angeles and the 29-31 July 1987 modeling episode for Atlanta. Episode selection and modeling procedures are described in the Modeling Protocol (Appendix B). In our modeling, we used the agency methodology and model input files as received for each episode, except for the following changes:

- Modification of temperature gradients for the Los Angeles episode, after consultation with SCAQMD modeling staff, to correct erroneous values in the original input files

- Adjustment of initial and boundary conditions to allow inclusion of four toxic air pollutants into the modeling episode

- Creation of new emission inventories to reflect the two alternative motor vehicle fuel scenarios for the year 2007 for each city.

Our goal in modeling was to build on the agency regulatory modeling analyses as closely as possible. Various model quality assurance (QA) and sensitivity simulations were carried out for each modeling domain to ensure the correct implementation of the episodes on our computer system. After confirming correct implementation of each episode, we performed a number of simulations to analyze the potential future impact of the two fuel scenarios. As part of our analysis of model output, we examined peak 1-hour concentrations of O_3, VOC, NO_x, and air toxics; 8-hour O_3 concentrations; population exposure to O_3 and air toxics; O_3 formation potential of emissions; and reactivity-weighted emissions.

In lieu of extensive sets of plots in an appendix presenting hourly isopleths for O_3 and tile plots of VOC and NO_x emissions, we provide as part of the final report animation files that include side-by-side comparisons of the emissions and photochemical modeling results. We prepared animations of hourly O_3 isopleths and VOC and NO_x emissions tile plots. Individual animations were prepared for each city for the following scenarios: base year with air toxics, base year with air toxics and no motor vehicle emissions, RFG scenario, and CNG scenario. These animations are in a file format suitable for linking to a Web page or viewing with public domain animation software.

1.4 Organization of this Report

The report is divided into eight sections (including this introductory section) and four appendices. In Section 2.0, we present a summary of the emissions analysis of motor vehicle emissions that forms the basis of the alternative fuel strategies we analyze in this report. Details of the motor vehicle emissions analysis is given in Appendix A.

Section 3.0 discusses the modifications made to UAM-IV photochemical model and the Carbon Bond IV chemical reaction mechanism (CBM-IV) to account for the photochemistry of four air toxic compounds: formaldehyde (FORM), acetaldehyde (ALD2), benzene (BENZ), and 1,3-butadiene (BUDI). The CBM-IV mechanism was altered to allow assessment of the impacts of these four air toxic compounds. This section describes the model implementation of the revised chemical schemes for toxics as well as changes made to model input preprocessors.

Sections 4.0 and 5.0, respectively, provide documentation of the setup and QA performed to verify proper functioning of the Los Angeles and Atlanta photochemical modeling episodes obtained from the respective regulatory agencies and used in this analysis. Sections 6.0 and 7.0 present the results of the photochemical modeling performed for the two cities using the motor vehicle emissions for the alternative fuel scenarios documented in Section 2.0. Finally, references are presented in Section 8.0.

Four appendices are a part of this report. Appendix A provides the documentation for the motor vehicle emissions analysis performed to estimate future year emissions from AFVs. Appendix B is the photochemical modeling protocol. Appendix C documents the emissions modeling performed to estimate the emissions of GHG and air toxics and to produce the photochemical model input files. Appendix D is an "electronic appendix" consisting of animated tile plots of the hourly emissions and predicted surface-level concentrations for each scenario, provided on a set of computer diskettes. These animations are designed for viewing using a public domain software program.

2.0 Motor Vehicle Emissions Analysis

The primary objective of the emissions analysis task is to devise a methodology for estimating emissions from alternative fuel vehicles, suitable for generating the emission inputs required by UAM-IV. The goal is to produce emission estimates for a motor vehicle fleet fueled by CNG, building on the regulatory modeling framework. In addition to estimating criteria pollutant emissions, the methodology must provide estimates of greenhouse gas and air toxics emissions from both conventional and alternative fuel vehicles. The procedures and emission factors used to estimate motor vehicle emissions for this study are described below. Details of the motor vehicle emissions analysis for criteria pollutants are given in Appendix A. Details of the CNG and air toxics emissions analysis are given in Appendix C.

2.1 Future Year Motor Vehicle Scenario Definition

The future year 2007 RFG and CNG scenarios were based upon full penetration of the most advanced vehicle technology currently available. We assumed that all CNG vehicles were dedicated to the use of CNG but were not optimized for use of CNG. We developed as part of this study comparable emission factor estimates for gasoline and CNG fueled vehicles. Emissions for the 2007 gasoline fuel scenarios were produced with the current emission factor models, MOBILE5a (U.S. EPA 1993a) and EMFAC7F (ARB 1994). The gasoline-based fuels were assumed to be California Phase 2 RFG for Los Angeles and LRVP gasoline for Atlanta. From the future year gasoline scenarios, we then developed the future year CNG scenario, which assumed 100% penetration of CNG into the light- and medium-duty vehicle fleet. As part of the regulatory modeling process, estimates of projected future motor vehicle activity had been produced for each urban area. Foundation files of hourly traffic characteristics for 2007, allocated to individual modeling grid cells, were obtained from SCAQMD and Georgia DNR. The motor vehicle emission estimates for all scenarios were developed using these foundation files.

Specific assumptions inherent in the alternative fuel scenarios were:

- 100% conversion of all on-road light- and medium-duty gasoline-powered vehicles to CNG.
- 100% conversion of light- and medium-duty motor vehicle fuel marketing and transportation sources to reflect use of CNG in place of current gasoline fuels.
- On-road emission estimates include estimates of incremental emissions due to on- and off-FTP operation. The FTP is the Federal Test Procedure. Off-FTP refers to operation outside the load and speed boundaries of the FTP.
- LRVP and RFG vehicle fleets reflect optimized vehicles that employ the most sophisticated technology for which emissions data are currently available.
- CNG vehicle fleets reflect dedicated, but not optimized, vehicles that employ the most sophisticated technology for which emissions data are currently available.
- RFG and LRVP emission factors and deterioration rate distributions reflect the assumptions and methodology in the EMFAC7F and MOBILE5a models, respectively.
- Current CNG ULEV emissions are representative of 2007 CNG ULEVs.

- Future year 2007 emission factors and deterioration rate distributions of the CNG fleet is based on the RFG and LRVP deterioration rate distributions.

2.2 Overview of Motor Vehicle Emissions Analysis Methodology

The emission factor models which are used to estimate motor vehicle emissions of criteria pollutants for regulatory applications are designed to characterize fleet-average emissions as a function of operating and environmental conditions. Models such as MOBILE5a and EMFAC7F have been developed using emissions test data from both prototype and in-use (gasoline-fueled) motor vehicles collected over a wide range of operating cycles and environmental conditions. For CNG fuel vehicles, by contrast, only a very limited amount of emissions test data is available, based on a small set of prototype vehicles and a limited range of operating conditions.

The emissions estimation approach which was devised for this study was designed to build on the existing framework of emission models for gasoline fuel motor vehicles. Using available test data for CNG fuel vehicles, a set of "adjustment factors" were developed that reflect the ratio between motor vehicle emissions fueled with CNG versus gasoline. These pollutant-specific adjustment factors were then applied to the hourly, gridded emission estimates for gasoline fuel vehicles, in order to calculate emissions for the CNG scenario. To obtain appropriate emission estimates for the CNG fuel scenarios in Los Angeles and Atlanta, it was necessary to develop two different sets of adjustment factors. The EMFAC7F emission factors for gasoline fuel vehicles for Los Angeles for 2007 reflect RFG and California emission control requirements, while the MOBILE5a emission factors used for Atlanta reflect conventional LRVP gasoline and federal control requirements.

Emissions of air toxics compounds for each fuel scenario were calculated by applying speciation profiles to the TOG emissions estimates. Different profiles were applied for evaporative and exhaust emissions, and for gasoline versus CNG fuel. For greenhouse gases, emission calculations were not used for air quality modeling, but are only intended to compare domain-wide emissions for different fuel scenarios. Alternative estimates for greenhouse gases from motor vehicles were developed based on energy consumption, speciation profiles, and direct emission factors.

The available data on motor vehicle emissions reflect both current technology and technology that is expected in the near future. The NREL supplied to Radian a database of all the motor vehicle emissions test data for alternative fuels and RFG available at NREL at the time of the study. These data include exhaust and evaporative emissions data for advanced technology CNG vehicles, as well as data for California RFG vehicles. We also performed a literature search and updated the NREL-supplied data with data from other sources. Of these data, only emissions data that reflect vehicles optimized for RFG or gasoline or dedicated for CNG were used in this study.

After assembling these data, we developed adjustment factors consisting of the ratio of fleet-average CNG emission factors to LRVP gasoline or RFG emission factors to reflect the use of CNG as the vehicle fuel. In addition, we developed estimates of the speciation of the vehicle exhaust and evaporative emissions. Our estimates of future year emissions account for future emission standards and the impact of expected control technology. The emissions adjustment factors account for emissions from vehicles operating under both FTP and off-FTP conditions of speed and load.

Off-FTP emissions from gasoline powered vehicles depart most from those expected under the FTP driving cycle during conditions of fuel enrichment under full power operation (hard accelerations and high speeds). Unlike gasoline powered vehicles, CNG fuel vehicles can operate at near-stoichiometric conditions under

full power. Therefore, CNG fueled vehicles may not experience increases in emissions from off-FTP operation comparable to those observed for gasoline powered vehicles.

We produced one set each of FTP and off-FTP operation adjustment factors for each fuel. Emissions data for CNG fueled vehicles are limited at this time. Therefore, our approach for CNG was to use our experience and engineering judgement to extrapolate available CNG emissions data to produce a consistent set of emission factors for FTP and off-FTP operation by vehicle type and operating mode.

Emission adjustment factors were developed for light-duty and medium-duty gasoline vehicles. The adjustment factors are a multiplicative factor that are applied to the MOBILE5a and EMFAC7F emission factors to yield emission factors for CNG powered vehicles, including off-FTP effects. The emission factor models themselves were not modified. The adjustment factors were applied as constant values, with no variation due to temperature, speed, or other parameters. Temporal and spatial variations in estimated motor vehicle emissions from CNG fuel vehicles will therefore mirror the variations in emissions from gasoline fuel vehicles as predicted by MOBILE5a or EMFAC7F.

2.3 Summary of Motor Vehicle Emission Analysis Results

The estimated fleet-average RFG, LRVP gasoline, and CNG emissions factors for 2007 for Los Angeles and Atlanta are shown in Table 2-1. These emission factors have been derived using the EMFAC7F (Los Angeles) and MOVILE5a (Atlanta) emission models which assume operation within the bounds of the FTP test procedure. When comparing these emission factors for TOG, it is important to note that each fuel produces a very different suite of emitted compounds. For CNG fuel vehicles, 95 percent of TOG exhaust emissions are methane. Speciation profiles for motor vehicle emissions of TOG are provided in Appendix A. Tables 2-2 and 2-3 present the estimated emission adjustment factors for Atlanta and Los Angeles, respectively, developed using the methodology and data discussed in Appendix A.

Table 2-1. Light- and Medium-Duty Fleet Composite Average Exhaust Emission Factors for FTP Operation for Year 2007 (units are grams/mile)

Pollutant	Los Angeles RFG Baseline	Atlanta LRVP Baseline	CNG
TOG	0.27	0.85	0.55
NO_x	0.53	1.1	0.20
CO	3.8	11.0	1.9

Table 2-2. Exhaust Emission Adjustment Factors for Atlanta for Year 2007

Pollutant	Vehicle Type[a]	Off-FTP Adjustment for LRVP gasoline	CNG Adjustment Factors[b]		
			A FTP CNG/gasoline	B Off-FTP	Total A*B
TOG	LDV	1.3	0.68	1.1	0.74
	LDT	1.2	0.63	1.1	0.69
	MDT	1.3	0.56	1.1	0.62
NO_x	LDV	2.0	0.19	1.5	0.29
	LDT	1.8	0.18	1.5	0.27
	MDT	1.6	0.20	1.5	0.30
CO	LDV	2.7	0.16	2.1	0.33
	LDT	2.2	0.15	2.1	0.31
	MDT	2.4	0.28	2.1	0.58

[a] Note: LDV = Light-duty gasoline vehicles
LDT = Light-duty gasoline trucks (0 - 6,000 pounds GVW)
MDT = Medium-duty gasoline trucks (6,000 - 8,500 pounds GVW)

[b] To obtain the adjusted exhaust emissions including off-FTP impacts for a given fuel, the FTP emission factor estimated using the MOBILE5a emission model is multiplied by the appropriate adjustment factors.

Table 2-3. Exhaust Emission Adjustment Factors for Los Angeles for Year 2007

Pollutant	Operating Mode	Vehicle Type	RFG	CNG Adjustment factors		
			Off-FTP Adjustment[a]	A CNG/RFG for FTP	B Off-FTP Adjustment[a]	Total (A*B)
TOG	Cold Start	LDV	1.3	0.95	1.1	1.0
		LDT	1.2	0.95	1.1	1.0
		MDT	1.3	0.95	1.1	1.0
	Hot Start	LDV	1.3	3.9	1.1	4.3
		LDT	1.2	3.9	1.1	4.3
		MDT	1.3	3.9	1.1	4.3
	Hot Stabilized	LDV	1.3	2.5	1.1	2.8
		LDT	1.2	2.5	1.1	2.8
		MDT	1.3	2.5	1.1	2.8
NO_x	Cold Start	LDV	2.0	0.76	1.5	1.1
		LDT	1.8	0.76	1.5	1.1
		MDT	1.6	0.76	1.5	1.1
	Hot Start	LDV	2.0	0.38	1.5	0.57
		LDT	1.8	0.38	1.5	0.57
		MDT	1.6	0.38	1.5	0.57
	Hot Stabilized	LDV	2.0	0.27	1.5	0.41
		LDT	1.8	0.27	1.5	0.41
		MDT	1.6	0.27	1.5	0.41
CO	Cold Start	LDV	2.7	0.55	2.1	1.2
		LDT	2.2	0.55	2.1	1.2
		MDT	2.4	0.55	2.1	1.2
	Hot Start	LDV	2.7	1.10	2.1	2.3
		LDT	2.2	1.10	2.1	2.3
		MDT	2.4	1.10	2.1	2.3
	Hot Stabilized	LDV	2.7	0.39	2.1	0.82
		LDT	2.2	0.39	2.1	0.82
		MDT	2.4	0.39	2.1	0.82

[a] To obtain the adjusted exhaust emissions including off-FTP impacts for a given fuel, the FTP emission factor estimated using the EMFAC7F emission model is multiplied by the appropriate adjustment factors.

The motor vehicle emissions estimates developed in this study are subject to significant limitations and uncertainties beyond those associated with emission estimates for conventional gasoline-fueled vehicles. Available test data to characterize emissions from CNG-fueled vehicles or from off-FTP operation of

gasoline-fueled vehicles is quite limited. The emissions data and procedures used to develop the adjustment factors are described in detail in Appendix A. The primary data set used to develop CNG adjustment factors for FTP operation consists of zero mile test data from seven prototype vehicles (3 LDV and 4 MDV) and one LDV engine, tested on a dynamometer. For off-FTP operation of gasoline fuel vehicles, the primary emissions data base represents 525 vehicle tests of 34 light-duty automobiles and trucks. For CNG-fueled vehicles, only preliminary test data for off-FTP operation is available. From the available data, it is not feasible to develop emission factors or adjustment factors that accurately reflect variations in emissions by vehicle type and operating mode. The emissions estimation procedures employed for this study are intended only to characterize the **relative** quantities of composite, fleet-average emissions for different fuel scenarios. Limitations and uncertainties inherent in our adjustment factors for on-FTP and off-FTP operation are summarized in Tables 2-4 and 2-5.

Table 2-4. Summary of Identified On-FTP Estimate Limitations

Limitation	Potential Impact
Emission adjustment factors for CNG were only estimated at standard test conditions. Corrections for non-standard conditions such as speed and temperature existing in the EMFAC7F and MOBILE5a models were assumed to be applicable to CNG vehicles.	Potential over-estimate of CNG emissions due to changes in temperature.
The vehicles on which the CNG test data were based are assumed to be representative of the fleet in general.	Unknown.
The amount of data available for estimating ULEV-capable CNG vehicle deterioration rates was extremely limited.	Potentially significant impact of unknown direction and magnitude.
CNG vehicle exhaust and evaporative speciation profiles were based on average gas composition. CNG composition is known to vary significantly.	Moderate potential impact on photochemistry.
Considerable variation in the individual species concentrations was seen in the RFG vehicle tests.	Moderate potential impact on photochemistry.

Table 2-5. Summary of Identified Off-FTP Estimate Limitations

Limitation	Potential Impact
Emission factors for the on-FTP portion were taken from the FTP test results of the vehicles.	Moderate potential impact.
Activity data used to compute the weighted average off-FTP emission rates were based on driving data collected from Atlanta during winter.	Moderate potential impact.
Off-FTP correction factors were developed using speed and acceleration to represent engine load.	Unknown.
Emissions data were generated from a set of late model vehicles, tuned for correct operation.	Unknown.

2.4 Emission Estimates for Greenhouse Gases and Air Toxics

Greenhouse gas emissions for CO_2, CH_4, and nitrous oxide (N_2O) from "affected" on-road mobile sources were calculated for the LRVP/RFG and CNG scenarios. "Affected" sources refer to passenger cars, LDTs and MDTs for which the emissions varied from one scenario to the next. Emissions from on-road mobile sources, heavy-duty gasoline trucks, all diesel vehicles, and motorcycles remained unchanged between scenarios and were therefore not included in this analysis.

For greenhouse gases, only domain-wide total emissions were calculated. The CO_2 emissions from affected sources were calculated using emission factors based on mass of carbon per unit of fuel energy content. The remaining greenhouse gas emissions were calculated using three different methods based, respectively, on vehicle miles traveled (VMT), energy (British Thermal Unit, BTU) content of the fuel, and speciated results from the GEMAP emissions modeling. The estimates derived from direct speciation are preferred. The results for the other two methods are given for comparison purposes. Gridded, hourly emissions of air toxics consisting of BENZ, BUDI, ALD2, and FORM were also calculated for the affected on-road mobile sources, based on direct speciation of the GEMAP emissions modeling results. Details of the estimation of greenhouse gas and air toxic emissions are given in Appendix C.

2.4.1 Emission Estimates for CO_2

Table 2-6 presents estimated CO_2 emissions for 2007 for light- and medium-duty vehicles fueled by gasoline or CNG. The emission factors used are for natural gas and gasoline combustion (U.S. DOE 1994). We assumed that the gasoline emission factors are representative of emissions from the combustion of either RFG or LRVP gasoline. Implicit in the use of these emission factors is the assumption that all carbon in the fuel is combusted completely to CO_2.

2.4.2 Emission Estimates for CH_4 and N_2O

Emissions estimates for CH_4 and N_2O were calculated using three methods:

- Directly by the emissions modeling system (requires an assumed N_2O to NO_x emission ratio to estimate N_2O emissions).
- Emission factors based on energy consumption.
- Emission factors based on VMT.

Our preferred estimates of CH_4 and N_2O emissions are based on the speciation profiles for exhaust and evaporative emissions. Nitrous oxide emissions were estimated based on model-input NO_x emissions. To obtain estimates of N_2O for gasoline-fueled vehicles, the NO_x emissions were multiplied by 0.04 (U.S. EPA 1995).

Table 2-6. Estimated Fuel Usage, Energy Usage, Carbon Emission Factors and CO_2 Emission Rates for Los Angeles and Atlanta for Year 2007 for Light- and Medium-Duty Gasoline and CNG Fueled Vehicles

Modeling Domain	Fuel	Gasoline Usage (10^6 Gal per day)	Energy Usage (10^{12} BTU per day)	Emission Factor (10^6 MT C per 10^{15} BTU)	CO_2 Emissions (U.S. Tons per day)[e]
Los Angeles	RFG	16.1[a]	2.0	19.4[b]	160,000
	CNG	16.1	2.0	14.5[c]	120,000
Atlanta	LRVP	6.76[d]	0.85	19.4[b]	67,000
	CNG	6.76	0.85	14.5[c]	50,000

[a] Source: BURDEN7F output for Los Angeles obtained from SCAQMD.
[b] Source: U.S. DOE, 1994. Table A4.
[c] Source: U.S. DOE, 1994. Table A3.
[d] Fuel usage based on an estimated VMT of 158 x 10^6 miles per day and an assumed average fuel economy of 23.4 miles per gallon based on BURDEN7F output for Los Angeles.
[e] All emissions are rounded to two or fewer significant figures.

For comparison purposes, we developed alternative estimates using two EPA emission factor approaches. Estimates of CH_4 and N_2O emissions using BTU-based and VMT-based factors are given in Tables 2-7 and 2-8 for Los Angeles and Atlanta, respectively. Both sets of emission factors were developed by U.S. EPA, but the BTU-based emission factors are preferred because, unlike the VMT-based factors, they do not require an inherent assumption of fuel economy (U.S. EPA 1995). For both cities, the speciation-based CH_4 emissions for the CNG scenario are significantly lower than those estimated using emission factors, while CH_4 estimates for the RFG/LRVP scenarios are higher. For N_2O, the trend is mixed with emission factors producing higher estimates for the Los Angeles scenario while the modeling approach produces higher N_2O emission for the Atlanta gasoline scenario. The inconsistent trend and large differences in the model and emission factor estimates indicate there is significant uncertainty in these estimates of greenhouse gas emissions.

Table 2-7. Estimated CH_4 and N_2O Emissions from Affected On-Road Mobile Sources in Los Angeles (tons/day)

Pollutant	Modeling Scenario	Preferred Estimate (Speciation)	Alternative Estimates	
			BTU-Based	VMT-Based
CH_4	RFG	30	19	18
	CNG	200	620	520
N_2O	RFG	8	15	15
	CNG	0	0	0

Note: All emission estimates are rounded to two or fewer significant figures

Table 2-8. Estimated CH_4 and N_2O Emissions from Affected On-Road Mobile Sources in Atlanta (tons/day)

Pollutant	Modeling Scenario	Preferred Estimate (Speciation)	Alternative Estimates	
			BTU-Based	VMT-Based
CH_4	LRVP	25	8.0	7.4
	CNG	140	260	200
N_2O	LRVP	15	6.3	6.0
	CNG	0	0	0

Note: All emission estimates are rounded to two or fewer significant figures

2.4.3 Emission Estimates for Air Toxics

Air toxics emissions of BUDI, BENZ, ALD2, and FORM were estimated both as gridded, hourly model input species and as daily totals for the entire Los Angeles and Atlanta modeling domains.

The air toxics emissions estimates presented in Table 2-9 for Los Angeles and Atlanta were calculated similarly to the CH_4 emissions. These chemicals are calculated from the speciated TOG emissions for each fuel scenario. The results presented in this table indicate that the CNG scenario is associated with lower estimates of primary emissions of all four air toxics compounds for both modeling domains.

Table 2-9. Estimated Air Toxic Emissions from Affected On-Road Mobile Sources in Los Angeles and Atlanta (tons/day)

Area	Modeling Scenario	Benzene	1-, 3-Butadiene	Acetaldehyde	Formaldehyde
Los Angeles	RFG	5.7	0.28	0.25	0.80
	CNG	0.03	0.02	0.02	0.15
Atlanta	LRVP	8.2	0.88	0.88	1.9
	CNG	0.02	0.01	0.01	0.11

Note: All emission estimates are rounded to two or fewer significant figures.

3.0 Development and Testing of a Toxics CBM-IV Chemical Mechanism for UAM-IV

In order to estimate ambient concentrations and exposures for identified air toxics compounds contained in motor vehicle emissions, it was necessary to modify the chemical mechanism in UAM-IV. The identification of acetaldehyde (ACET) as a toxic chemical of concern required that the chemical lumping of higher aldehydes in the present version of the CBM-IV mechanism be revised in order to break out ACET as a separate chemical species. This disaggregation requires significant changes in the CBM-IV mechanism used in UAM-IV version 6.21. Other changes are required for better simulation of gas phase chemistry for the toxic species BENZ and BUDI. These revisions to the CBM-IV chemistry were made by Killus (1995) for this project and are described below. The modifications to the chemical mechanism produce changes in predicted ozone concentrations. A series of tests were conducted to ensure that the new mechanism was operating properly and to document and quantify any predicted changes in ozone photochemistry.

3.1 Modifications of the CBM-IV Surrogate Approximation

The technique of "surrogate approximation" is used in the CBM-IV mechanism to reduce the number of state (transported) species. It is common in atmospheric models to account for a group of chemically-similar compounds by using a single compound as a "surrogate", e.g., using propene as a surrogate for all 1-olefins (OLE). UAM also uses another form of surrogate approximation, by treating a number of highly reactive compounds as if they had already reacted to form products. Thus, a very reactive compound such as cis-2-butene can be approximated as an emission of two molecules of its reaction product ACET. Tests have shown the UAM surrogate approximation technique to give adequate results in most situations.

The present highly aggregated version of the Carbon Bond chemical reaction mechanism known as CBM-IV has 10 primary organic species. Three of these species are highly lumped surrogates: paraffins (PAR), OLE, and ALD2, representing ACET and higher aldehydes (HALD). The other explicit surrogate chemical species include FORM, toluene (TOL), xylene (XYL), isoprene (ISOP), ethene (ETH), and the alcohols ethanol (ETOH), and methanol (MEOH). The complete chemical mechanism has 33 species and is represented by 86 chemical reactions. The new toxics CBM-IV mechanism has 42 species, as listed in Table 3-1, and 109 chemical reactions. The complete chemical mechanism is documented in Table 3-2. The last 9 species listed in Table 3-1 and the last 23 reactions in Table 3-2 are those added for the new mechanism. With the introduction of new species (ACET, IOLE, HALD, HPAN, C_3O_3) the related reactions in the original mechanism have also been modified.

The explicit treatment of ACET in UAM is not straightforward because the original formulation lumped all non-formaldehyde aldehyde species into a single category. It is necessary to distinguish ACET both from other higher aldehyde species and from reactive compounds that form ACET. This change was accomplished by adding two new "species": HALD, for other higher aldehydes, and IOLE, for internal olefins such as cis-2-butene and trans-2-butene, which form ACET as a reaction product. The addition of HALD, in turn, requires a new species "HPAN" to represent the PAN-analog reaction products of HALD.

The photolysis rate for ACET is considerably smaller than the rate for other higher aldehydes (Moortgat et al., 1989). With a smaller photolysis rate, ACET will react more slowly, which can result in higher predicted ACET concentrations and lower concentrations of radicals produced via photolysis. For the new species IOLE, a new set of chemical reactions (Reactions 89 to 92 in Table 3-2) was added to the chemical mechanism, based on Atkinson et al (1994) and Atkinson (1990). The reaction pathways to form HALD

from OLE and PAR are based on similar product pathways in the original CBM-IV mechanism (Geary et al., 1988).

Three air toxics compounds, BENZ, BUDI, and acrolein (ACRO), were installed as "ghost" state variables, with no feedback to O_3 photochemistry. The emission and decay of these compounds is described explicitly, while their effects on O_3 photochemistry are treated via their contributions to the Carbon Bond surrogates already in the model. The "ghost" variable approach will give reasonable results as long as the species in question is a relatively minor constituent of a class of compounds and is not itself a reaction product. The simplifying assumption of "ghost" species makes the addition of BENZ, BUDI, and ACRO to the UAM chemistry routines, and the testing of those additions, both simple and straightforward. Reactions for the "ghost" species are numbered 87, and 99 through 103 in Table 3-2. They have no effect on the chemistry, and will track concentrations of the three compounds so long as the reacting species (OH, O_3, and NO_3) are correctly simulated.

Three chemical reactions involving propane and acetone (Reactions 104-106) were also added to the toxics chemical mechanism and are listed in Table 3-2. For the present study, these reaction have been disabled, since they do not involve any toxic species of concern.

3.2 Testing of the CBM-IV Toxics Chemical Mechanism

The implementation of the changes to the CBM-IV chemistry for this project has been tested under a variety of conditions. The modified chemical mechanism solver was installed in a chemical box model, BOXCHEM, which functions as a numerical smog chamber. The results for a series of test cases are discussed in Killus (1995). The testing indicates that predicted peak ozone is reduced slightly for the revised mechanism, compared to the unmodified CBM-IV chemistry.

The BOXCHEM model was exercised in two modes. In the first mode, the compounds were introduced as initial conditions with no emissions. In the second mode, emissions were input as 30% of the initial conditions for each time step. The BOXCHEM was operated for both nighttime (zero photolysis) and midday conditions. The most relevant tests were for midday conditions. During these midday tests the chamber was operated for a 6-hour simulation period in the afternoon with a constant temperature of 298°K and water vapor concentration (a source of hydroxyl radicals) of 20,000 ppm. An error tolerance was set to 1% for NO and HO_2. The predicted concentrations were saved every 30 minutes as a period ending snapshot.

Plots of the modeled concentration for midday conditions for seven chemical species are given in Figure 3-1 for each type of BOXCHEM simulation. The ending digit of the simulation identifier (see legend box in the lower right of the figure) indicates the mode in which BOXCHEM was exercised. Figure 3-1a indicates that typically 5-8% more ozone is produced by the original unmodified chemistry. Also, there is no effective difference between simulations with and without "ghost" species toxics as was expected.

Differences in ozone production are reflected in changes in the nitrogen chemistry. In the new chemical scheme, there are 10 chemical species (including nitrate and excluding NTR) and 9 in the old scheme. The new addition is the higher PAN analogs (HPAN). Of all the species, all but a percent or so of the total nitrogen is sequestered in the PANs, HNO_3, N_2O_5, NO_2, AND NO. A summary of the nitrogen species concentrations at the end of the 6-hour afternoon simulation is shown in Table 3-3. The table indicates that the TOXIC chemistry scheme results in less NO_x to participate in ozone chemistry. One reason is that HPAN facilitates the conversion of NO_x to a nitrate and represents a significant nitrogen reservoir, as shown in Table 3-3.

The time versus concentration plots for NO_2 and PAN are shown in Figures 3-1b and 3-1c, respectively. For all of the test cases the NO_2 initially jumps then decays with the passage of time. The rate of decrease is larger for the toxics chemistry. The decrease in the rate of PAN formation (and buildup) in the toxics chemistry case is evident.

The radical (OH) concentrations were examined. Figure 3-1d shows that the expanded CBM chemical mechanism results in lower radical concentrations regardless of the presence of emission species. The situation is a little more complicated for the peroxy radicals (C_20_3). When emissions of peroxy radicals are added, the time series in Figure 3-1e indicates that for some times more peroxy radicals are present under the expanded CBM scheme than the original, but at the end of the experiment more radicals are produced with the original chemistry.

In the base simulation, ALD2 contains all of the aldehydes other than formaldehyde. In the case of the toxics chemistry, ALD2 only contains acetaldehyde, with all remaining higher aldehydes lumped into HALD. The time series of ALD2 is given in Figure 3-1f. An interesting finding is that there is more acetaldehyde as ALD2 in the expanded CBM simulations than all of the aldehydes present in ALD2 in the base simulation. The reduced photolysis for acetaldehyde (ACET) relative to the larger photolysis in the original CBM higher aldehydes (ALD2) contributes to the overall increase in total aldehyde concentrations in the expanded CBM chemistry. The slower photolytic destruction results in fewer radicals being formed.

The reactions of the "ghost" toxic species such as benzene and 1,3-butadiene was examined. The time series of benzene is shown in Figure 3-1g. Benzene reacts very slowly, so there is essentially very little difference between the cases when benzene is and is not allowed to react. When the toxics switch is enabled, the 1-3-butadience concentrations plunge from 3.0×10^{-3} ppm at the start of the experiment to 1.3×10^{-5} six hours later.

Table 3-1. Chemical Species in the Toxics Version of the CBM-IV Mechanism

Species Name	Representation
Nitric oxide	NO
Nitrogen dioxide	NO_2
Nitrogen trioxide (nitrate radical)	NO_3
Dinitrogen pentoxide	N_2O_5
Nitrous acid	HONO
Nitric acid	HNO_3
Peroxynitric acid (HO_2NO_2)	PNA
Oxygen atom (singlet)	0^1D
Oxygen atom (triplet)	O
Hydroxyl radical	OH
Water	H_2O
Ozone	O_3
Hydroperoxy radical	HO_2
Hydrogen peroxide	H_2O_2

Carbon monoxide	CO
Formaldehyde (CH_2O)	FORM
Acetaldhyde (RCHO)	ACET
Peroxyacyl radical ($CH_3C(O)OO\cdot$)	C_2O_3
Peroxyacyl nitrate ($CH_3C(O)OONO_2$)	PAN
Paraffin carbon bond (C-C)	PAR
Secondary organic oxy radical	ROR
Olefinic carbon bond (C=C)	OLE
Ethene (CH_2=CH_2)	ETH
Toluene (C_6H_5-CH_3)	TOL
Cresol and higher molecular weight phenols	CRES
Toluene-hydroxyl radical adduct	TO_2
Methylphenoxy radical	CRO
High molecular weight aromatic oxidation ring fragment	OPEN
Xylene (C_6H_4-$(CH_3)_2$)	XYL
Methylglyoxal ($CH_3C(O)C(O)H$)	MGLY
Isoprene	ISOP
NO-to-NO_2 operation	XO_2
NO-to-nitrate operation	XO_2N
Sulfate	SULF
Nitrate	NTR
Internal olefins	IOLE
Higher PAN anlogs (e.g.PPN)	HPAN
Higher aldehydes (R_nCHO)	HALD
Benzene (C_6H_6)	BENZ
1-, 3-butadiene ($(CH_2)_2CHCH$)	BUDI
Acrolein (CH_2CFORM)	ACRO
Propane (C_3H_8)	PRPA
Acetone (CH_3COCH_3)	AONE
Higher peroxacyl radicals	C_3O_3
Total number of chemical species	**42**

Table 3.2 The Toxics version of the Carbon Bond Mechanism IV

Reaction No.	Reaction	Pre-factor ppm^{-n} hr^{-1}	Temperature dependency	Rate constant at 298K ppm^{-n} hr^{-1}
		Inorganic Reactions		
(R1)	$NO_2 + h\nu \rightarrow NO + O$	radiation dependent	none	na
(R2)	$O + O_2 + M \rightarrow O_3 + M$	0.503E+07	$e^{1175/T}$	0.600E+02
(R3)	$O_3 + NO \rightarrow NO_2 + O_2$	0.155E+06	$e^{-1370/T}$	0.160E+04
(R4)	$O + NO_2 \rightarrow NO + O_2$	0.825E+05	none	0.825E+06
(R5)	$O + NO_2 + M \rightarrow NO_3 + M$	0.138E+05	$e^{687/T}$	0.139E+06
(R6)	$O + NO + M \rightarrow NO_2 + M$	0.194E+05	$e^{602/T}$	0.146E+06
(R7)	$O_3 + NO_2 \rightarrow NO_3 + O_2$	0.106E-05	$e^{-2450/T}$	0.284E+01
(R8)	$O_3 + h\nu \rightarrow O + O_2$	radiation dependent	none	na
(R9)	$O_3 + h\nu \rightarrow O^1D$	radiation dependent	none	na
(R10)	$O^1D + M \rightarrow O + M$	0.688E+07	$e^{390/T}$	0.255E+08
(R11)	$O^1D + H_2O \rightarrow 2\ OH$	0.196E+03	none	0.196E+03
(R12)	$O_3 + OH \rightarrow HO_2 + O_2$	0.141E+06	$e^{-940/T}$	0.600E+04
(R13)	$O_3 + HO_2 \rightarrow OH + 2\ O_2$	0.126E+04	$e^{-580/T}$	0.180E+03
(R14)	$NO_3 + h\nu \rightarrow 0.89\ NO_2 + 0.89\ O + 0.11\ NO$	radiation dependent	none	na
(R15)	$NO_3 + NO \rightarrow 2\ NO_2$	0.115E+07	$e^{250/T}$	0.265E+07
(R16)	$NO_3 + NO_2 \rightarrow NO + NO_2 + O_2$	0.220E+04	$e^{-1230/T}$	0.354E+02
(R17)	$NO_3 + NO_2 + M \rightarrow N_2O_5 + M$	0.471E+05	$e^{256/T}$	0.111E+06
(R18)	$N_2O_5 + H_2O \rightarrow 2\ HNO_3$	0.114E-03	none	0.114E-03
(R19)	$N_2O_5 + M \rightarrow NO_3 + NO_2 + M$	0.127E-19	$e^{-10897/T}$	0.167E+03
(R20)	$NO + NO + O_2 \rightarrow 2\ NO_2$	0.156E-02	$e^{530/T}$	0.923E-02
(R21)	$NO + NO_2 + H_2O \rightarrow 2\ HONO$	0.960E-09	none	0.960E-09
(R22)	$OH + NO \rightarrow HONO$	0.383E+05	$e^{806/T}$	0.588E+06

Reaction No.	Reaction	Pre-factor ppm^{-n} hr^{-1}	Temperature dependency	Rate constant at 298K ppm^{-n} hr^{-1}
(R23)	$HONO + h\nu \rightarrow OH + NO$	radiation dependent	none	na
(R24)	$OH + HONO \rightarrow NO_2$	0.586E+06	none	0.586E+06
(R25)	$HONO + HONO \rightarrow NO + NO_2$	0.900E-03	none	0.900E-03
(R26)	$OH + NO_2 + M \rightarrow HNO_3 + M$	0.922E+05	$e^{713/T}$	0.101E+07
(R27)	$OH + HNO_3 + M \rightarrow NO_3 + H_2O + M$	0.329E+06	$e^{1000/T}$	0.131E+05
(R28)	$HO_2 + NO \rightarrow OH + NO_2$	0.165E+07	$e^{240/T}$	0.736E+06
(R29)	$HO_2 + NO_2 \rightarrow HO_2NO_2$ (PNA)	0.0	$e^{749/T}$	0.0
(R30)	HO_2NO_2 (PNA) $+ M \rightarrow HO_2 + NO_2 + M$	0.0	$e^{-10121/T}$	0.0
(R31)	$OH + HO_2NO_2$ (PNA) $\rightarrow NO_2 + H_2O + O_2$	0.0	$e^{380/T}$	0.0
(R32)	$HO_2 + HO_2 \rightarrow H_2O_2$	0.524E+04	$e^{1150/T}$	0.249E+06
(R33)	$HO_2 + HO_2 + H_2O \rightarrow 2\ H_2O_2$	6.461E-07	$e^{5800/T}$	0.131E+02
(R34)	$H_2O_2 + h\nu \rightarrow 2\ OH$	radiation dependent	none	na
(R35)	$OH + H_2O_2 \rightarrow HO_2 + H_2O$	0.283E+06	$e^{-187/T}$	0.151E+06
(R36)	$OH + CO + O_2 \rightarrow HO_2 + CO_2$	0.193E+05	none	0.193E+05
	Formaldehyde (FORM) Reactions			
(R37)	$FORM + OH + O_2 \rightarrow HO_2 + CO + H_2O$	0.900E+06	none	0.900E+06
(R38)	$FORM + h\nu \rightarrow 2\ HO_2 + CO$	radiation dependent	none	na
(R39)	$FORM + h\nu \rightarrow CO + H_2$	radiation dependent	none	na
(R40)	$FORM + O \rightarrow OH + HO_2 + CO$	0.258E+07	$e^{-1550/T}$	0.142E+05
(R41)	$FORM + NO_3 \rightarrow HNO_3 + HO_2 + CO$	0.558E+02	none	0.558E+02
	Acetaldehyde (ACET) Reactions			
(R42)	$ACET + O \rightarrow C_2O_3 + OH$	0.104E+07	$e^{-986/T}$	0.382E+05
(R43)	$ACET + OH \rightarrow C_2O_3$	0.622E+06	$e^{250/T}$	0.144E+07

Reaction No.	Reaction	Pre-factor ppm^{-n} hr^{-1}	Temperature dependency	Rate constant at 298K ppm^{-n} hr^{-1}
(R44)	ACET + NO_3 $\xrightarrow{O_2}$ C_2O_3 + HNO_3	0.2222E+03	none	0.222E+03
(R45)	ACET + hν $\xrightarrow{2O_2}$ FORM + XO_2 + CO + 2 HO_2	radiation dependent		
(R46)	C_2O_3 + NO $\xrightarrow{O_2}$ FORM + XO_2 + HO_2 + NO_2	0.310E+07	e^{-180T}	0.169E+07
(R47)	C_2O_3 + NO_2 → PAN	0.230E+06	$e^{380/T}$	0.822E+06
(R48)	PAN → C_2O_3 + NO_2	0.720E-20	$e^{-13500/T}$	0.152E+01
(R49)	C_2O_3 + C_2O_3 → 2 FORM + 2 XO_2 + 2 HO_2	0.222E+06	none	0.222E+06
(R50)	C_2O_3 + HO_2 → 0.79 FORM + 0.79 XO_2 + 0.79 HO_2 + 0.79 OH	0.576E+06	none	0.576E+06
(R51)	OH → FORM + XO_2 + HO_2	0.391E+06	$e^{-1710/T}$	0.126E+04
	Alkane Reactions			
(R52)	PAR + OH → 0.87 XO_2 + 0.13 XO_2N + 0.11 HO_2 + 0.06 ACET + 0.76 ROR - 0.11 PAR + 0.05 HALD	0.722E+05	none	0.722E+05
(R53)	ROR → 0.6 ACET + 0.96 XO_2 + 0.94 HO_2 + 0.04 XO_2N + 0.02 ROR - 2.10 PAR + 0.5 HALD	0.375E+19	$e^{-8000/T}$	0.823E+07
(R54)	ROR → HO_2	0.573E+07	none	0.573E+07
(R55)	ROR + NO_2 →	0.132E+07	none	0.132E+07
	Alkene Reactions			
(R56)	O + OLE → 0.32 ACET + 0.38 HO_2 + 0.28 XO_2 + 0.30 CO + 0.20 FORM + 0.02 XO_2N + 0.22 PAR + 0.20 OH + 0.31 HALD	0.105E+07	$e^{-324/T}$	0.355E+06
(R57)	OH + OLE → FORM + 0.5 ACET + XO_2 + HO_2 - PAR + 0.5 HALD	0.464E+06	$e^{504/T}$	0.252E+07

Reaction No.	Reaction	Pre-factor ppm^{-n} hr^{-1}	Temperature dependency	Rate constant at 298K ppm^{-n} hr^{-1}
(R58)	O_3 + OLE → 0.25 ACET + 0.74 FORM + 0.33 CO + 0.44 HO_2 + 0.25 HALD + 0.22 XO_2 + 0.10 OH - PAR	0.126E+04	$e^{-2105/T}$	0.138E+01
(R59)	NO_3 + OLE → 0.91$X0_2$ + FORM + 0.5 ACET + 0.09 XO_2N + NO_2 - PAR + 0.5 HALD	0.681E+03	none	0.681E+03
(R60)	O + ETH → FORM + 0.70 $X0_2$ + CO + 1.70 HO_2 + 0.30 OH	0.924E+06	$e^{-792/T}$	0.648E+05
(R61)	OH + ETH → XO_2 + 1.56 FORM + HO_2 + 0.22 HALD	0.180E+06	$e^{411/T}$	0.715E+06
(R62)	O_3 + ETH → FORM + 0.42 CO + 0.12 HO_2	6.111E+04	$e^{-2633/T}$	0.162E+00
	Aromatic Reactions			
(R63)	OH + TOL → 0.08 XO_2 + 0.36 CRES + 0.44 HO_2 + 0.56 TO_2	0.186E+06	$e^{322/T}$	0.549E+06
(R64)	TO_2 + NO → 0.08 $X0_2$ + 0.36 CRES + 0.44 HO_2 + 0.56 TO_2	0.720E+06	none	0.720E+06
(R65)	TO_2 → HO_2 + CRES	0.150E+05	none	0.150E+05
(R66)	OH + CRES → 0.40 CRO + 0.60 XO_2 + 0.60 HO_2 + 0.30 OPEN	.0366E+07	none	0.366E+07
(R67)	NO_3 + CRES → CRO + HNO_3	0.195E+07	none	0.195E+07
(R68)	CRO + NO_2 →	0.120E+07	none	0.120E+07
(R69)	OPEN + hν → C_2O_3 + CO + HO_2	radiation dependent	none	na
(R70)	OH + OPEN → XO_2 + C_2O_3 + 2 HO_2 + 2 CO + FORM	0.264E+07	none	0.264E+07
(R71)	O_3 + OPEN → 0.03 ACET + 0.62 C_2O_3 + 0.70 FORM + 0.03 XO_2 + 0.69 CO + 0.08 OH + 0.76 HO_2 + 0.20 MGLY	0.482E+01	$e^{-500/T}$	0.90E+00
(R72)	OH + XYL → 0.70 HO_2 + 0.50 XO_2 + 0.20 CRES + 0.80 MGLY + 1.10 PAR + 0.30 TO_2	0.147E+07	$e^{116/T}$	0.217E+07

Reaction No.	Reaction	Pre-factor ppm^{-n} hr^{-1}	Temperature dependency	Rate constant at 298K ppm^{-n} hr^{-1}
(R73)	$OH + MGLY \rightarrow XO_2 + C_2O_3$	0.156E+07	none	0.156E+07
(R74)	$MGLY + h\nu \rightarrow C_2O_3 + CO + HO_2$	radiation dependent	none	na
	Isoprene Reactions			
(R75)	$O + ISOP \rightarrow 0.60\ HO_2 + 0.80$ ACET + 0.55 OLE + $0.50\ XO_2 + 0.50$ CO + 0.45 ETH + 0.90 PAR	0.162E+07	none	0.162E+07
(R76)	$OH + ISOP \rightarrow$ FORM + $XO_2 + 0.67\ HO_2 + 0.40$ MGLY + $0.20\ C_2O_3$ + ETH + 0.20 ACET + $0.13\ X0_2N$	0.852E+07	none	0.852E+07
(R77)	$O_3 + ISOP \rightarrow$ FORM + 0.40 ACET + 0.55 ETH + 0.20 MGLY + 0.06 CO + 0.10 PAR + $0.44\ HO_2 + 0.10$ OH	0.108E+01	none	0.108E+01
(R78)	$NO_3 + ISOP \rightarrow XO_2N$	0.282E+05	none	0.282E+05
	Operator Reactions			
(R79)	$XO_2 + NO \rightarrow NO_2$	0.7200E+06	none	0.720E+06
(R80)	$XO_2 + XO_2 \rightarrow$	0.153E+09	$e^{1300/T}$	0.12E+06
(R81)	$XO_2N + NO \rightarrow$	0.600E+05	none	0.600E+05
	Sulfur Reactions			
(R82)	$OH + SO_2 \rightarrow$ SULF	0.389E+05	$e^{1600/T}$	0.666E+05
(R83)	$SO_2 + O_3 \rightarrow$ SULF	0.490E-02	none	0.490E-02
	Alcohol Reactions			
(R84)	$OH + MEOH \rightarrow$ FORM + HO_2	0.960E+05	none	0.960E+05
(R85)	$OH + ETOH \rightarrow$ ACET + HO_2	0.143DE+06	$e^{176/T}$	0.258E+06
	Null Reaction			
(R86)	NR	0.681E+04	$e^{1300/T}$	0.534E+06
	Benzene Reaction			
(R87)	BENZ + OH → OH	0.109E+06	none	0.109E+06

Reaction No.	Reaction	Pre-factor ppm^{-n} hr^{-1}	Temperature dependency	Rate constant at 298K ppm^{-n} hr^{-1}
	Disaggregated Aldehyde Reactions			
(R88)	IOLE + OH → 1.5 ACET + 0.5 HALD + HO_2 + XO_2	0.566E+07	none	0.566E+07
(R89)	IOLE + O → 1.425 ACET + 0.475 HALD + 0.1 HO_2 + 0.1 XO_2 + 0.1 CO + 0.1PAR	0.204E+07	none	0.204E+07
(R90)	IOLE + O_3 → 0.75 ACET + 0.25 HALD + 0.2 OH + .25 CO	0.186E+02	none	0.186E+02
(R91)	IOLE + NO_3 → 1.5 ACET + 0.5 HALD + NO_2	0.344E+05	none	0.344E+05
(R92)	HALD + OH → C_3O_3	0.144E+07	none	0.144E+07
(R93)	HALD + hν → ACET + 2 × HO_2 + CO + XO_2 - PAR	radiation dependent	none	na
(R94)	HALD + O → OH + C_3O_3 + - PAR	0.382E+05	none	0.382E+05
(R95)	HALD + NO_3 → C_3O_3 + HNO_3 - PAR	0.242E+03	none	0.242E+03
(R96)	C_3O_3 + NO_2 → HPAN	0.230E+06	$e^{-380/T}$	0.643E+05
(R97)	HPAN → C_3O_3 + NO_2	0.337E+21	$e^{-14000/T}$	0.133E+01
(R98)	C_3O_3 + NO → NO_2 + ACET + HO_2 + XO_2	0.310E+07	$e^{-180/T}$	0.567E+07
	Toxic Compound Reactions			
(R99)	BUDI + OH → OH + ACRO	0.594E+07	none	0.594E+07
(R100)	BUDI + O_3 → O_3 + ACRO	0.600E+00	none	0.600E+00
(R101)	BUDI + NO_3 → NO_3	0.870E+04	none	0.870E+04
(R102)	ACRO + OH → OH	0.180E+07	none	0.138e+07
(R103)	ACRO + O_3 → O_3	0.666E-01	none	0.666E-01
(R104)	PRPA + OH → XO_2 + HO_2 + AONE	0.108E+06	none	0.108E+06
(R105)	AONE + OH → C_2O_3 + FORM + XO_2	0.348E+05	none	0.348E+05
(R106)	AONE + hν → FORM + XO_2 + C_2O_3	radiation dependent	none	na
	Radical Reactions			
(R107)	C_3O_3 + C_3O_3 → 2 XO_2 + 2 ACET + 2 HO_2	0.222E+06	none	0.222E+06

Reaction No.	Reaction	Pre-factor $ppm^{-n}\ hr^{-1}$	Temperature dependency	Rate constant at 298K $ppm^{-n}\ hr^{-1}$
(R108)	$C_3O_3 + HO_2 \rightarrow 0.79\ ACET + 0.79\ XO_2 + 0.79\ HO_2 + 0.79\ OH + 0.21\ PAA$	0.576E+06	none	0.576E+06
(R109)	$C_2O_3 + C_3O_3 \rightarrow 2\ XO_2 + ACET + FORM + 2\ HO_2$	0.444E+06	none	0.444E+06

* See Appendix A for notes.

Table 3-3. Final Predicted Concentrations for the Major Nitrogen Species from the 6-Hour Daytime BOXCHEM Simulation CBM and TOXIC (units are ppm)

Chemical Species	CBM Simulation	TOXIC Simulation
NO	6.5×10^{-5}	5.9×10^{-5}
NO_2	3.2×10^{-3}	2.9×10^{-3}
HNO_3	0.057	0.049
PAN	0.066	0.054
HPAN	NA	0.025

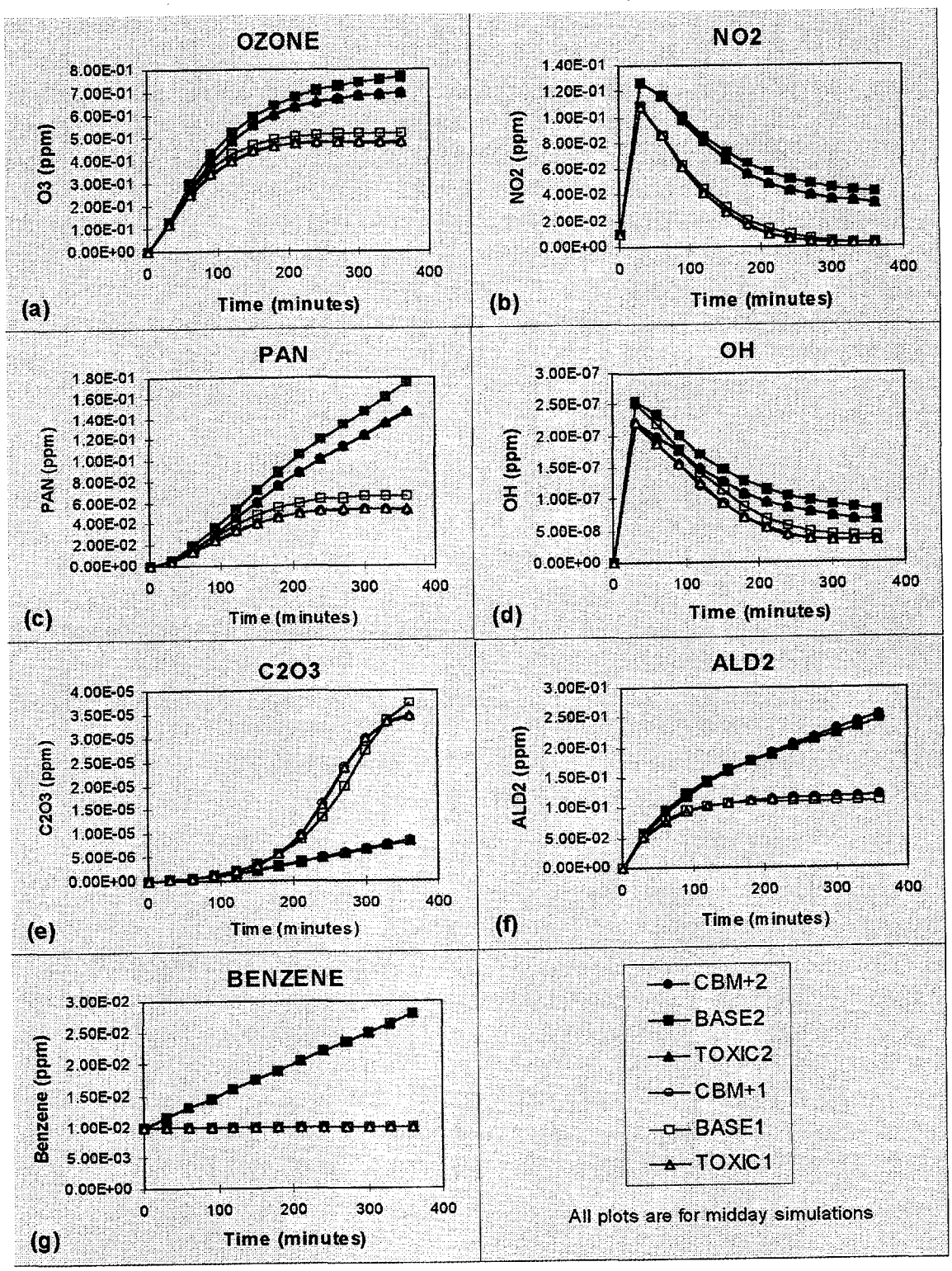

Figure 3.1. BOXCHEM comparison of CBM-IV, Base, and Toxics mechanisms for midday simulation

4.0 Model Setup and Quality Assurance for Los Angeles

The modeling episode for the Los Angeles area chosen for this study is the 26-28 August 1987 episode developed by the SCAQMD. This section discusses the setup and testing performed for the Los Angeles modeling domain, before the alternative fuel scenarios were modeled. Two quality assurance model runs were made: one base case run (designated QA1) to duplicate the regulatory application, and a corresponding run (designated QA2) using toxics chemistry.

4.1 Modeling Scenario and Sources of Model Inputs

The model inputs used for Los Angeles are essentially those developed by SCAQMD for their 1994 SIP attainment modeling. The model inputs were reviewed in the modeling protocol (Appendix B). In the protocol, the meteorological conditions of the episode, the processes used to create the meteorological input files, and the quality of the SCAQMD files are discussed. For Los Angeles, the base case runs represent the 1987 emissions scenario. Table 4-1 summarizes the Los Angeles modeling domain, and how UAM-IV was applied to the domain. Table 4-2 summarizes the sources of the model input files. The meteorology inputs, including winds, surface temperatures, mixing heights, and domain-wide average scalars are all from the SCAQMD modeling files. The only exception was a minor correction in the temperature gradients appearing in the UAM-IV METSCALARS file.

Table 4-1. A Summary of Los Angeles Modeling Domain Characteristics

Model Domain Parameter	Numerical Values Used
Universal Transverse Mercator (UTM) zone and origin	Zone 12 at 275 km E, 3670 km N
Number of cells in easting and northing	65 cells by 36 cells
Size of grid cells in the horizontal	5 x 5 km
Number of model layers	5
Number of layers below diffusion break	2
Number of layers above diffusion break	3
Region top	2,000 m
Minimum layer thickness below diffusion break	25 m
Minimum layer thickness above diffusion break	150 m

Table 4-2. Summary of Input Data Sources for the Los Angeles Episode

Modeling criteria	UAM
Modeling period selected	26-28 August 1987
Modeling domain	Los Angeles SCAQMD modeling domain used for 1994 AQMP
Meteorological fields	SCAQMD files generated using the hybrid Systems Applications International Mesoscale Model (SAIMM)/objective analysis approach
Boundary conditions	Use SCAQMD files developed for the base year (1987) simulation. Toxics are added based on observations
Initial conditions	Use SCAQMD files developed for the base year simulation. Toxics are added based on observations
Point-source emissions	Base-year (1987) emissions are from SCAQMD. Future-year 2007 emissions estimated from linear interpolation of South Coast Association of Governments (SCAG) estimated 2000 and 2010 projection factors and SCAQMD 1990 point source inventory.
Biogenic emissions	Midrange of base-year day-specific emissions using the Biogenic Emission Information System (BEIS) with inputs supplied by SCAQMD
Surface emissions	Base year (1987) emissions are from SCAQMD. For 2007, EMFAC7F mobile emissions. Stationary source emissions estimated as described above for point sources.

Before running the model, the point source preprocessor was applied to create a file of elevated point source emissions. The SCAQMD used a version of UAM-IV with the PAN chemistry corrections, but the code was not an official 6.2X version. Version 6.21 was used throughout this study. One other small difference is that the MAXITER parameter in the CHEM2B subroutine was set to 50 to prevent the model run from crashing on 26 August, as per tip #9 from the UAM USERTIPS.TXT file available from EPA OAQPS on the SCRAM electronic bulletin board.

4.2 Modification of Initial Input Data Sets for Toxic Compounds

For the toxics chemistry simulation, explicit breakout of the ALD2 surrogate into ACET and HALD (described in Section 3) requires modifications to emissions and initial and boundary concentration files. A processor was developed that performed the respeciation using mass conservation of carbon. The following modifications were made to the AIRQUALITY, BOUNDARY, and TOPCONC files used by UAM-IV:

- Ambient ACET concentrations were set equal to 0.65 of the original ALD2 concentrations.
- HALD concentrations were set equal to 0.23 of ALD2 concentrations.
- BENZ concentrations were set equal to 0.50 of TOL concentrations.

- BUDI concentrations were set equal to 0.30 of OLE concentrations.

For the toxics comparison simulation, BENZ emissions were set to one quarter of TOL emissions and BUDI emissions were set equal to 0.20 of OLE emissions closer to the toxic emission totals given in Harley and Cass (1994) and .

To determine whether initial concentrations of toxics were appropriate, the initial mass of each compound was compared with the predicted mass at the end of the second day. Results of this mass balance analysis are given in Table 4-3. The results show that the initial mass for each species is not drastically different from the final mass loadings, suggesting that the initial conditions are reasonable. The top and side boundary conditions were evaluated by reviewing the cumulative fluxes of material over the modeling period. The FORM fluxes that were specified by SCAQMD were not modified. However, the mass loading suggests that boundary fluxes are competing with the internal processes such as the chemistry. The loss of ACET through advection suggests that boundary concentrations are generally low enough that emitted and chemically produced ACET is being exported from the domain. BENZ reacts slowly and so inappropriate boundary concentrations would show up in the flux budget. However, we can see that the emissions outstrip the net export of BENZ by more than a factor of two. BUDI is destroyed rather rapidly. The boundary fluxes suggest that BUDI boundary concentrations may be too high. Most of the BUDI mass is localized near the inflow boundaries.

Table 4-3. A Summary of Major Sources and Sinks of the Toxic Chemicals in the Los Angeles Modeling Domain for the Base Year (1987) (units are tons [CH_4 equivalent mass])

Specie	Emission	Advection	Chemistry	Initial mass	Final mass
FORM	34	474	-580	425	344
ACET	75	-130	91	227	268
BENZ	114	-41	-5	278	346
BUDI	34	101	-137	6	4

4.3 Evaluation of Base Case Simulation without Air Toxics

The initial simulation was performed using the UAM-IV inputs as they were received from SCAQMD. (One exception is the use of corrected temperature gradients for QA1, as described in Section 3 and in the protocol.) This simulation, denoted QA1, was for the base year (1987). The SCAQMD did not supply a model output hourly averaged concentration file for direct verification. Therefore, verification was accomplished using information from SCAQMD's final report (SCAQMD 1994). The daily maximum 1-hour average O_3 concentration patterns from both runs for 27 August are compared in Figure 4-1.[1] The maximum 1-hour O_3 concentration predicted by SCAQMD was 160.9 ppb, while the maximum predicted in QA1 is 160.3 ppb. Differences of up to 1 ppb are commonly encountered in photochemical modeling when the identical simulation is run on different computer platforms. The predicted spatial patterns match closely, particularly for areas above 120 ppb.

[1] Figures in this section have been placed together following the text.

The daily maximum 1-hour average surface O_3 concentration pattern for 28 August is shown in Figure 4-2, which again shows that the highest concentrations occur in the same locations for both runs. The maximum, which occurs in Riverside County, is 190.5 ppb for the SCAQMD simulation and is 188.9 ppb for the QA1 simulation, a difference of 1.6 ppb. This difference is slightly larger than the 1 ppb target identified in the protocol. This small difference is not surprising, however, particularly since the temperature gradient corrections represent a change in inputs between the two runs.

Figure 4-3 illustrates the time series of hourly ozone predictions at two monitoring sites, Azusa and Norco, along with the observed ozone concentrations. For QA1, the predictions represent grid cell average concentrations. We do not know what procedure was used to determine the SCAQMD predictions at monitoring sites. Close agreement is seen between the QA1 and SCAQMD time series. Substantial model under-prediction is evident at both sites, and is most extreme for 28 August at Azusa.

4.4 Comparison of Base Year with and without Toxic Compound Chemistry

The toxics QA simulation is denoted as QA2. Model inputs are the same as QA1, except that the inputs for the aldehydes and IOLE have been converted in the initial, boundary, and emissions files as described above in Section 4.2. Results for QA1 and QA2 were compared, first in terms of predicted concentrations, and then based on mass budgets. Some differences in the O_3 and aldehyde concentrations are expected, as described in Section 2. The disaggregated toxics chemistry tends to produce less O_3 than the original CB-IV chemistry as noted earlier in Section 3.

The maximum daily 1-hour surface O_3 concentration patterns for QA1 and QA2 are presented in Figures 4-4 and 4-5. The maximum concentrations for the toxics simulation are lower than for QA1. Differences between QA1 and QA2 are slightly greater on 28 August. The only place where there are higher predicted O_3 concentrations for QA2 is over the ocean. The spatial pattern of daily maxima and the locations of predicted peaks are nearly identical for QA1 and QA2.

The differences in the maximum daily O_3 concentrations from the QA1 and QA2 simulations are shown in Figures 4-6 and 4-7 for 27 and 28 August, respectively. On 27 August, the difference plot indicates that reductions in O_3 in the 10 to 20 ppb range occurred over a broad area. The maximum difference is 19 ppb, slightly more than 10% of the peak predicted concentration. Differences in individual grid cells can be larger than the difference between domain-maximum concentrations. For 27 August, the predicted QA2 domain maximum, 148.7 ppb, is only 11.6 ppb lower the maximum of 160.3 ppb for QA1, as seen in Figure 4-4. On 28 August, the concentration differences increase, with a maximum difference of 42.3 ppb. This difference is much larger than the 13.1 ppb difference between domain maximum values. In a region with steep gradients in predicted concentrations, a shift of one or two grid cells in the peak location between QA1 and QA2 can produce these large differences. The time series plots in Figures 4-3 show the time series of O_3 at Azusa and Norco for both the QA1 and the QA2 simulations. The largest differences appear to occur at the time when the maximum O_3 is predicted.

The daily maximum fields of oxides of nitrogen (NO_x) and VOC for QA1 and QA2 were also plotted and compared. The daily maximum 1-hour average surface VOC concentrations for 28 August are shown in Figure 4-8. The concentration field shows very little difference in the maximum predicted VOC concentrations. The peak concentrations differ by only 1 ppb. Figure 4-9 displays the daily maximum 1-hour average NO_x concentrations. Visually, there is no difference between the QA1 and the QA2 fields. The maximum difference is less than 2 ppb. The daily maximum FORM concentration field was plotted for both QA1 and QA2. The results are shown in Figure 4-10. The QA1 simulation predicts higher peak FORM concentrations (18.2 vs. 15.8 ppb).

4.5 Mass Budget Analysis

A mass budget analysis was conducted to provide further comparison of the QA1 and QA2 simulations. The cumulative production and destruction of selected species for 27-28 August are presented in Table 4-4. This table indicates that the chemistry of ACET has been significantly altered by the disaggregation of the CBM-IV chemical scheme. There is a net destruction of ALD2 in the original scheme (using the FORM photolysis rates) but there is a net production of ACET in the toxics chemistry case. The difference is partly due to the altered ACET destruction by photolysis. Mass destruction of such species as OLE and ETH is relatively unchanged.

Table 4-4. A Summary of the Chemical Production of O_3 and Other Chemicals over the Period 27-28 August in the Los Angeles Modeling Domain (units are tons)

Chemical Specie	Base Run (QA1)	Toxics Chemistry Run (QA2)
O3	17074	14672
OLE	-478	-478
TOL	-667	-663
XYL	-603	-602
FORM	-546	-580
ALD2/ACET	-68 (ALD2)	91 (ACET)
ETH	-501	-498
HPAN	NA	24
PAN	520	492
HNO3	4372	4338

Table 4-4 indicates that the chemistry of CBM-IV organic species that are not affected by the change in the chemical mechanism seems to be relatively unchanged as well. However, minor perturbations (5% or less over two days) do seem to be present in the NO_x chemistry for the CBM-IV toxics scheme. The concentration of HPAN varies over several orders of magnitude between midnight and noon with HPAN being formed by radical reactions during the day and decomposition resulting in a rapid HPAN destruction at night. Net production of HPAN for a midnight to midnight simulation is realtively small as shown in Table 4-4, unlike the BOXCHEM which covers an afternoon period. The impact of adding HPAN on night-time No_x is small since NO_2 lost during the day is returned at night as a result of decompostion. The reduction in ozone production ($\sim 14\%$) is due to day-time sequestering of NO_x by HPAN and by a slowing of aldehyde chemistry production of XO_2 radical which mediates the NO to NO_2 conversion.

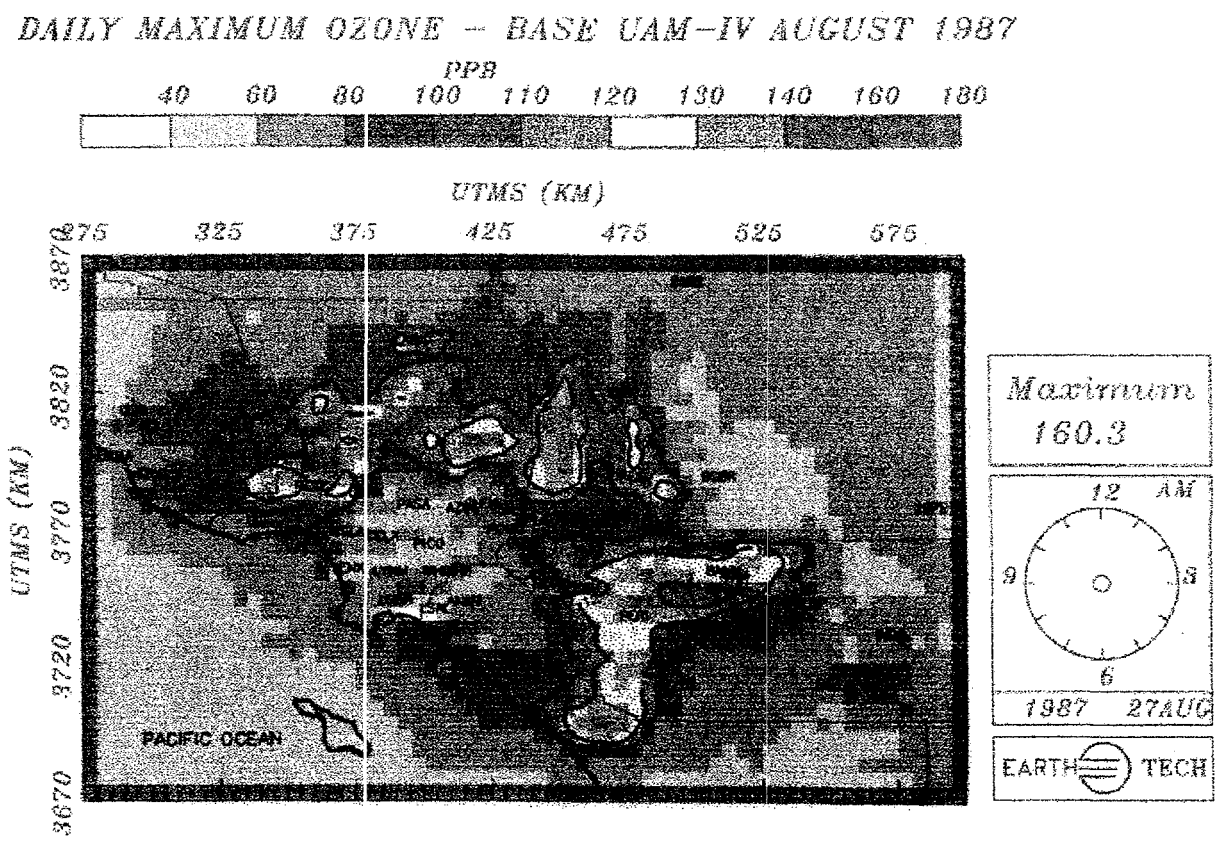

Figure 4-1. **Comparison of daily maximum 1-hour surface O_3 concentrations for 27 August for SCAQMD simulation (isopleths in pphm) and QA1 simulation (tiles in ppb).**

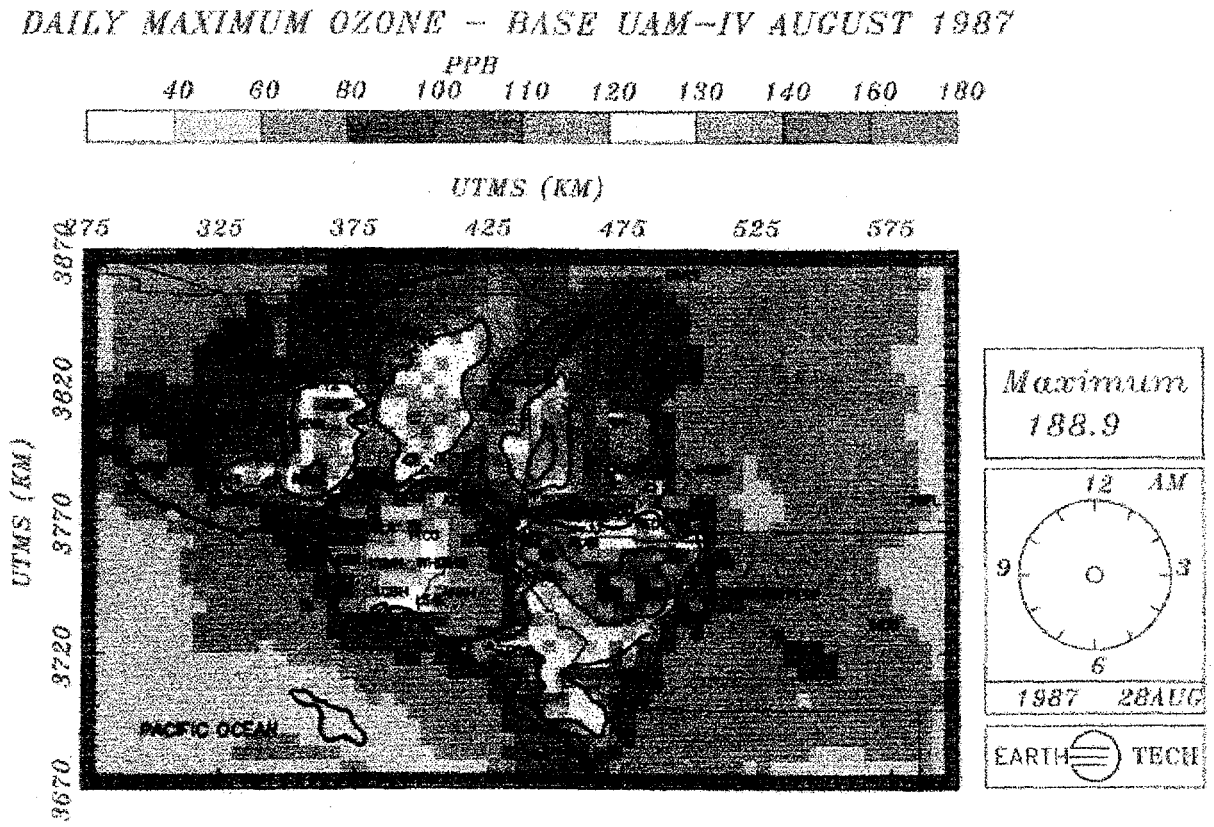

Figure 4-2. Comparison of daily maximum 1-hour surface O_3 concentrations for 28 August for SCAQMD simulation (isopleths in pphm) and QA1 simulation (tiles in ppb).

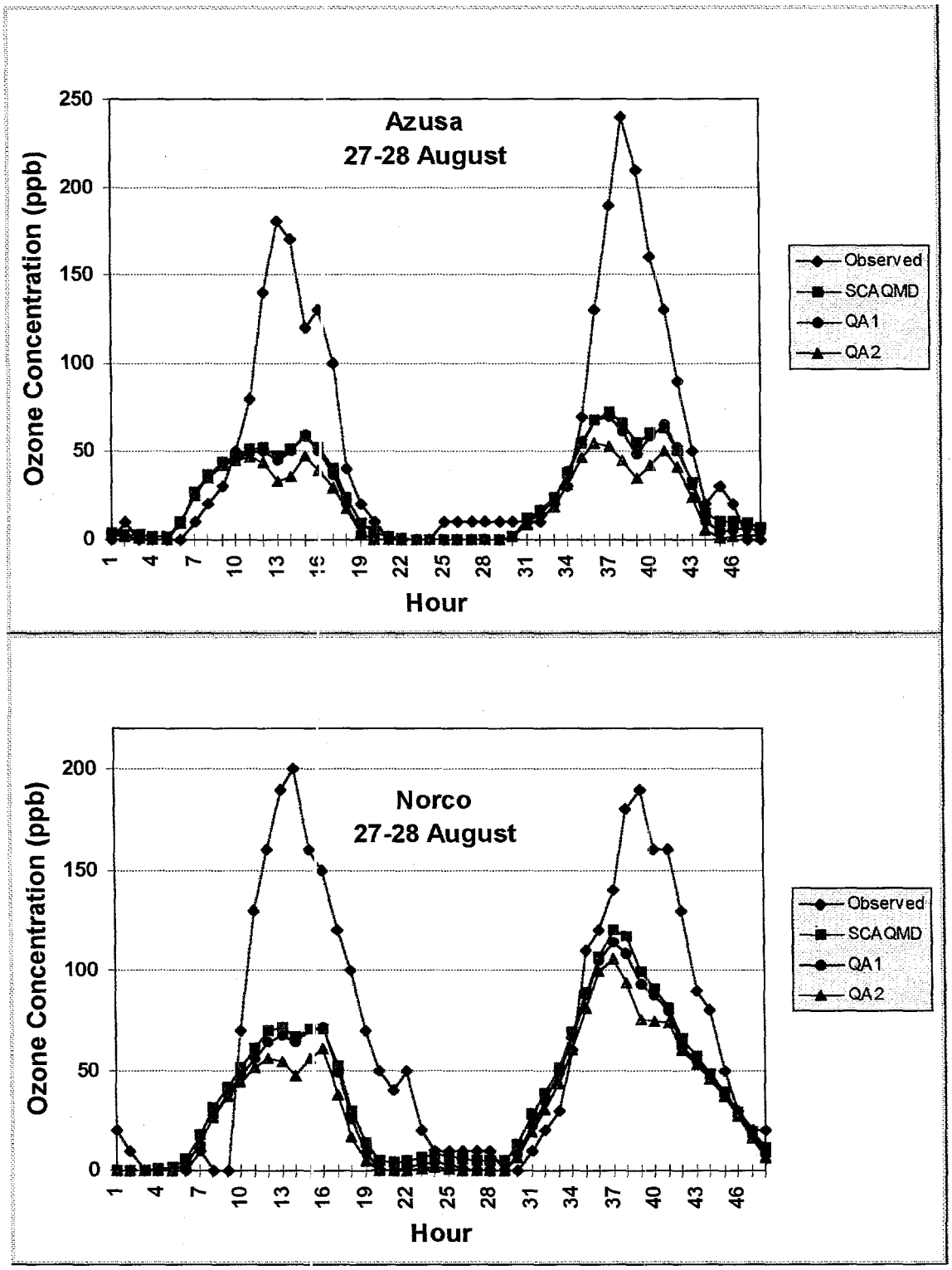

Figure 4-3. Hourly observed and predicted 1-hour surface ozone concentrations at Azusa (top) and Norco (bottom) for 27-28 August 1987 AQMP episode.

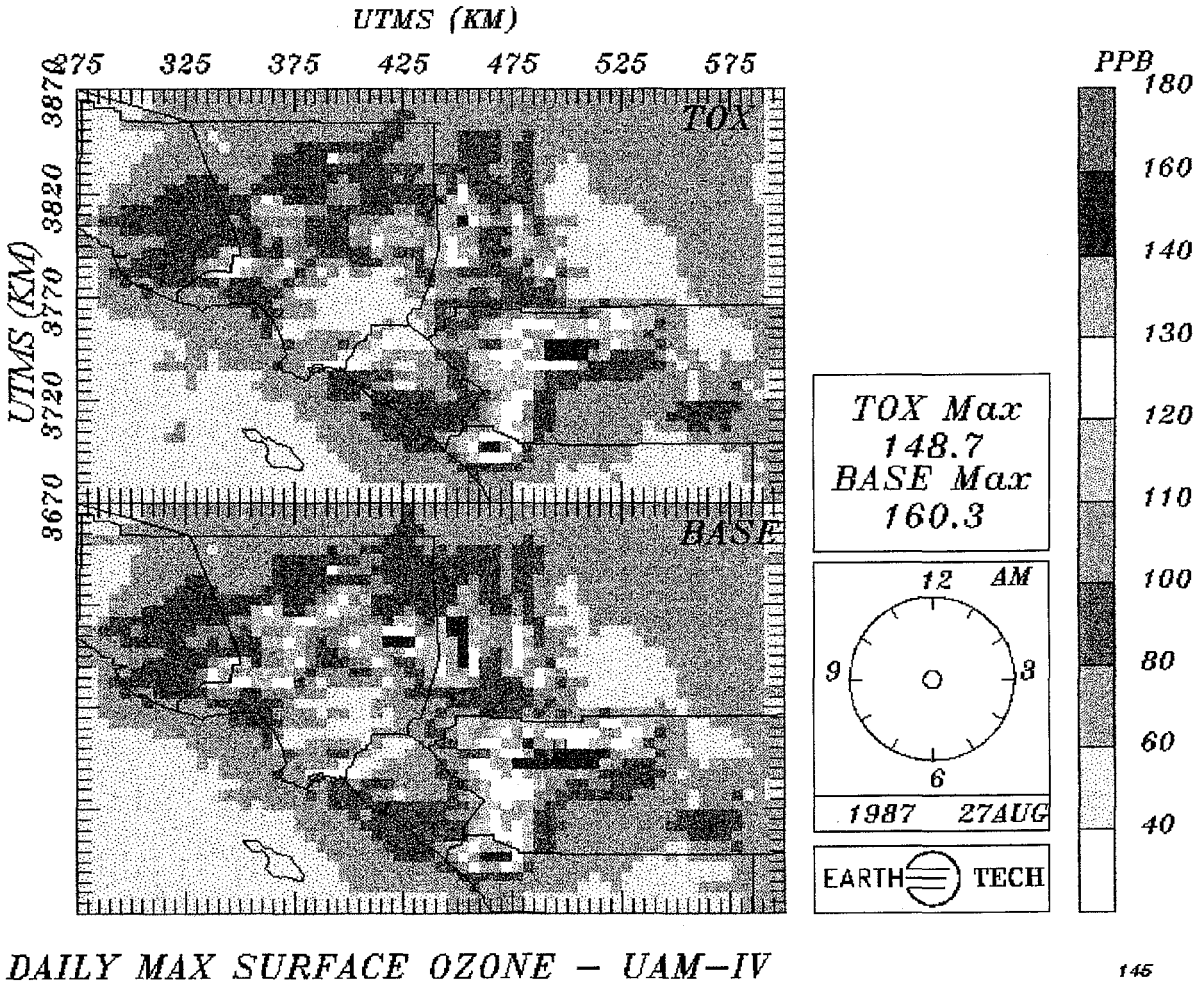

Figure 4-4. **Daily maximum 1-hour surface O_3 concentrations for Los Angeles for 27 August for QA1 (Base) and QA2 (Air Toxics) QA simulations.**

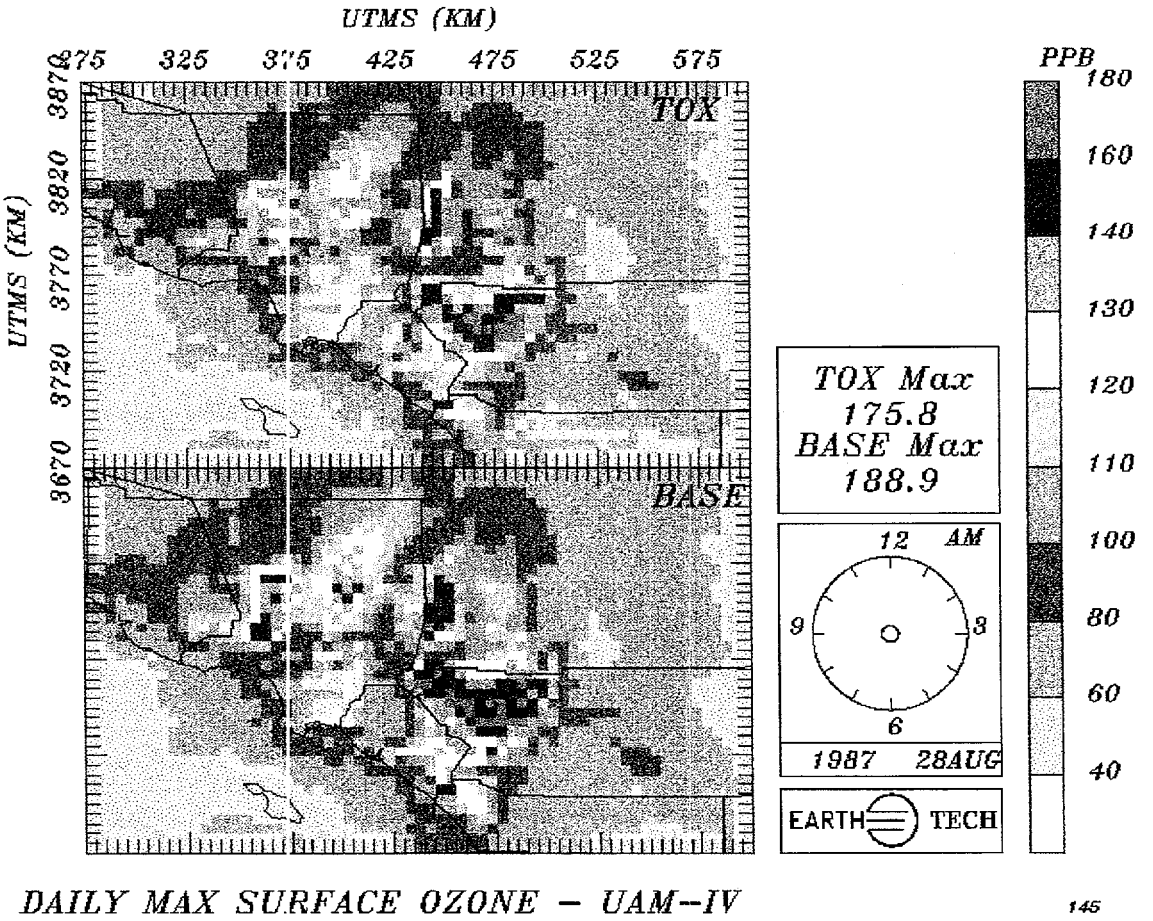

Figure 4-5. **Daily maximum 1-hour surface O_3 concentrations for Los Angeles for 28 August for QA1 (Base) and QA2 (Air Toxics) QA simulations.**

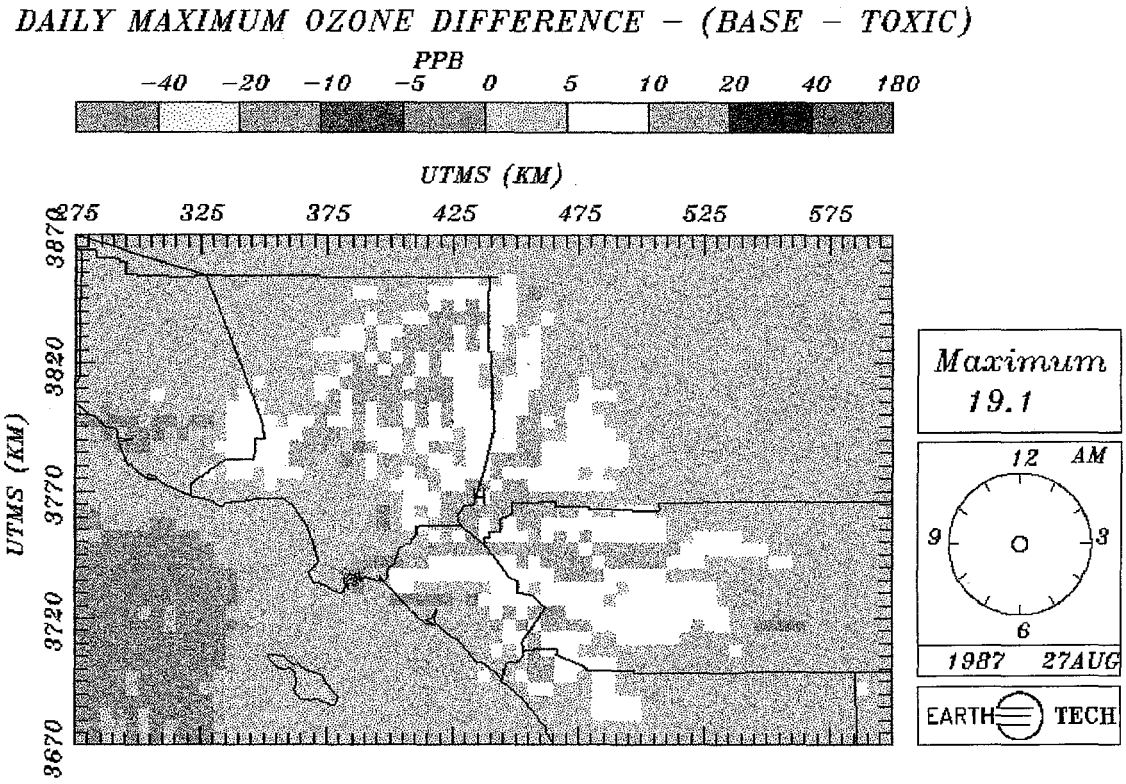

Figure 4-6. **Difference in daily maximum 1-hour surface O_3 concentrations for Los Angeles for 27 August for QA1 (Base) minus QA2 (Air Toxics) QA simulations.**

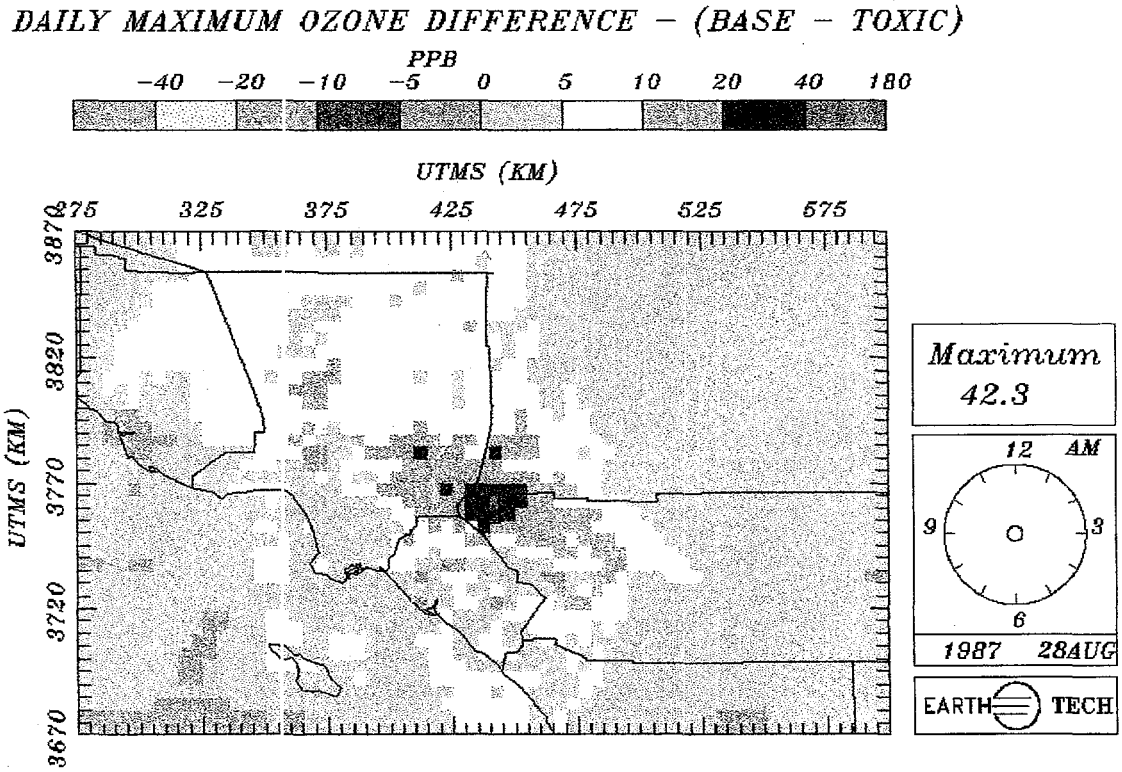

Figure 4-7. Difference in daily maximum 1-hour surface O_3 concentrations for Los Angeles for 28 August for QA1 (Base) minus QA2 (Air Toxics) QA simulations.

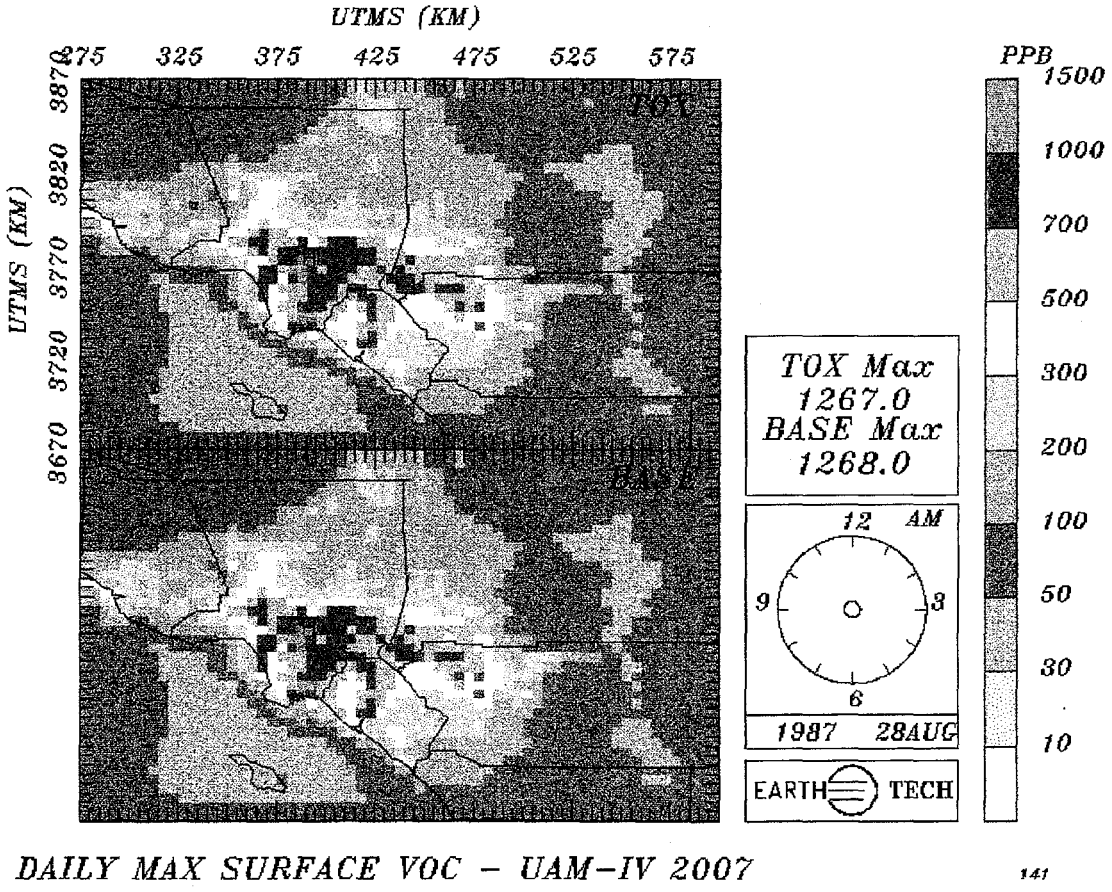

Figure 4-8. Daily maximum 1-hour surface VOC concentrations for Los Angeles for 28 August for QA1 (Base) and QA2 (Air Toxics) QA simulations.

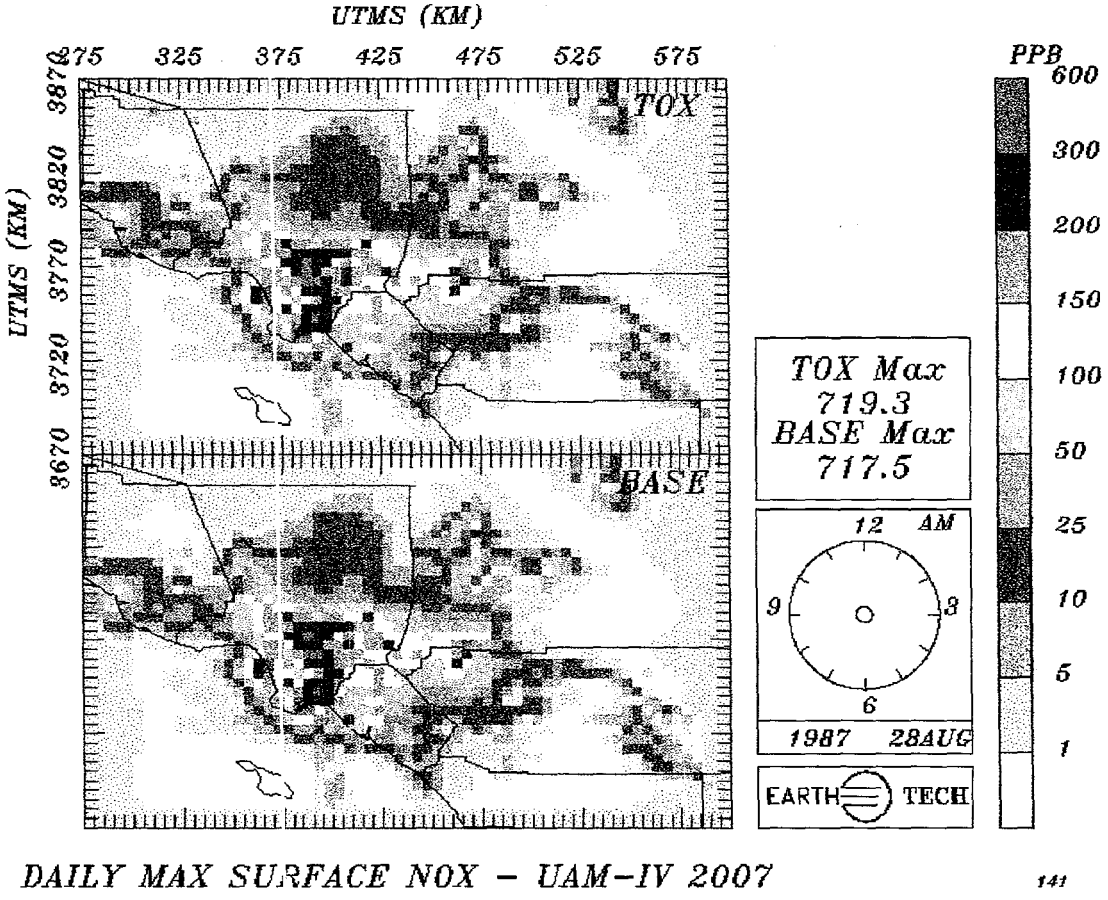

Figure 4-9. **Daily maximum 1-hour surface NO_x concentrations for Los Angeles for 28 August for QA1 (Base) and QA2 (Air Toxics) QA simulations.**

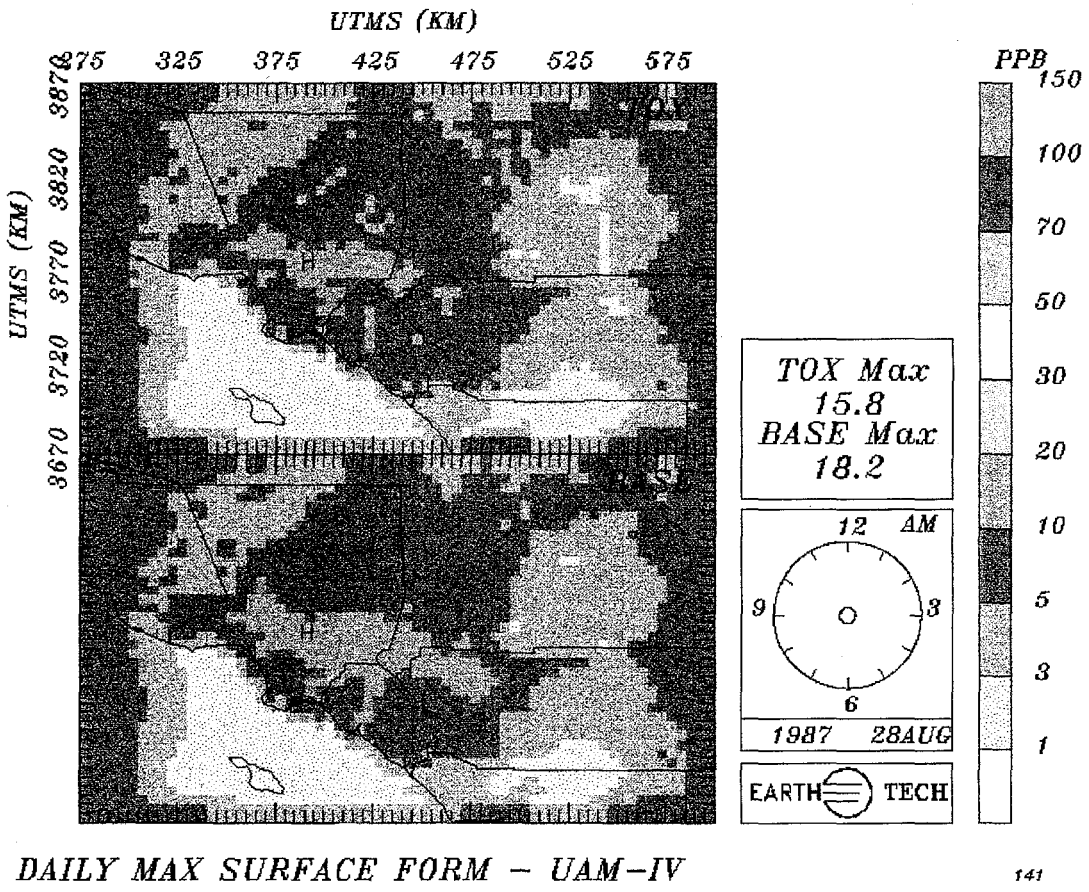

Figure 4-10. Daily maximum 1-hour surface FORM concentrations for Los Angeles for 28 August for QA1 (Base) and QA2 (Air Toxics) QA simulations.

5.0 Model Setup and Quality Assurance for Atlanta

The modeling episode for the Atlanta area chosen for this study was the 29-31 July 1987 episode developed by the Georgia DNR for their 1994 SIP revision. This section discusses the setup and testing performed for the Atlanta modeling domain. Two QA model runs were made: one base run to duplicate the regulatory application, and a corresponding run with toxics chemistry. For the Atlanta episode, the base run represents a 1999 emissions scenario provided by Georgia DNR.

5.1 Modeling Scenario and Sources of Model Inputs

The model inputs used for Atlanta are essentially those developed by the DNR for their 1994 SIP modeling. The model inputs were reviewed in the modeling protocol (Appendix B). In the protocol, the meteorological conditions of the episode, the processes used to create the meteorological input files, and the quality of the DNR files are discussed. Table 5-1 summarizes the modeling domain and how UAM-IV was applied to the domain. Table 5-2 summarizes the sources of the model input files.

Modeling was conducted using the DNR meteorology. The winds, surface temperatures, mixing heights, and the meteorological domain-wide average scalars were used as received from the DNR. In changing from the UAM-IV with standard CBM-IV chemistry to the toxics version described in Section 3, it was necessary to change the chemical speciation in the emissions files, the initial condition files, and the boundary condition files.

Table 5-1. A Summary of Atlanta Modeling Domain Characteristics

Model Domain Parameter	Numerical Values Used
UTM zone and origin	Zone 16 at 660 km E, 3665 km N
Number of cells in easting and northing	40 cells by 40 cells
Size of grid cells in the horizontal	4 x 4 km
Number of model layers	5
Number of layers below diffusion break	2
Number of layers above diffusion break	3
Region top	2,200 m
Minimum layer thickness below diffusion break	25 m
Minimum layer thickness above diffusion break	150 m

Table 5-2. Summary of Input Data Sources for the Atlanta Episode

Modeling criteria	UAM
Modeling period selected	29-31 July 1987.
Modeling domain	Atlanta domain used for 1994 SIP modeling by Georgia DNR.
Meteorological fields	Model inputs supplied by DNR - meteorological parameters developed by Systems Applications International (SAI) from the SAI Mesoscale Model (SAIMM).
Boundary conditions	Are set to 1999 DNR values. Toxics are treated in the same manner as for Los Angeles
Initial conditions	Initial conditions on 29 July developed by DNR for 1999. Modifications for toxics as for Los Angeles.
Point source emissions	For base run, used 1999 emissions obtained from DNR. For 2007 scenarios, point source emissions projected from state 1990 inventory to 2007 using BEA growth factors and NO_x reasonably achievable control technology (RACT) and VOC reasonable further progress (RFP) requirements.
Biogenic emissions	Same day-specific BEIS biogenic emissions as used by DNR.
Surface emissions	For base run, used 1999 emissions from DNR. Projection of Vehicle miles traveled (VMT) to 2007 using extrapolation of DNR 1999 growth factors. MOBILE5a mobile emission factors with modified, unspecified maintenance requirements and low RVP gasoline. Area source growth factors based on census and economic data to scale from 1990 inventory to 2007.

Prior to exercising the model, the point source preprocessor was exercised to create a file of elevated point source emissions. For simulations with no toxics (QA1), the UAM-IV version 6.21 was used.

5.2 Modification of Initial Input Data Sets for Toxic Compounds

The explicit breakout of ALD2 into acetaldehyde (ACET) and HALD requires modifications to emissions and initial and boundary concentration files. A processor was developed that performed the respeciation using mass conservation of carbon. The following modifications were made to the AIRQUALITY, BOUNDARY, and TOPCONC files used by UAM-IV:

- ACET concentrations were set equal to 0.65 of the original ALD2 concentrations.
- HALD concentrations were set equal to 0.23 of ALD2 concentrations.
- BENZ concentrations were set equal to 0.50 of the prevailing TOL concentrations.
- BUDI concentrations were set equal to 0.30 of OLE concentrations.

For the toxics comparison simulation, BENZ emissions were set to 0.30 of TOL emissions and BUDI emissions were set equal to 0.50 of the FORM emissions close to the toxic emission budget given in Harley and Cass (1994).

To determine whether initial concentrations of toxics were appropriate, the initial mass of each compound was compared with the predicted mass at the end of the second day. The results in Table 5-3 show that, with the exception of BENZ, the initial mass of each species is not very different from the final mass loading, suggesting that the initial conditions are reasonable. The top and side boundary conditions were examined via the cumulative fluxes of material over the modeling period. The FORM fluxes that were specified by the DNR were not modified. However, the mass loading suggests that boundary fluxes are competing with the internal processes such as the chemistry. The emissions of ACET approximately balance losses by chemistry and advective export with no evidence of inflow boundary fluxes seriously perturbing the model chemistry. BENZ reacts slowly and so inappropriate boundary concentrations would show up in the flux budget. We can see that the emissions outstrip the net export of BENZ by over a factor of seven, giving rise to a systematic trend toward increased BENZ mass loading during the days simulated. Because BUDI is destroyed rather rapidly, the boundary inflow flux suggests that the BUDI boundary concentrations may be too high with respect to emissions because the emitted mass is less than a third of the mass lost due to chemical destruction. The mass imbalance is localized near the inflow boundaries because of the rapid destruction, however, so no adjustment was made.

Table 5-3. A Summary of Major Sources and Sinks of the Toxic Chemicals in the Atlanta Modeling Domain for the Base Run for 30-31 July 1987 (units are tons [CH_4 equivalent mass])

Specie	Emission	Advection	Chemistry	Initial Mass	Final Mass
FORM	9	-43	30	105	103
ACET	129	-85	-42	81	83
BENZ	53	7	-1	30	90
BUDI	5	11	-16	5	5

5.3 Evaluation of Base Run without Air Toxics

The initial simulation (QA1) was performed using the UAM-IV inputs as they were received from the DNR. The DNR supplied a model output hourly averaged concentration file for 1999 for direct verification. The daily maximum 1-hour average O_3 concentration patterns for July 30 are shown in Figure 5-1 for the QA1 and DNR simulations.[1] The maximum O_3 concentration predicted by the DNR is 160.3 ppb while the maximum predicted for QA1 is 160.4 ppb. Visually, there is no difference between the two concentration patterns. The daily maximum 1-hour average O_3 concentration pattern for the second day (31 July) is shown in Figure 5-2, which again shows no apparent difference between the two sets of daily maximum concentrations.

[1]Figures in this section have been placed together following the text.

5.4 Comparison of Base Run with and without Toxic Compound Chemistry

The toxics QA simulation is denoted QA2. Model inputs for QA2 are the same as for QA1, except for the modifications necessary to treat the toxic species, as discussed in Section 5.2. Results for QA1 and QA2 were compared, first in terms of predicted concentrations, and then based on mass budgets. Some differences in the O_3 and aldehyde concentrations are expected, as described in Section 2.0. The disaggregated toxics chemistry produces less O_3.

The daily maximum 1-hour average surface O_3 concentration patterns for QA1 and QA2 are presented in Figures 5-3 and 5-4 for 30 and 31 July, respectively. Generally, the maximum concentrations for QA2 are lower than for QA1, with the differences increasing from the first day to the second. On 30 July, predicted maximum concentrations west of Atlanta are noticeably lower for QA2. On 31 July, predicted O_3 concentrations southeast of Atlanta are lower for QA2. The locations of the peaks in the concentration fields are basically the same for QA1 and QA2.

The time series plots in Figure 5-5 show predicted surface O_3 concentrations at Dawsonville and MLK MARTA Station for both QA1 and QA2. The largest differences, while slight, occur at midday when the maximum O_3 is predicted. The differences in the maximum daily O_3 concentration pattern are shown in Figures 5-6 and 5-7 for 30-31 July, respectively. On 30 July, the difference plot indicates that predicted O_3 for QA2 is 5 to 10 ppb lower over a broad area northwest of Atlanta. The maximum grid cell difference is 10 ppb, although the domain maximum concentrations agree within 1 ppb. On 31 July (Figure 5-7), the concentration differences increase, with a maximum difference of 22 ppb. This maximum difference in the O_3 pattern occurs in the vicinity of Cedar Grove. The domain maximum O_3 prediction for QA2 is 167 ppb, compared to 176 ppb for QA1.

The daily maximum fields of NO_x and VOC for QA1 and QA2 were also compared. The daily maximum 1-hour average surface VOC concentrations for 31 July are shown in Figure 5-8. The concentration fields show very little difference between QA1 and QA2 simulations. The peak concentration differed by less than one ppb. Figure 5-9 displays the daily maximum 1-hour average surface NO_x concentrations for 31 July. Visually, there is no difference between the QA1 and QA2 fields. The maxima differ by less than 0.1 ppb. The daily maximum 1-hour surface FORM concentration fields are shown for QA1 and QA2 for 31 July in Figure 5-10. The QA1 simulation shows slightly higher peak FORM concentrations (23.7 vs. 22.8 ppb) when compared to the toxics chemistry simulation.

5.5 Mass Budget Analysis

A mass budget analysis was also conducted to compare chemical production for the QA1 and QA2 simulations. First, the cumulative chemistry over the two episode days was examined. The net production and destruction of selected species are presented in Table 5-4. This table indicates that the chemistry of ALD2 has been significantly altered by the disaggregation of the CBM-IV chemical scheme. The amount of ALD2 destroyed in the original scheme is larger than the combined destruction of ACET and HALD2 in the toxics scheme. This result is probably due to the slower photolysis of ACET.

Table 5-4 indicates that the chemistry of CBM-IV organic species that are not affected by the change in the chemical mechanism seems to be relatively unchanged as well. The fact that less O_3 (10% less) is being produced seems to be due mainly to the reduced rate of production of species which mediate the NO to NO_2 conversion (e.g. XO_2 radical species). The aldehyde destruction chemistry is a significant producer of XO_2.

Table 5-4. A Summary of the Chemical Production of O_3 and Other Chemicals over the Period 30-31 July 1987 in the Atlanta Modeling Domain (units are tons)

Chemical Specie	Base Run (QA1)	Toxics Chemistry Run (QA2)
O3	5173	4622
OLE	-196	-197
TOL	-185	-190
XYL	-175	-177
FORM	39	30
ALD2/ACET	-74 (ALD2)	-42 (ACET)
ETH	-20	-27
PAN	512	458
HNO3	2056	2068
HPAN	-	17

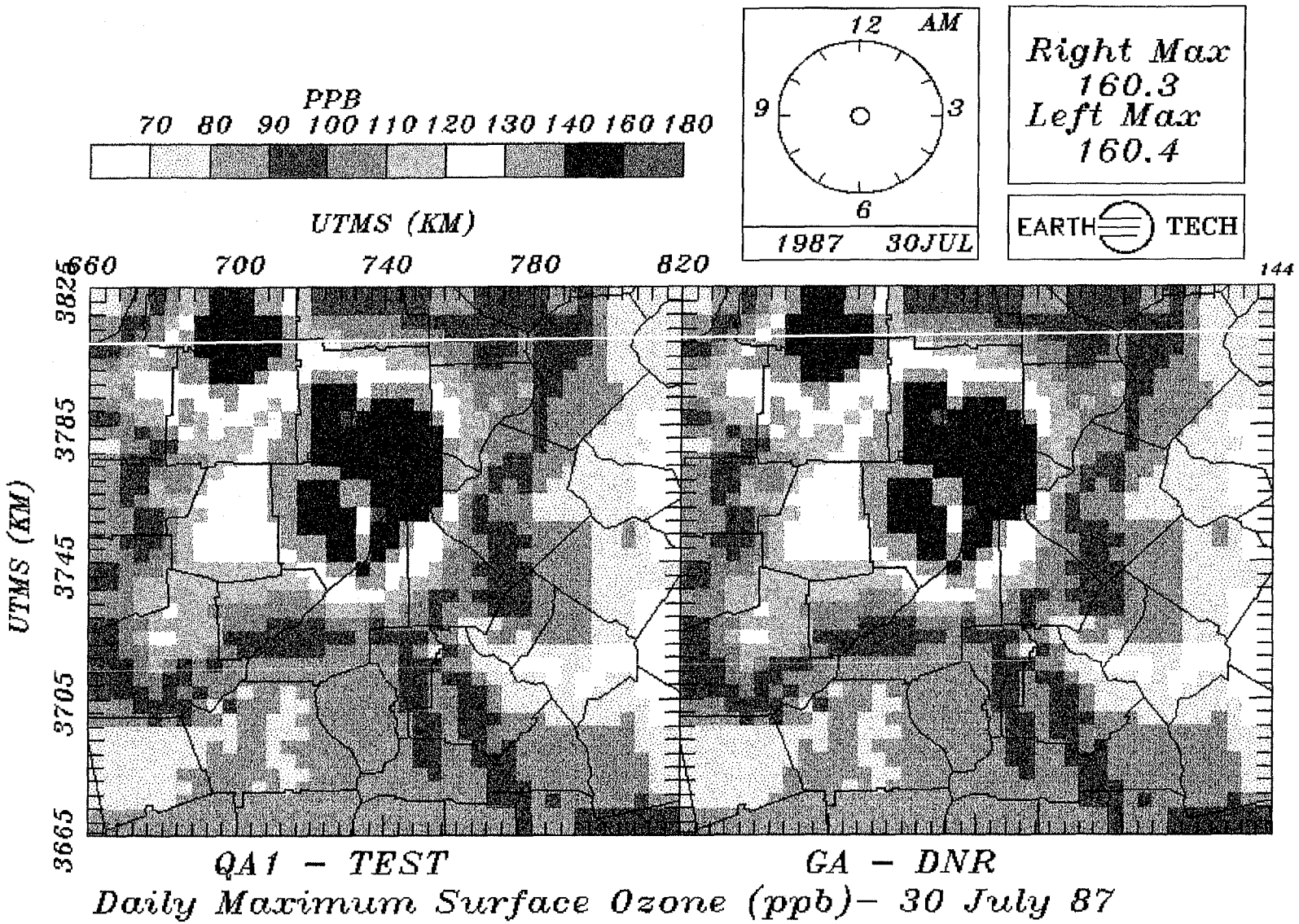

Figure 5-1. Comparison of daily maximum 1-hour O_3 concentrations for 30 July for DNR simulation and QA1 simulation. (1999 emissions)

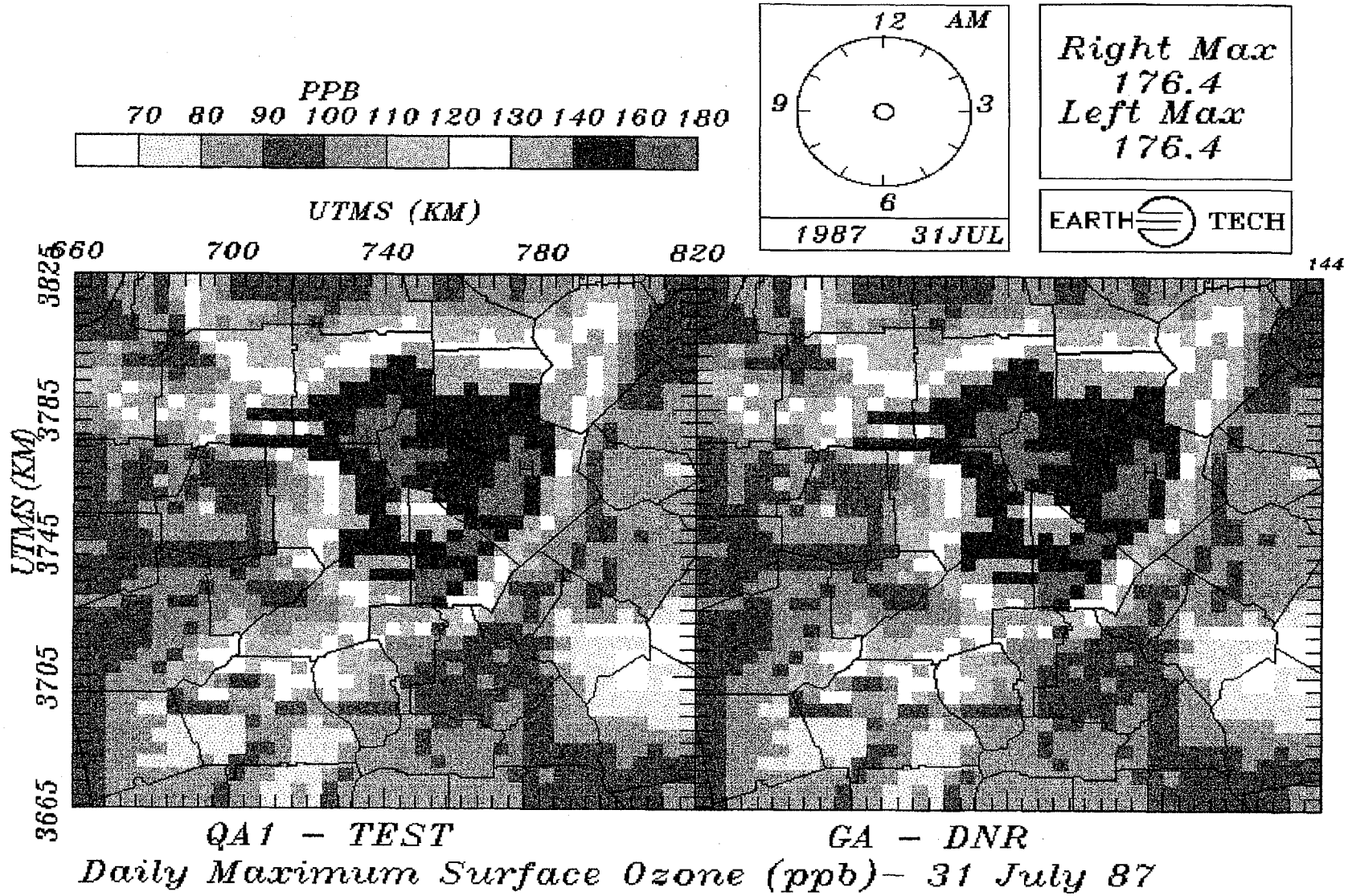

Figure 5-2. Comparison of daily maximum 1-hour O_3 concentrations for 31 July for DNR simulation and QA1 simulation. (1999 emissions)

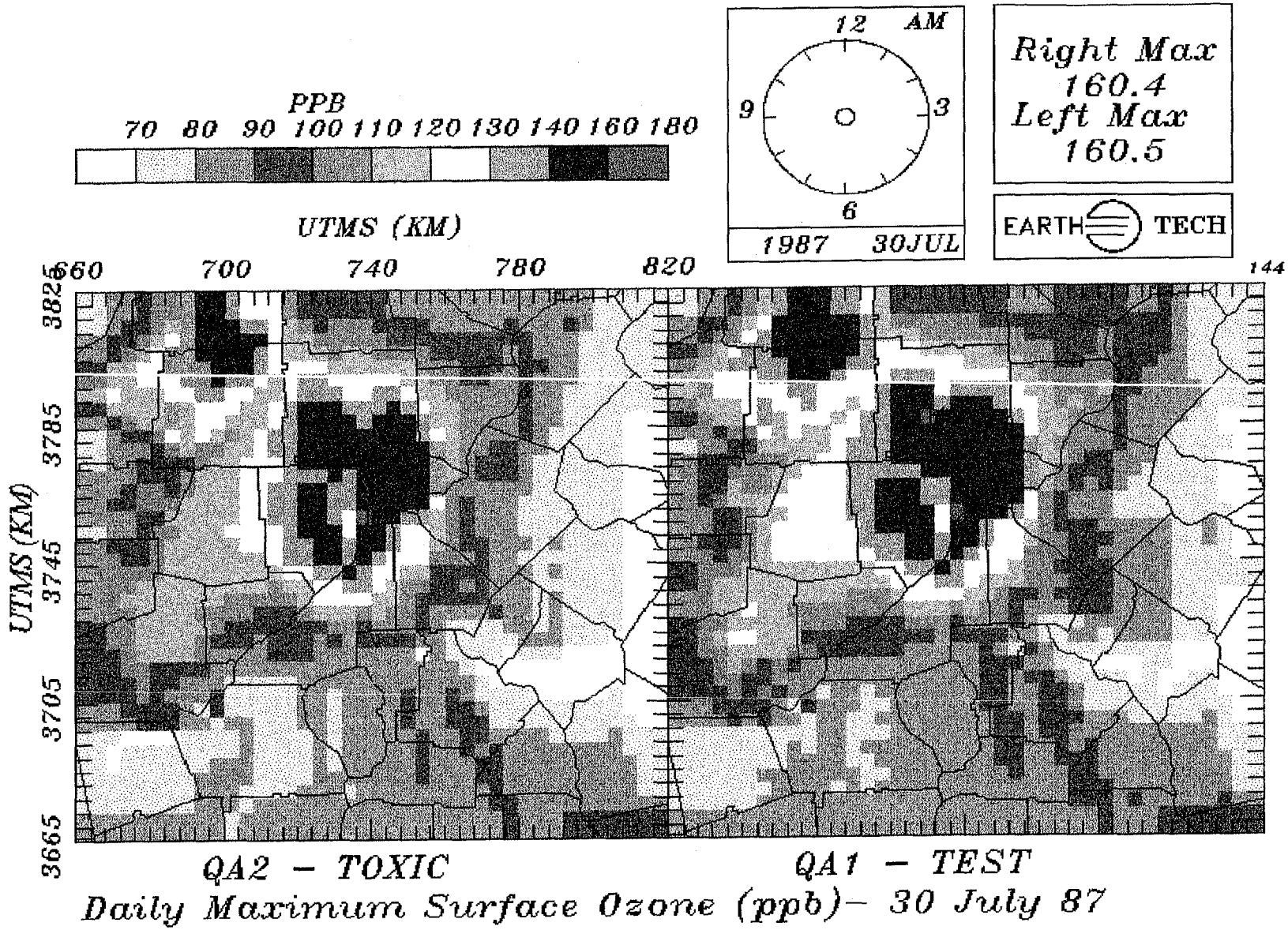

Figure 5-3. Comparison of daily maximum 1-hour surface O_3 concentrations for 30 July for Atlanta for QA1 (Base) and QA2 (Air Toxics) QA simulations. (1999 emissions)

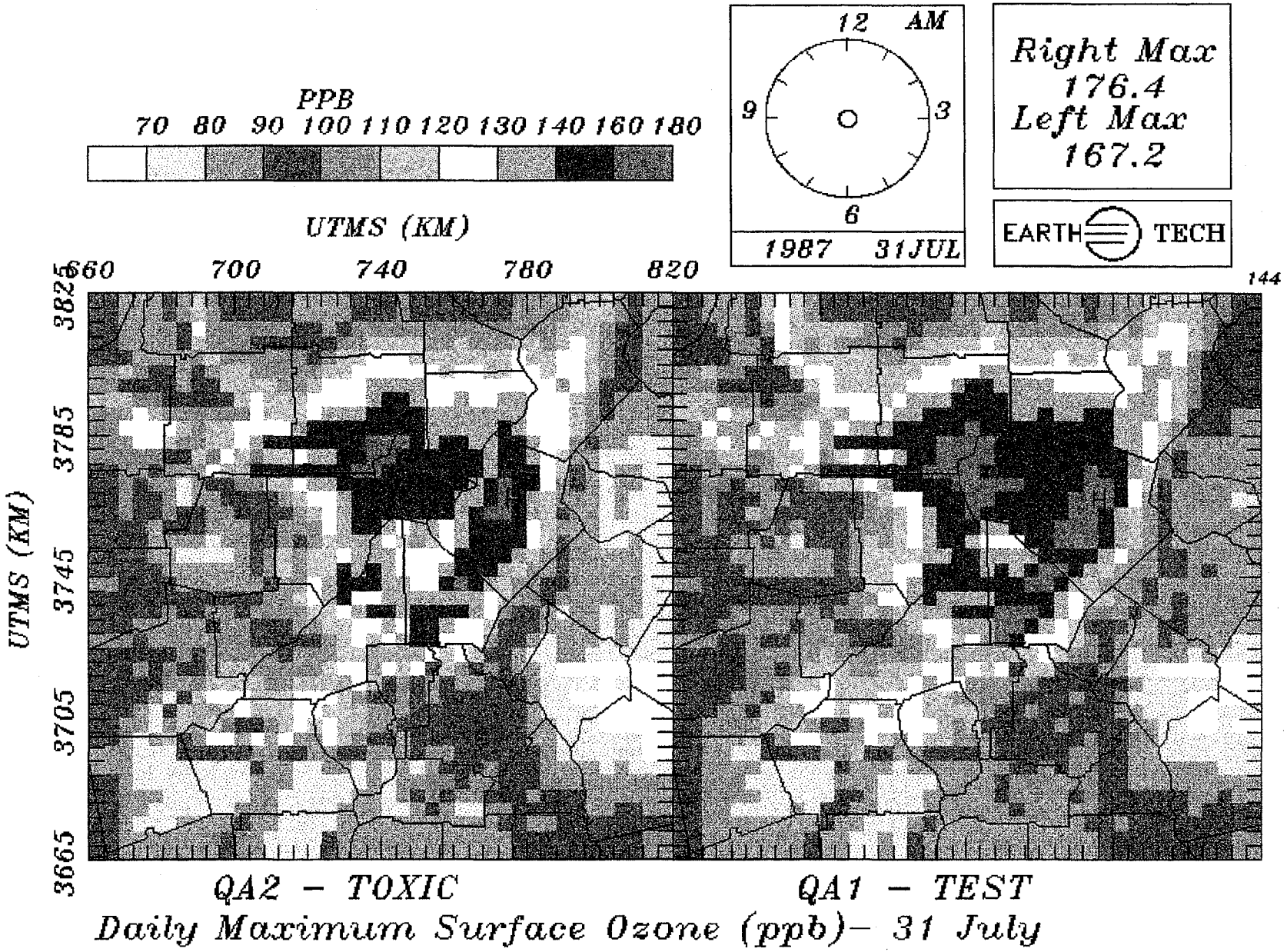

Figure 5-4. Comparison of daily maximum 1-hour surface O_3 concentrations for 31 July for Atlanta for QA1 (Base) and QA2 (Air Toxics) simulations. (1999 emissions)

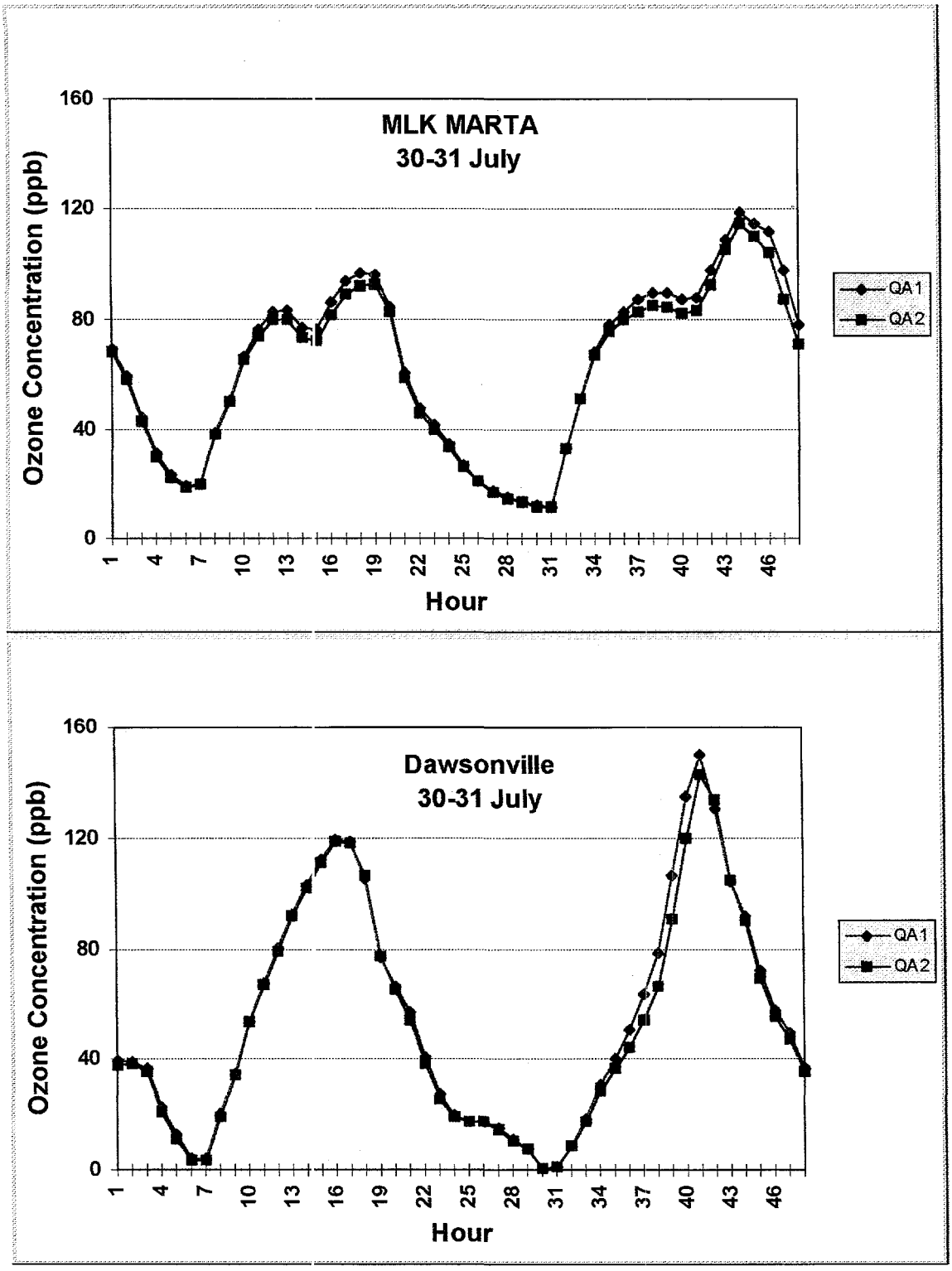

Figure 5-5. Hourly predicted 1-hour surface ozone concentrations at MLK MARTA (top) and Dawsonville (bottom) for 30-31 July 1987 for QA1 (Base) and QA2 (Air Toxics) simulations.

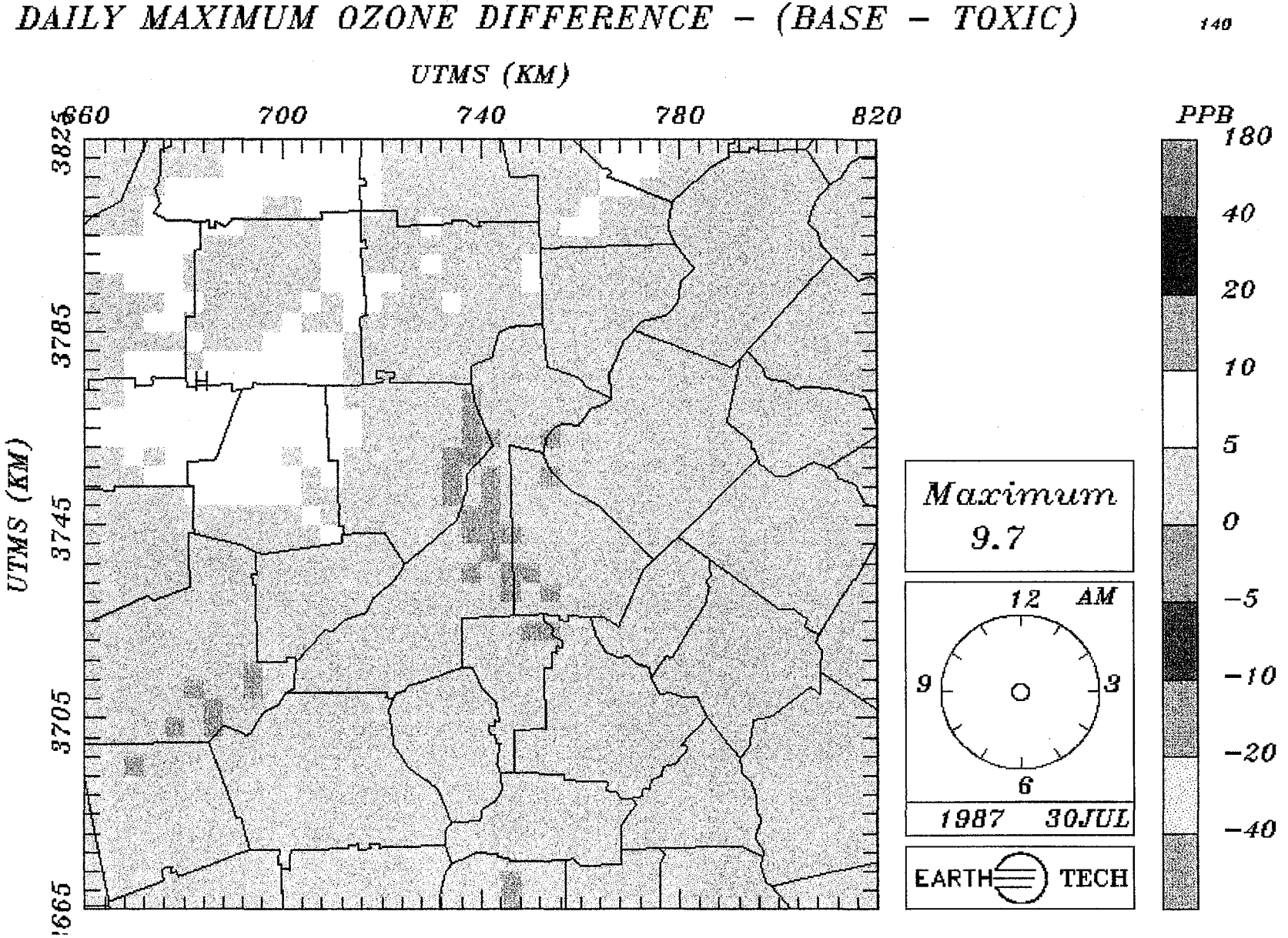

Figure 5-6. Difference in daily maximum 1-hour surface O_3 concentration for Atlanta for 30 July for QA1 (Base) minus QA2 (Air Toxics) QA simulations. (1999 emissions)

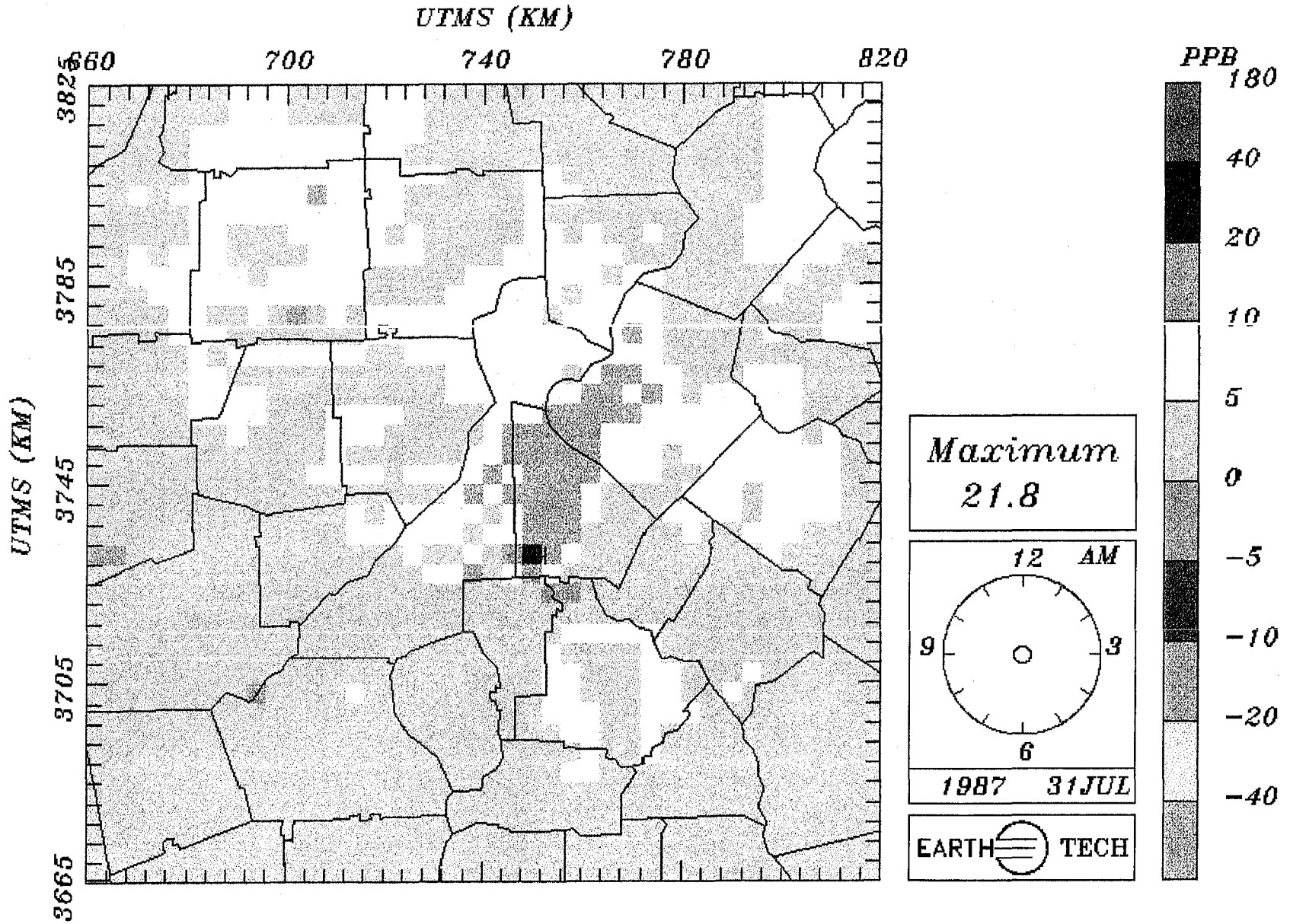

Figure 5-7. **Difference in daily maximum 1-hour surface O_3 concentration for Atlanta for 31 July for QA1 (Base) minus QA2 (Air Toxics) QA simulations. (1999 emissions)**

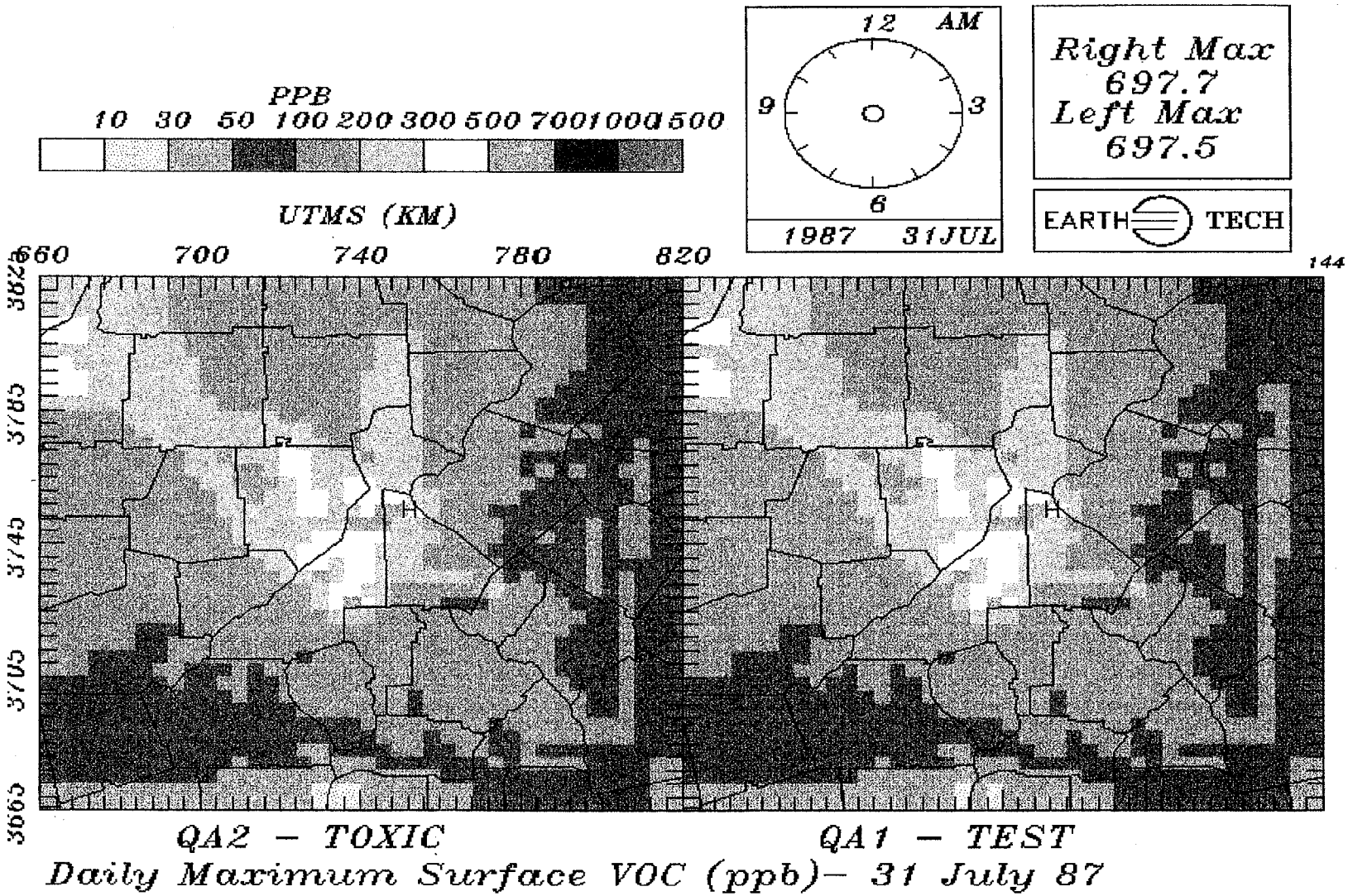

Figure 5-8. Daily maximum 1-hour surface VOC concentrations for Atlanta for 31 July for QA1 (Base) and QA2 (Air Toxics) QA simulations. (1999 emissions)

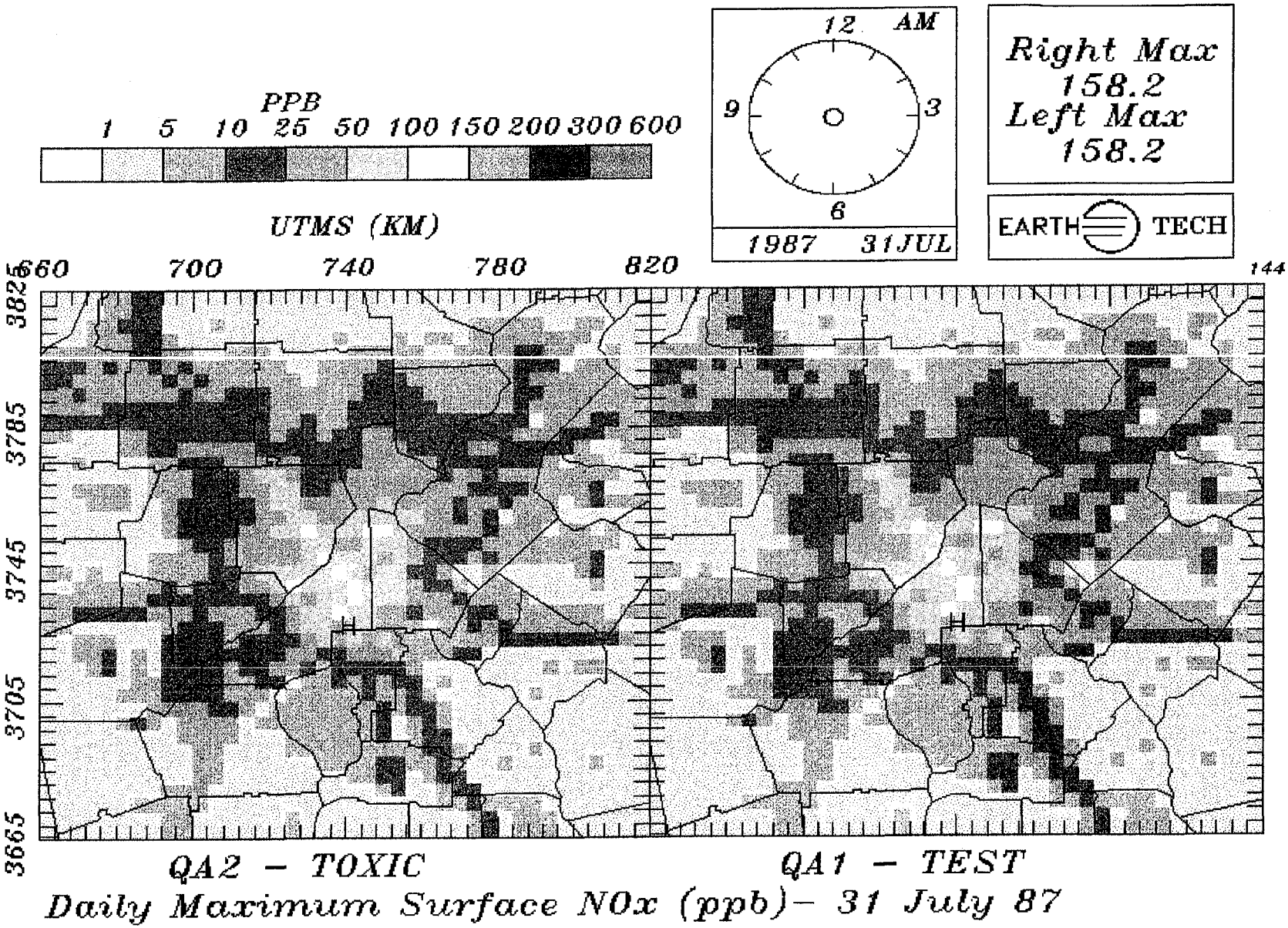

Figure 5-9. Daily maximum 1-hour surface NO_x concentrations for Atlanta for 31 July for QA1 (Base) and QA2 (Air Toxics) QA simulations. (1999 emissions)

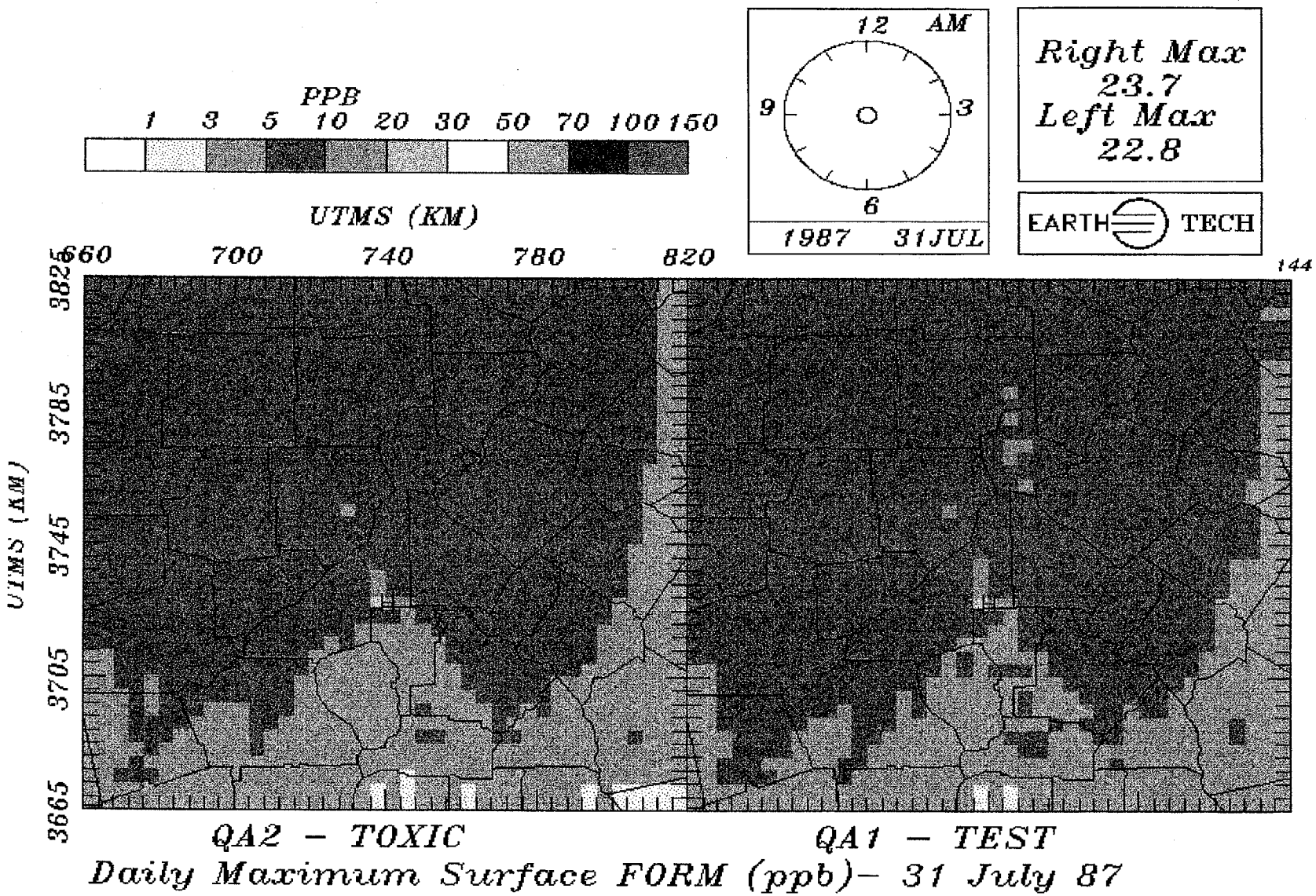

Figure 5-10. Daily maximum 1-hour surface FORM concentrations for Atlanta for 31 July for QA1 (Base) and QA2 (Air Toxics) QA simulations. (1999 emissions)

6.0 Analysis of Future Year Modeling Results for Los Angeles

Three future UAM-IV model simulations were made for the year 2007. The 1987 base year emissions had appropriate growth and control factors applied to project the emissions to the year 2007. Such projections become rather uncertain after a few years because of the vagaries of the economy, unforeseen shifts in demography, and the complex interplay between evolving emission control programs. The use of AFVs will result not only in changes in the on-road mobile emissions component, but also in emission changes associated with fuel processing and distribution.

Three emission inventories were prepared for the future year modeling. The first contained all point and area source emissions in the Los Angeles area except those associated with on-road vehicles, plus gasoline fuel distribution and marketing. In addition, it contained emissions for all diesel vehicles, both on- and off-road, and emissions for all heavy-duty gasoline-fueled motor vehicles. This emissions scenario was called S1, and when modeled, provides an indication of what fraction of the surface O_3 concentrations are due to sources other than light- and medium-duty gas vehicles. The sources comprising the S1 scenario was called the *unaffected sources* since they were not involved in or affected by motor vehicle fuel substitution.

The second inventory consisted of emissions from all light- and medium-duty gasoline on-road motor vehicle using RFG as fuel. In addition, it included emissions from those point and area sources associated with gasoline-fuel distribution and marketing. These emissions, when added to the S1 inventory emissions, produced the 2007 RFG scenario. This scenario was used to estimate the future year O_3 air quality for an inventory representing a gasoline-fueled motor vehicle fleet. In a similar manner, an emissions scenario was developed that assumed all light- and medium-duty gasoline vehicles were instead dedicated to use of CNG. This inventory, when added to the S1 inventory, produced the CNG scenario inventory.

As indicated in the introduction, a major focus of this study is to quantify the degree to which the use of CNG may affect ambient concentrations and population exposures to O_3 and toxics during a severe O_3 episode. In this section we present and analyze the results of the three UAM simulations where the changes in model inputs reflect the effects of alternative motor vehicle fuels.

6.1 Surface Emissions Inventory Description

Our focus is on surface emission sources of VOCs and NO_x the major precursors of O_3.[1] [2] Of secondary interest are the emissions of the toxic compounds FORM, ACET, BENZ, and BUDI. The surface emissions inventory consists of four major components; biogenics, low-level points, off-road area emissions (fixed plus stationary), and on-road mobile emissions. We summarize the VOC and NO_x emissions components for each of the three emissions inventories in Table 6-1. In this table the daily tonnages of emissions for NO_x are expressed as NO_2 equivalents and the VOCs are expressed in terms of

[1] In the SCAQMD, VOC emissions are typically referred to as ROG. For consistency with the Atlanta nomenclature, we will use the term VOC in this section.

[2] Organic emissions in Sections 6 and 7 are stated as VOCs, while emission factors in Section 2 are stated as TOG. One important distinction between TOG and VOC emissions is that TOG includes methane, while VOC does not.

CH_4 equivalent mass for only the primary CB-IV species (e.g., no BENZ or BUDI). For comparison, elevated point source emissions are also contained in Table 6-1.

As expected, the emissions data indicate that biogenic emissions in Los Angeles constitute a relatively minor fraction of the total VOC emissions budget. No soil NO_x emissions were contained in the SCAQMD emission inventory. Motor vehicle emissions of NO_x are dominated by diesel vehicles and heavy duty trucks, which are included in unaffected sources. For S1, area and low point emissions represent approximately 60-70% of the total VOC and NO_x emissions. The CNG fueled vehicle emissions add essentially no VOCs and only one-fourth the amount of NO_x emissions of RFG fueled vehicles.

Table 6-1. Estimated Emissions in Los Angeles Modeling Domain for 2007 for S1 Scenarios and RFG and CNG Scenario Incremental Emissions

Pollutant	Source Type	Unaffected Sources (tons/day)	Future Year Motor Vehicle Incremental Emissions (tons/day)	
			RFG	CNG
VOC	Motor Vehicle	28	141	3.7
	Area	234	19	2.7
	Low Level Point	163	3.2	0.5
	Elevated Point	3.2	0	0
	Biogenics	160	0	0
	Total VOC[a]	560	160	6.9
NO_x	Motor Vehicle	148	198	54
	Area	229	0	0
	Low Level Point	109	0	0
	Elevated Point	12	0	0
	Biogenics	0	0	0
	Total NO_x[a]	500	200	54

[a] Totals are rounded to two significant figures and are VOC as non methane hydrocarbon containing no CO and CH_4.

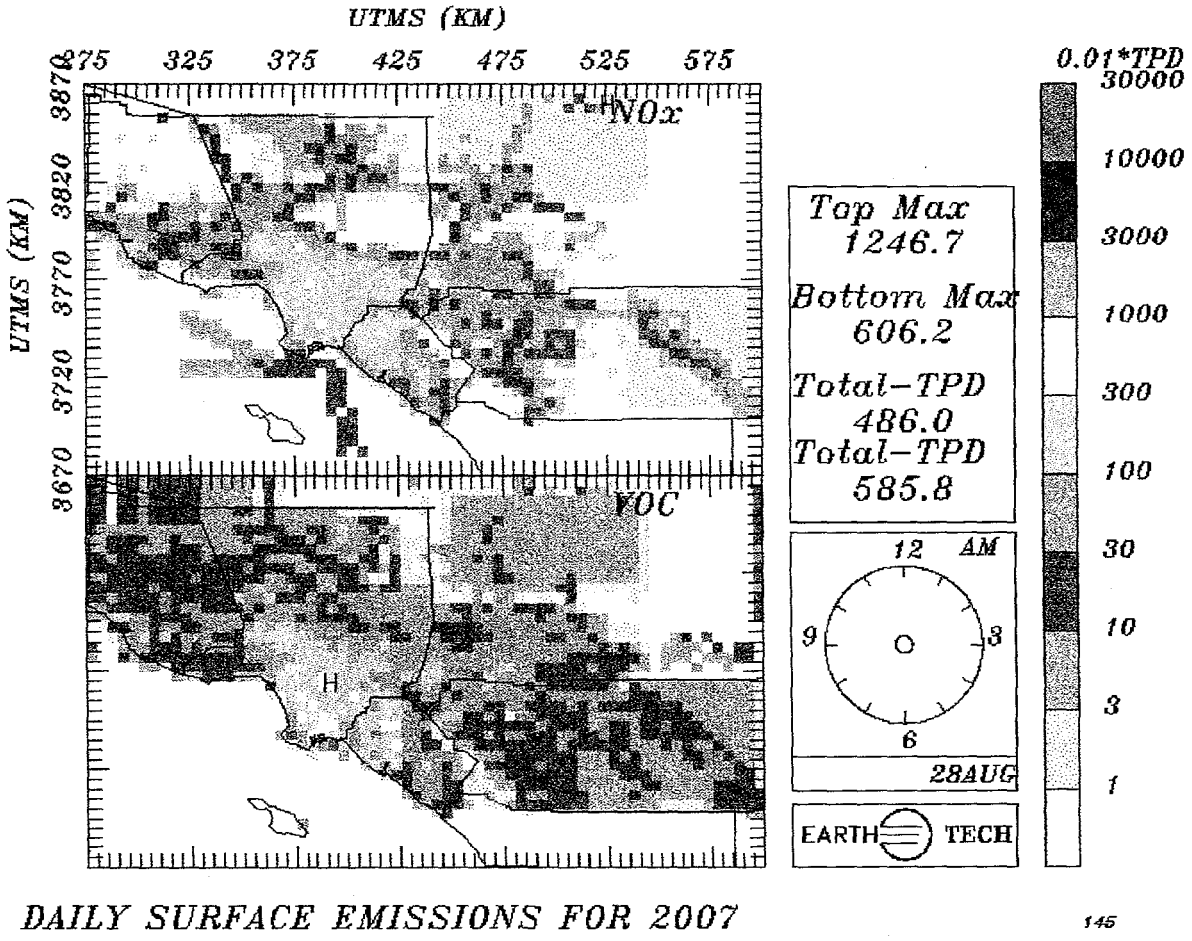

Figure 6-1. Daily VOC and NO_x emission density plots with on-road light- and medium-duty vehicle emissions removed for Los Angeles for 28 August for 2007.

The spatial distribution of surface emissions of NO_x and VOC for the S1 inventory is shown in Figure 6-1. This figure indicates that within the modeling domain there are no emissions from San Diego County. Also evident is the absence of any VOC emissions from the desert areas of San Bernardino County. This pattern of emissions is consistent with the emissions summaries presented in SCAQMD (1994). Although the peak NO_x emission rate per cell is more than twice as large as that of VOCs (12 vs. 6 ton/day) there is more total tonnage of VOCs emitted per day than NO_x. The greatest VOC emissions are in downtown Los Angeles and near Long Beach, which is expected given the petroleum industrial concentration. The largest non-elevated point NO_x emissions occur near the Victorville and Barstow areas. There seems to be a spurious column of VOC emissions in the most easterly cells in San Bernardino County. Major highways and shipping routes show up as corridors of elevated NO_x emissions.

The diurnal patterns of domain-total NO_x and VOC emissions by major component for the S1 inventory are shown in Figure 6-2. Diesel emissions peak around 0700 LST in the morning and again around 1700 LST in the evening. Surprisingly, biogenic emissions appear to peak later in the day around 1800 LST before collapsing to a small value during the night. Low-level point source VOC emissions show an activity profile that resembles a square wave signal between 0800 and 1500 LST corresponding to the work day. The off-road and on-road emission profiles are very similar, suggesting that both are dominated by similar emission processes and activity profiles.

The speciation of the RFG on-road mobile emissions is presented in Table 6-2. This table shows several interesting features, including a significant lack of FORM emissions from RFG fueled vehicles. From standard gasoline, one expects of the order 2% of the CH_4 equivalent mass to be FORM. For RFG, there appears to be very little FORM or ACET present. There are relatively large emissions of aromatic compounds (TOL and XYL) as well as the toxic compound BENZ. Conversely, as one would expect, motor vehicles emit very small, if any amounts of a biogenic compound such as isoprene.

Table 6-2. RFG Scenario Selected Speciation of Gasoline Powered On-Road Motor Vehicle Emissions for Los Angeles for 2007 Expressed as CH_4 Equivalents from GEMAP

Toxics CB-IV Species	Domain Wide Emissions (tons/day)
PAR	92
XYL	27
TOL	25
BENZ	7.7
OLE	5.5
ETH	3.7
FORM	0.71
ACET	0.19
HALD	3.2
BUDI	0.17
ISOP	0.15

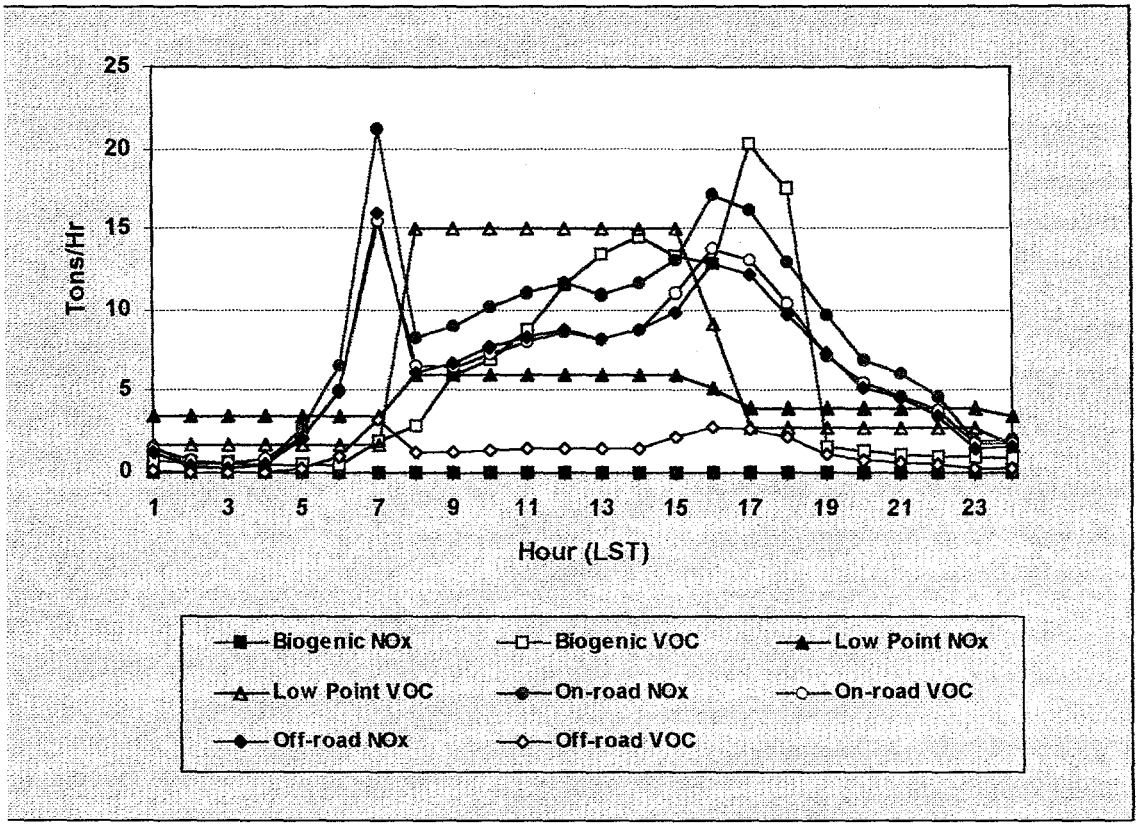

Figure 6-2. Diurnal trend in NO_x and VOC emissions for Los Angeles by emission category for 2007.

The spatial pattern of daily VOC emissions due to RFG and CNG fueled vehicles is presented in Figure 6-3. This figure indicates that the RFG fueled vehicle emissions are over an order of magnitude larger than those due to CNG fueled vehicles. Emissions of VOCs from both CNG and RFG fuel use peak in the corridor between the coast and downtown Los Angeles.

Figure 6-4 illustrates the spatial pattern of daily NO_x emissions due to RFG and CNG fueled vehicles in the Los Angeles modeling domain. As in the case of VOC emissions, the NO_x emissions peak in the downtown Los Angeles area. The spatial pattern is the same for both fuels. The maximum daily grid-cell and domain-wide total emission rates for NO_x from RFG fueled vehicles are each almost four times those from CNG fueled vehicles.

6.2 Intercomparisons of Maximum Hourly Ozone

The spatial patterns of predicted daily maximum 1-hour O_3 with and without RFG fueled vehicles are displayed in Figure 6-5 for 27 August and Figure 6-6 for 28 August. On 27 August, the difference in maximum O_3 is 5 ppb. For the RFG scenario, the maximum is predicted in the San Bernardino mountains north of Pasadena. For Scenario S1, the maximum O_3 is predicted between Reseda and Burbank. On 28 August, the difference in maximum O_3 is 13 ppb, with the RFG maximum predicted just west of Rubidoux.

The predicted daily maximum 1-hour concentrations with RFG and with CNG fueled vehicles are compared in Figure 6-7 for 27 August and in Figure 6-8 for 28 August. The spatial patterns of predictions with CNG fueled vehicles resemble the S1 scenario more closely than the RFG scenario. Statistics describing predicted peak O_3 for the three 2007 Los Angeles emission scenarios are summarized in Table 6-3. Domain-maximum predicted concentrations with CNG increase by 1 ppb and 5 ppb, respectively, for 27 and 28 August. The domain-average daily maximum prediction for 27 August is the same for all three scenarios, indicating that the addition of motor vehicle emissions produces decreases in predicted peak O_3 in some parts of the domain. For 28 August, the domain-average predicted maximum increased by 1.1 ppb with RFG and 0.3 ppb with CNG.

Table 6-3. Daily Maximum and Average O_3 Concentrations in the Los Angeles Modeling Domain for 2007 (units are ppb)

Statistic	Emission Scenario	27 August	28 August
Maximum daily 1-hour	S1	128	137
Maximum daily 1-hour	RFG	133	150
Maximum daily 1-hour	CNG	129	142
Domain average 1-hour	S1	47.5	50.4
Domain average 1-hour	RFG	47.5	51.5
Domain average 1-hour	CNG	47.5	50.7

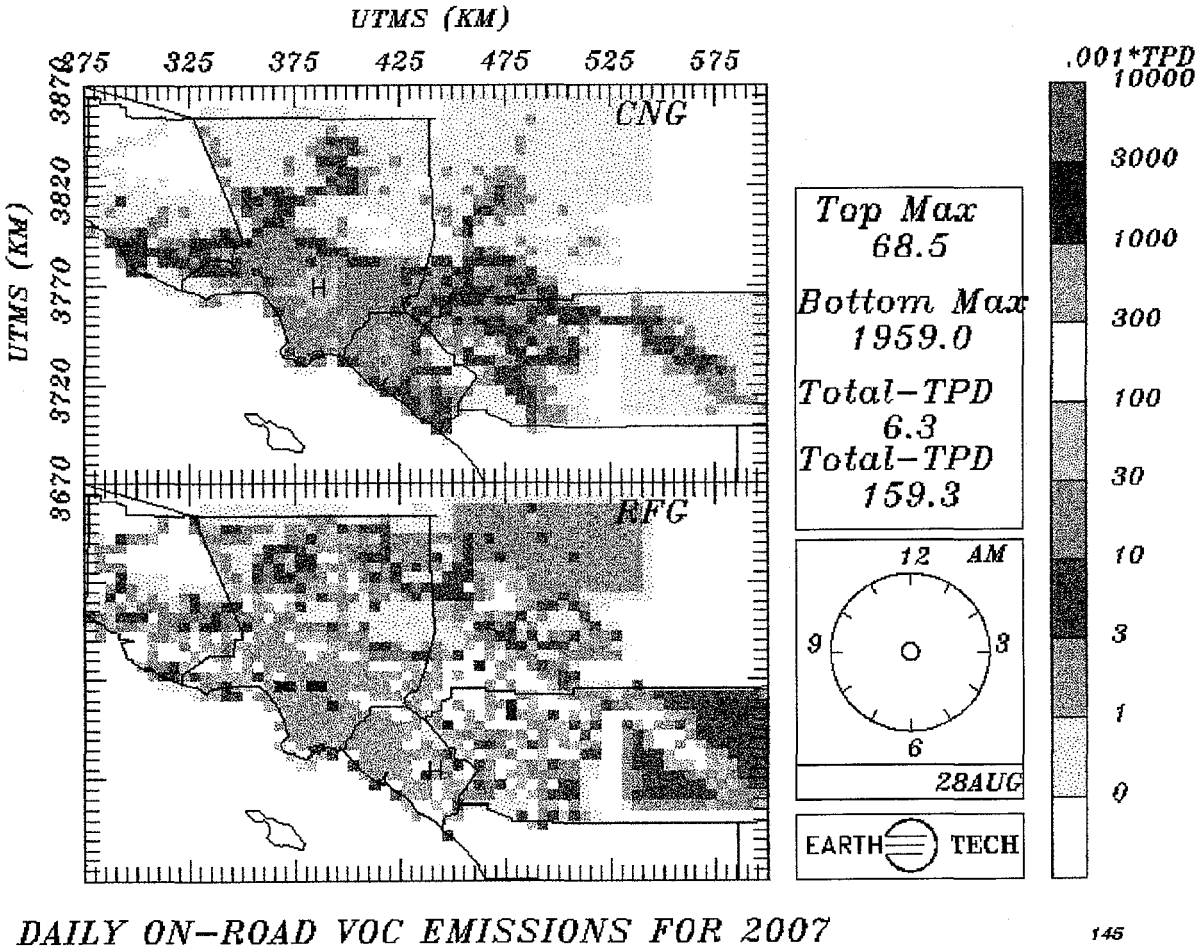

Figure 6-3. Daily VOC emission density plots for CNG and RFG scenarios for Los Angeles for 28 August for 2007.

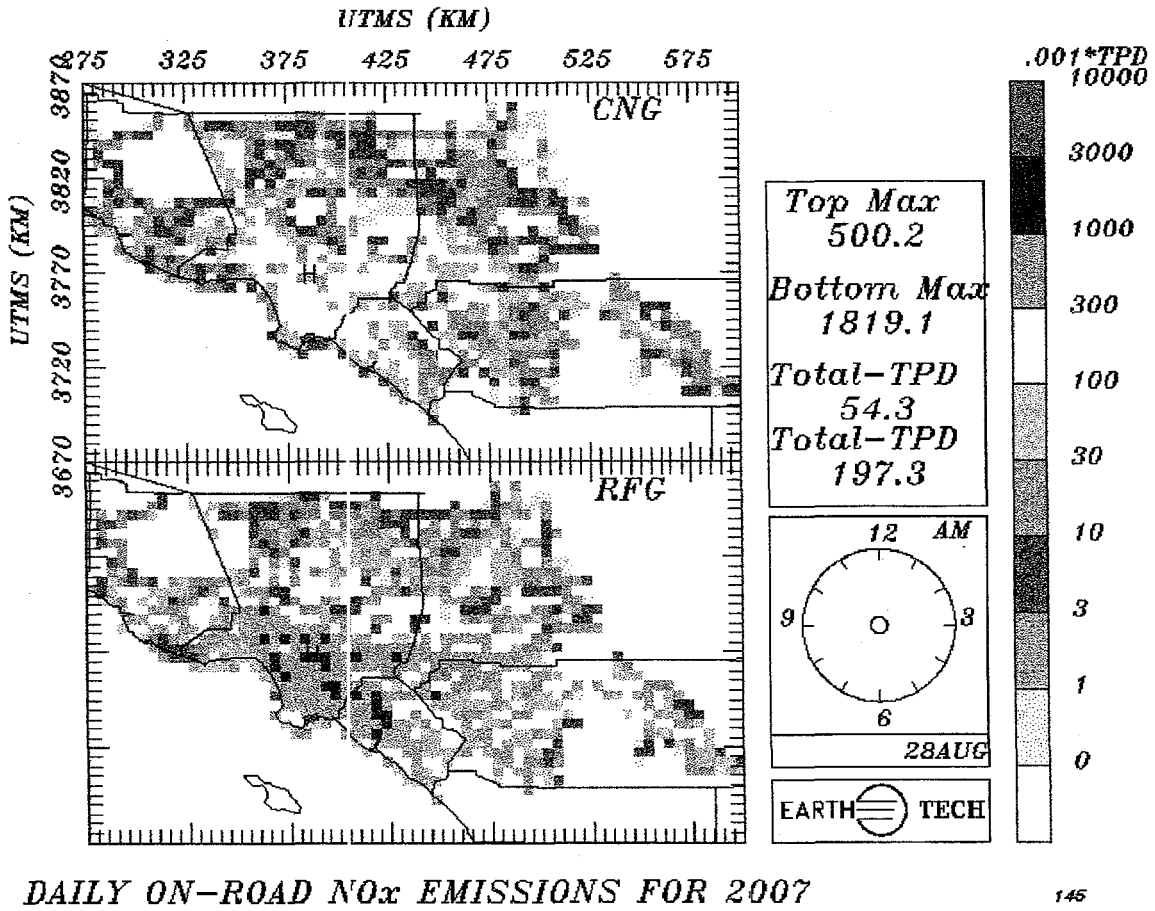

Figure 6-4. Daily NO_x emission density plots for CNG and RFG scenarios for Los Angeles for 28 August for 2007.

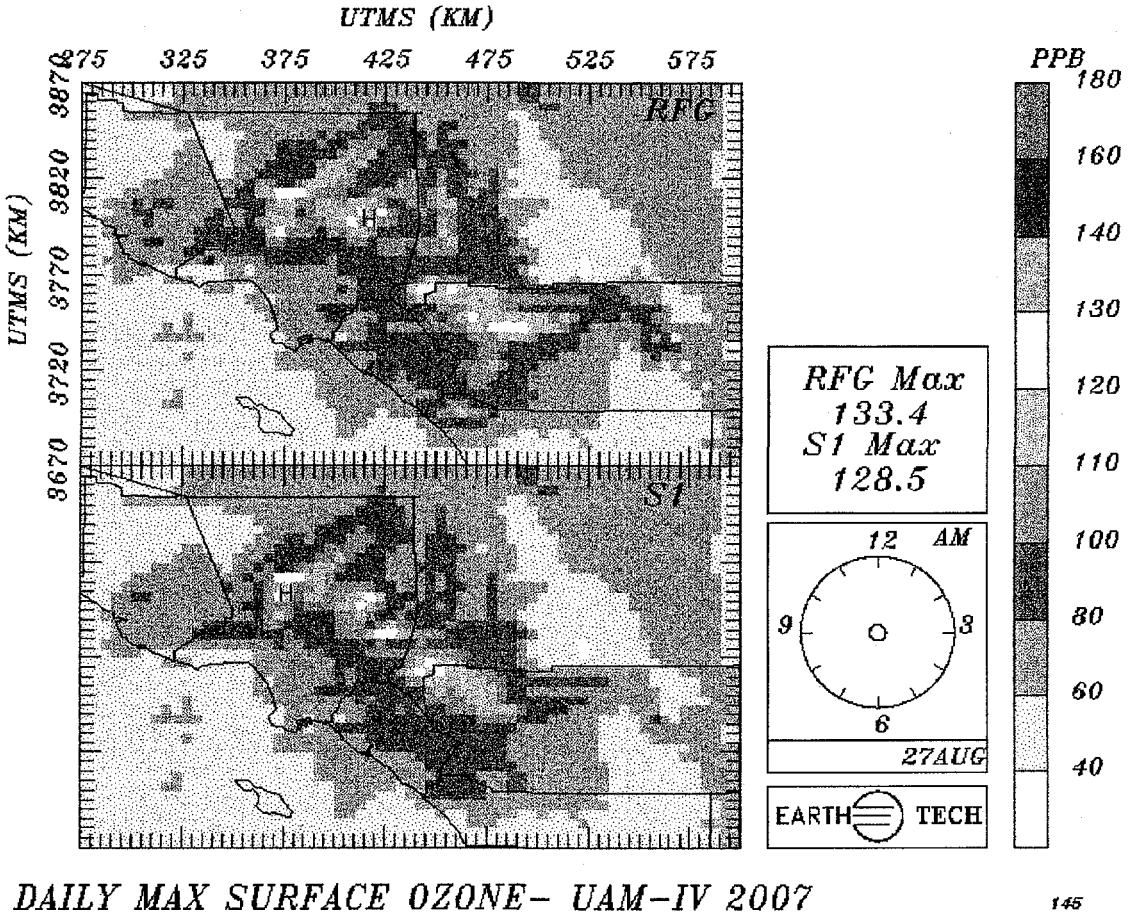

Figure 6-5. Daily maximum 1-hour O_3 concentrations with and without on-road motor vehicles for the RFG scenario for Los Angeles for 27 August for 2007.

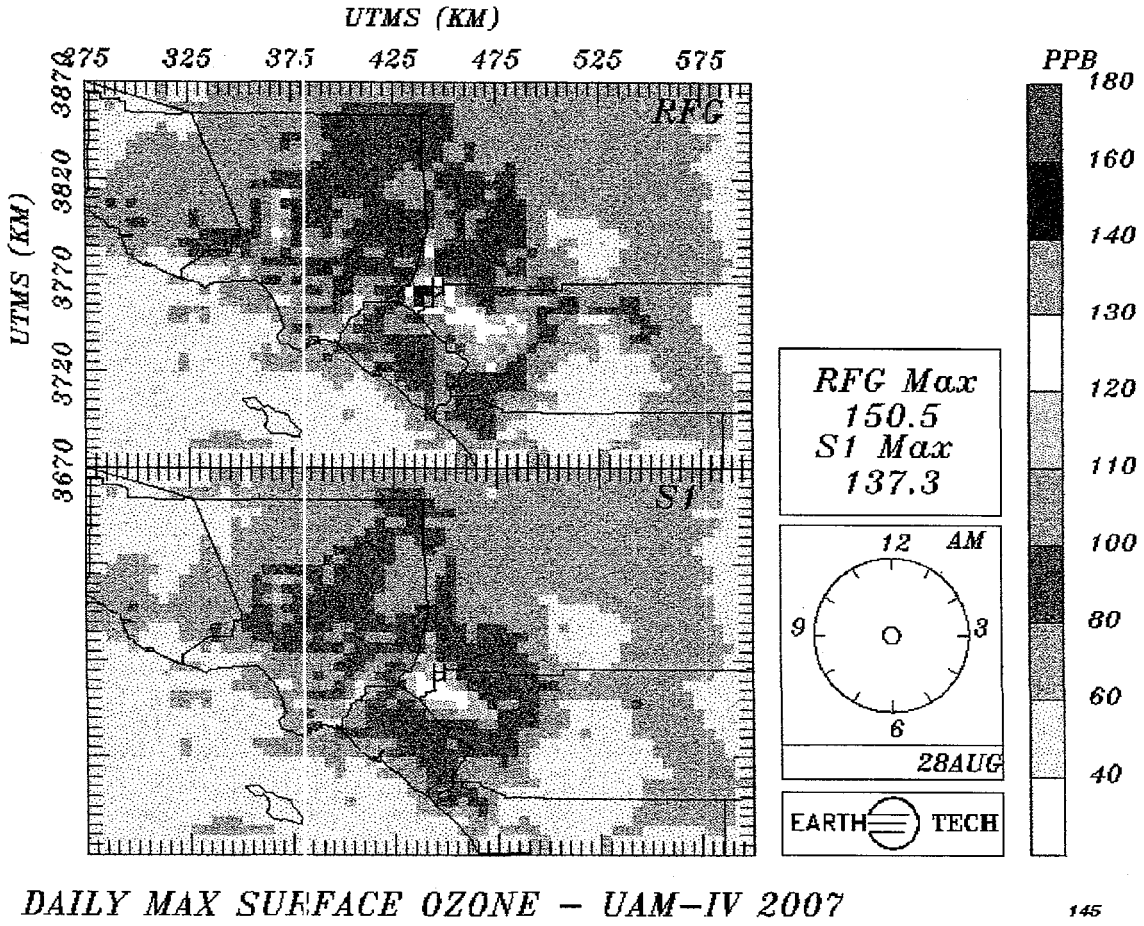

Figure 6-6. Daily maximum 1-hour O_3 concentrations with and without on-road motor vehicles for the RFG scenario for Los Angeles for 28 August for 2007.

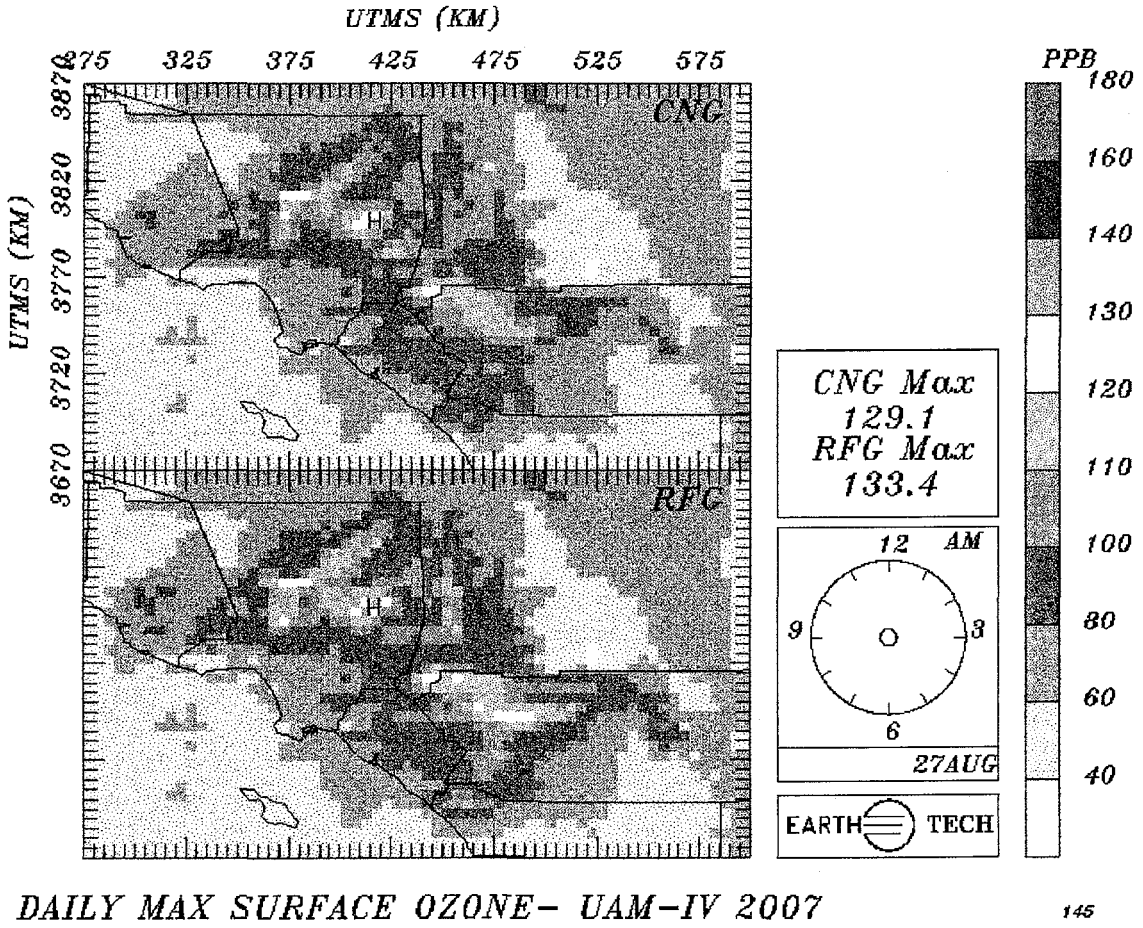

Figure 6-7. Daily maximum 1-hour O_3 concentrations for RFG and CNG scenarios for Los Angeles for 27 August for 2007.

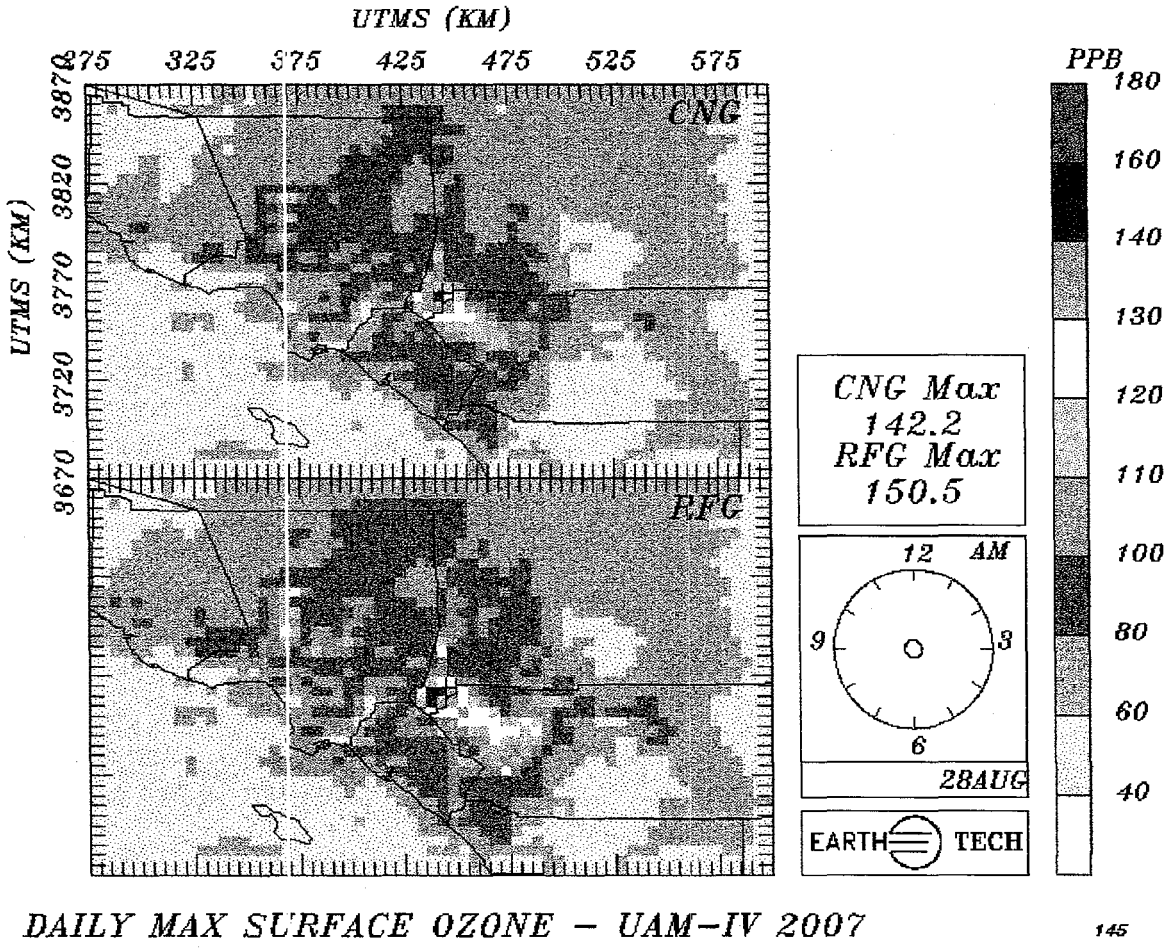

Figure 6-8. Daily maximum 1-hour O_3 concentrations for RFG and CNG scenarios for Los Angeles for 28 August for 2007.

The surface (UAM layer 1) daily maximum 1-hour VOC concentrations with RFG and CNG fueled vehicles are shown in Figure 6-9 for 28 August. For both scenarios, the peak VOC concentrations occur in the vicinity of Lennox and Long Beach with a secondary maximum in and around the city of Riverside. The maximum VOC concentration for the RFG scenario is only about 10% higher than for the CNG scenario, despite a factor of five difference in motor vehicle emissions.

The daily maximum 1-hour NO_x concentrations for RFG and CNG scenarios are shown in Figure 6-10. Since the highest concentrations of NO_x are caused by other source categories such as large point sources, domain-maximum values are the same for the two scenarios. Comparing the spatial patterns of NO_x concentrations, the largest differences show up in major highway corridors such as the Riverside-Palm Springs corridor and the I-5 beltway between Anaheim and Irvine in Orange County.

6.3 Intercomparisons of Maximum 8-Hour O_3

The patterns of daily maximum 8-hour average O_3 concentrations on 28 August (Figure 6-11) are similar to those of daily maximum 1-hour concentrations in Figure 6-8. The peak 8-hour average O_3 concentration due to RFG fueled vehicles is approximately 6 ppb higher than that for CNG fueled vehicles (e.g., 112 ppb vs. 106 ppb). The maximum predicted concentrations for both fuel scenarios are located just to the west of Riverside. Riverside County has by far the highest 8-hour average concentrations. Statistics for peak 8-hour O_3 predictions are summarized in Table 6-4. Differences between scenarios are very small for 27 August. For 28 August, the RFG scenario produced a 10% increase (10 ppb) in the domain maximum, relative to S1, while the CNG scenario produced a 4% increase. Domain-average 8-hour concentrations increased by 0.2 ppb for CNG and 0.6 ppb for RFG.

6.4 Intercomparisons of O_3 and Toxic Exposures

The SCAQMD study region fills the central portion of the modeling domain. Population exposure estimates were made using 1990 census data that were gridded on a 10x10 km grid by the SCAQMD. The population density is displayed in Figure 6-12. The maximum population density is located in downtown Los Angeles. Several secondary maxima occur, including one in northern Orange County (i.e., Anaheim), one in the Rasceta-Burbank corridor, and the Pomona-Redlands-Riverside triangle. Smaller, isolated maxima occur in places like Palm Springs, Indio, and Victorville. The maximum population density is approximately one to two thousand people per square kilometer in Los Angeles proper. As can be noted from Figure 6-12, the SCAQMD data file used for the exposure assessment has numerous grid cells with zero population, which indicates a data base limitation for sparsely populated areas.

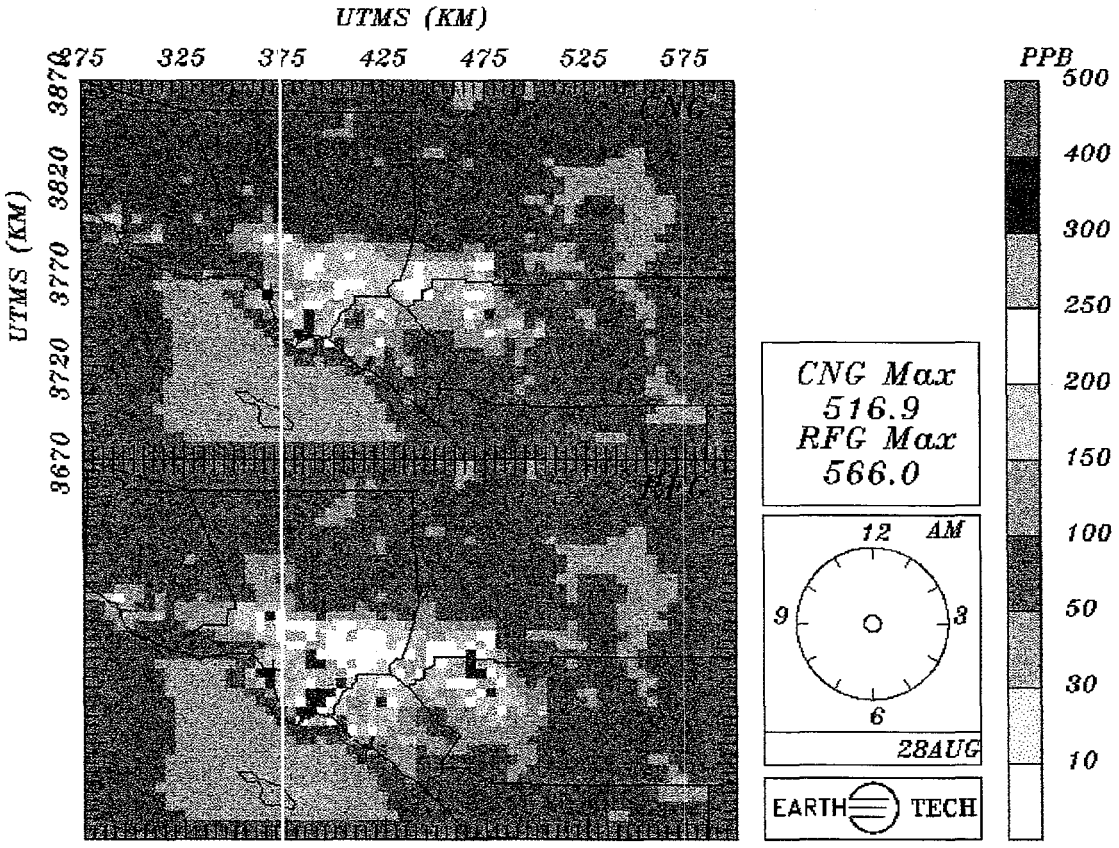

Figure 6-9. Daily maximum 1-hour VOC concentrations for RFG and CNG scenarios for Los Angeles for 28 August for 2007.

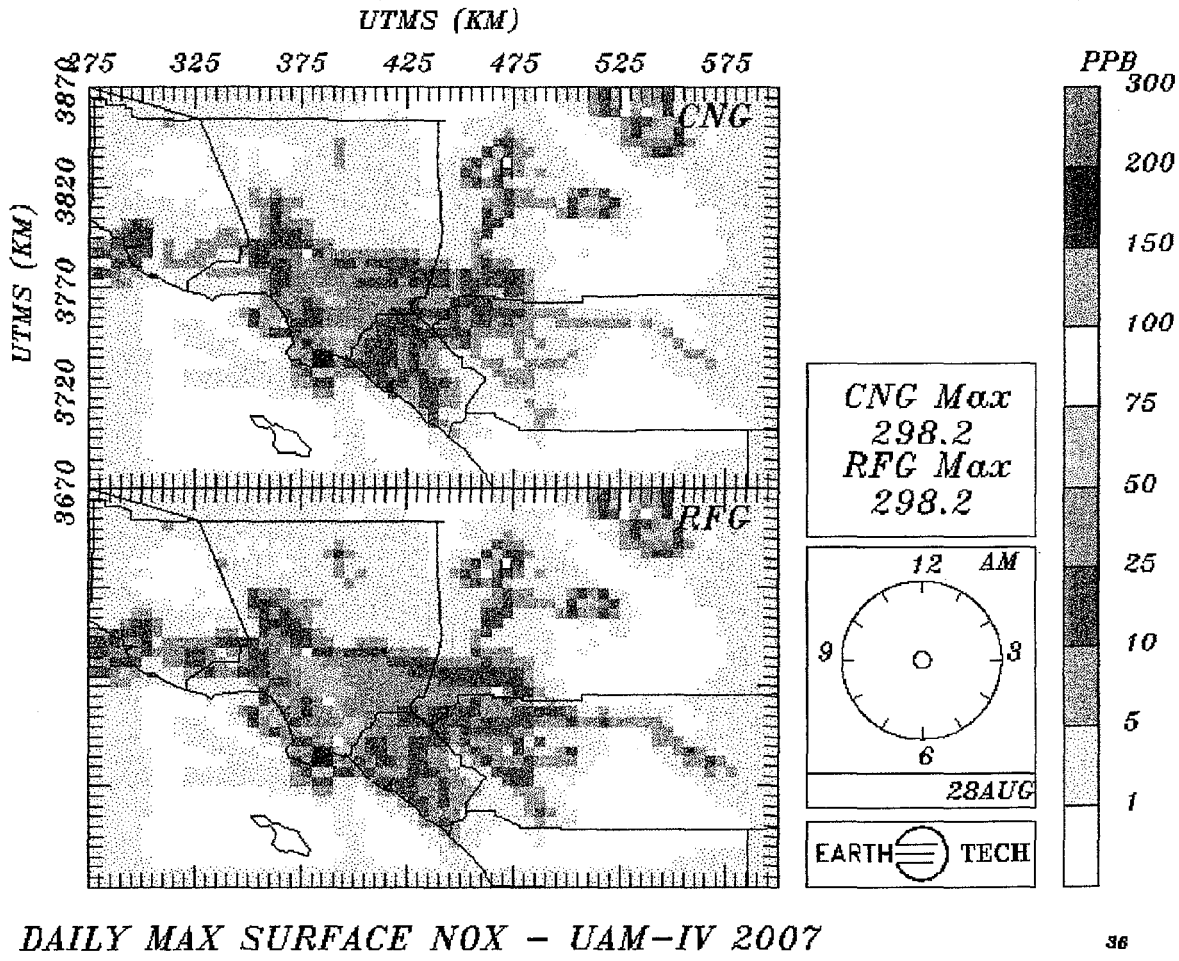

Figure 6-10. Daily maximum 1-hour NO_x concentrations for RFG and CNG scenarios for Los Angeles for 28 August for 2007.

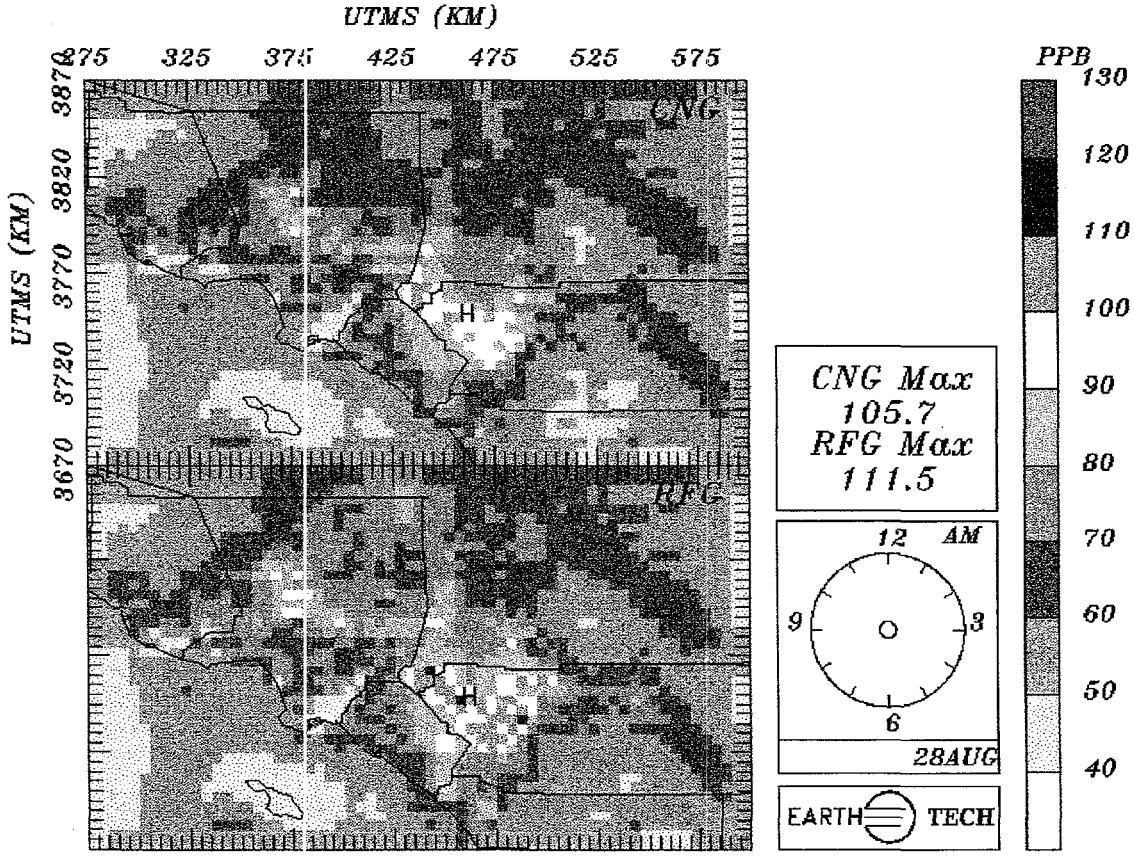

Figure 6-11. Daily maximum 8-hour O_3 concentration for RFG and CNG scenarios for Los Angeles for 28 August for 2007.

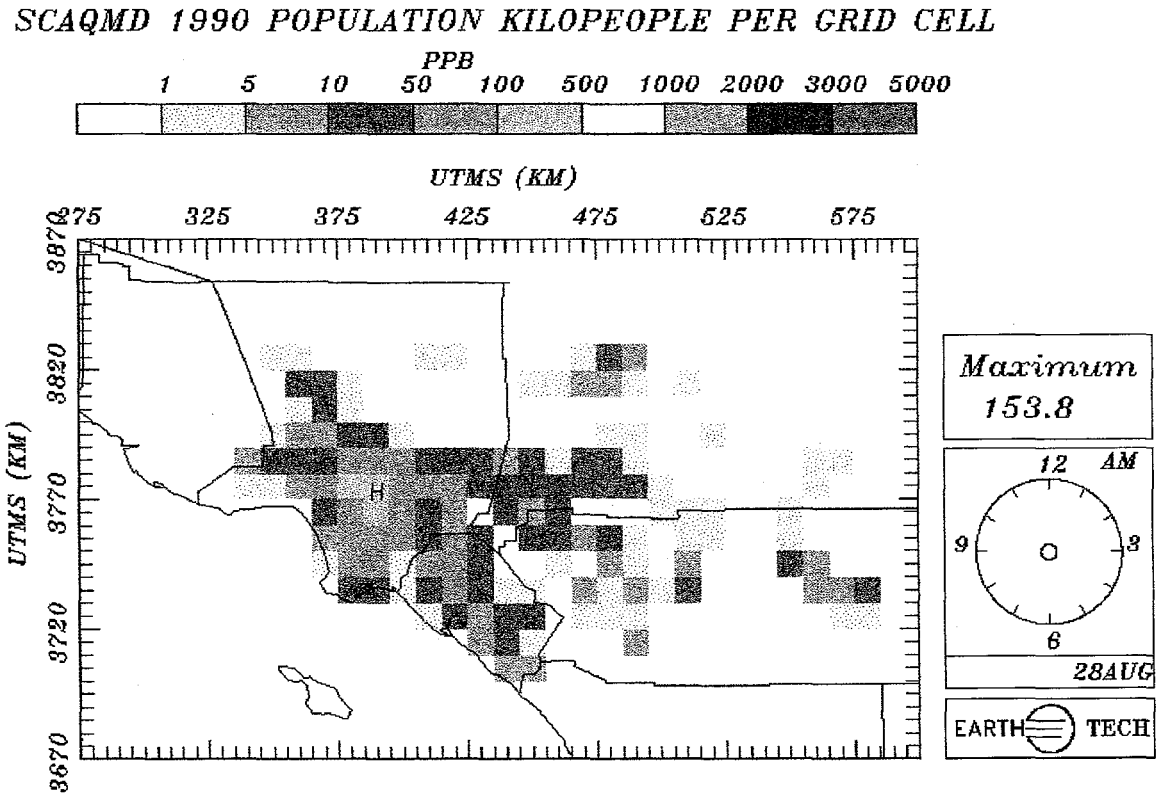

Figure 6-12. Population density in Los Angeles area for 1990.

Table 6-4. Daily Maximum and Average 8-Hour O_3 Concentrations in the Los Angeles Modeling Domain for 2007 (units are ppb)

Statistic	Emission Scenario	27 August	28 August
Maximum daily	S1	105	102
Maximum daily	RFG	106	112
Maximum daily	CNG	105	106
Domain average	S1	45.2	45.8
Domain average	RFG	45.1	46.4
Domain average	CNG	45.2	46.0

The exposure to O_3 was estimated on a daily basis as the sum over all hours of the product of the hourly predicted O_3 in a cell times the number of people in the grid cell. The domain-wide sum of exposure to O_3 is summarized in Table 6-5. The units are parts per million times million people times hours. Two sets of exposure estimates are presented, the first (No Threshold) representing all hourly concentrations in all grid cells, the second (80 ppb Threshold) representing only those hours and cells with predicted concentrations exceeding 80 ppb. The No Threshold results are larger by more than a factor of 100, reflecting the lower O_3 predictions that occur in most cells for most hours. For both episode days, the No Threshold exposures are highest for the S1 scenario. At night, increased NO_x emissions lead to lower predicted O_3 concentrations, which may explain why the RFG scenario (with the highest NO_x emissions) produces the lowest exposure estimates. With a concentration threshold of 80 ppb, exposure estimates are consistent with peak O_3 predictions. The RFG scenario produces the highest exposure estimates for both episode days, and the S1 scenario the lowest.

Table 6-5. Population Exposure to Predicted Surface O_3 Concentrations in Los Angeles for 2007 (units are 10^6 people x ppm-hours)

	No Threshold		80 ppb Threshold	
Emission Scenario	27 August	28 August	27 August	28August
S1	13.6	14.5	.026	.048
RFG	12.4	13.8	.057	.114
CNG	13.2	14.2	.036	.078

The pattern of O_3 exposure (No Threshold) for the RFG and CNG fueled vehicle cases is illustrated in Figure 6-13 for 28 August when the largest overall exposures were predicted. The peak in the O_3 exposure occurs

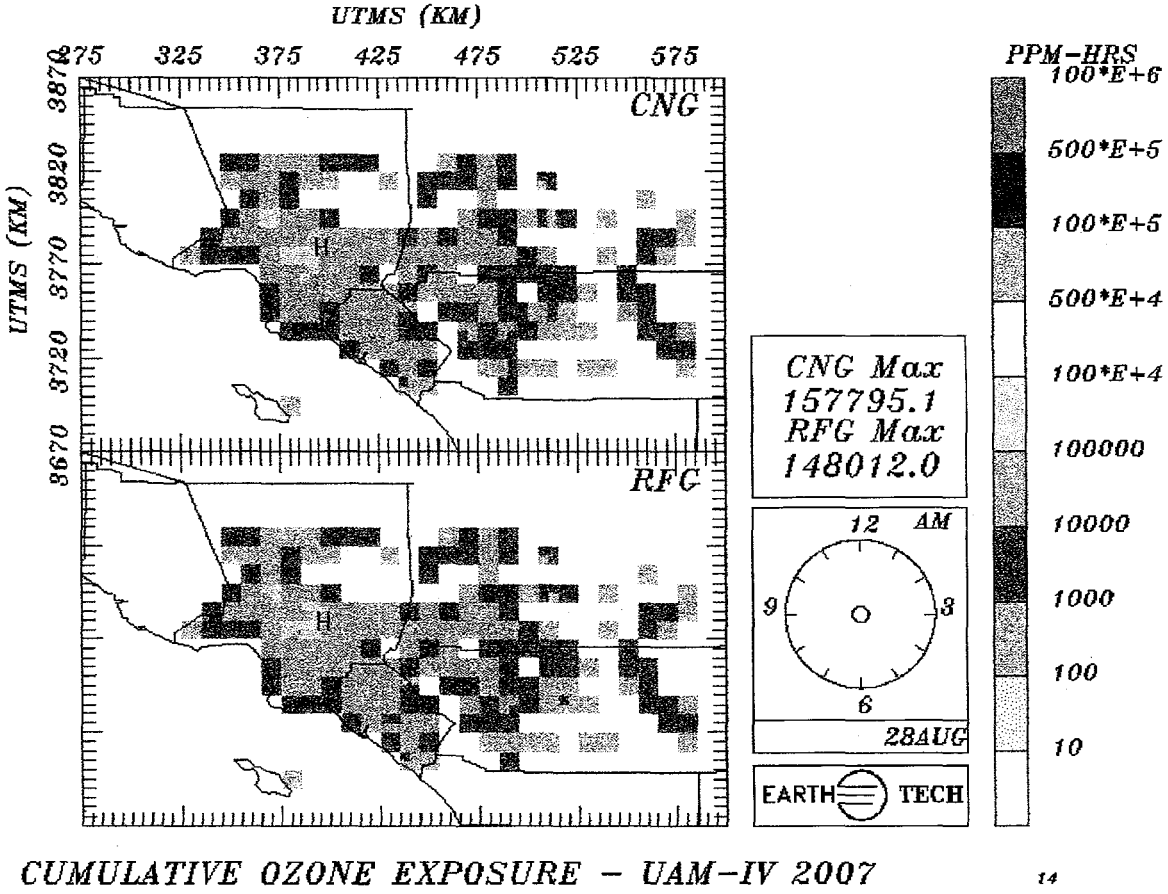

Figure 6-13. Cumulative O_3 exposure for RFG and CNG scenarios for Los Angeles for 28 August for 2007.

in the vicinity of downtown Los Angeles, which might be expected given the population density. The largest differences in O_3 exposure occur in the Reseda-Burbank-Los Angeles corridor. The surface NO_x concentrations in this corridor are relatively large. The predicted O_3 time series at Burbank in the base simulation (not shown) indicates that surface O_3 concentrations fall very close to zero at night. The low night-time O_3 and elevated NO_x concentrations suggest that the titration of O_3 by NO (at night) is a key factor in the No Threshold exposure results.

The maximum daily 1-hour concentrations and the population exposure to the four toxic compounds (FORM, ACET, BENZ, and BUDI) are summarized in Table 6-6. Emissions of the two "ghost" species, BENZ and BUDI, were only assigned for motor vehicle sources. Concentration predictions for these two species are therefore based only on motor vehicle emissions, plus contributions from initial and boundary concentrations. The species FORM and ACET were assigned for all VOC emission sources, based on source emission profiles. Several observations can be made from this table including the following:

- Predicted FORM concentrations and population exposures are the largest of any of the toxic compounds.
- The largest concentrations and exposures occur on 28 August with the exception of the maximum ACET concentration.
- The largest predicted toxic concentrations and exposures occur for the RFG scenario.
- The CNG fueled vehicle scenario and the unaffected source scenario are most similar in terms of the maximum predicted concentrations and exposures.

The cumulative FORM exposure patterns for the RFG and CNG fueled vehicle cases are shown in Figure 6-14 for 28 August. Note that the units are ppb-people-hours. The figure indicates that the highest predicted exposure occurs in the vicinity of downtown Los Angeles. The exposures to FORM in the RFG scenario are most different from those for the CNG scenario in and around Los Angeles. The spatial pattern of population exposure to toxic compounds for the CNG scenario resembles the exposure pattern for the S1 scenario more closely than the RFG pattern.

6.5 Relative O_3 Formation Potential Analysis

The individual chemical species included within VOC emissions do not all contribute equally to O_3 formation. Since the chemical composition of VOC emissions from RFG and CNG fueled vehicles is quite different, a method of comparing VOC emissions on the basis of reactivity or ozone-forming potential would provide further insight regarding the environmental impact of AFVs. Several approaches for making this comparison were considered in the protocol (Appendix B), including the maximum incremental reactivity (MIR) metric defined by Carter (1994).

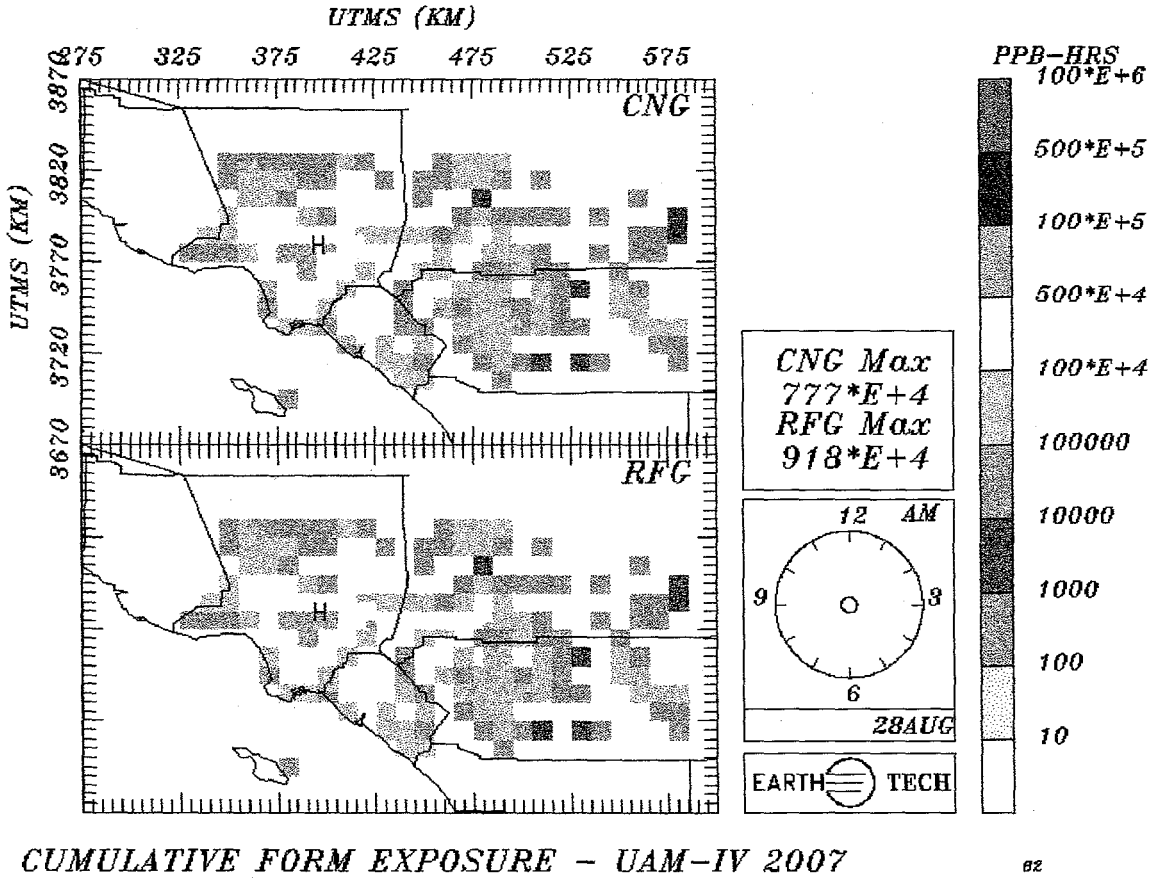

Figure 6-14. Cumulative FORM exposure for RFG and CNG scenarios for Los Angeles for 28 August for 2007.

Table 6-6. Daily Maximum 1-Hour Concentrations and Domain-wide Cumulative Populations Exposures to Each of the Four Toxic Compounds in Los Angeles Modeling Domain for 2007 (units are ppb-people-hours)

Statistic	Date	Emission scenario[1]	FORM	ACET	BENZ	BUDI
Maximum daily 1-hour	27 August	S1	16.0	4.20	1.28	0.25
		RFG	16.3	5.40	2.00	0.27
		CNG	16.0	4.20	1.28	0.25
Cumulative exposure	27 August	S1	1.13	0.565	0.138	0.0027
		RFG	1.18	0.626	0.191	0.0055
		CNG	1.13	0.567	0.139	0.0030
Maximum daily 1-hour	28 August	S1	16.4	4.00	1.20	0.25
		RFG	16.8	5.40	2.00	0.25
		CNG	16.5	4.10	1.30	0.25
Cumulative exposure	28 August	S1	0.876	0.531	0.135	0.0014
		RFG	0.956	0.622	0.208	0.0038
		CNG	0.875	0.533	0.137	0.0016

[1] No emissions of BUDI, BENZ for S1 scenario

For this study, one would like to be able to calculate the ozone formation potential (ozone formed per unit emission) that would result from use of a given alternative fuel. Multiple model runs in which small emissions increments are applied independently to each CB-4 species that is emitted by use of a given fuel are made, and the resulting formation potentials are summed to yield the composite ozone formation potential of the fuel. However, there is a conflict between using a small enough emissions increment to maintain linearity in the resulting chemical calculations and using a large enough increment to produce a statistically detectable change in ozone concentration.

For this study, a method of establishing a statistically significant yet linearity-preserving emission increment for each specie was not available. The scope of the study did not allow development of either direct differentiation versions (e.g., ADIFOR - Bischof, 1994) or direct decoupled method versions (e.g., Yang et al., 1997) of UAM-IV to yield incremental emissions sensitivities. Also, this study involves a specific episode with specific space- and time-varying meteorological conditions and overall emissions, so using generic specie ozone formation potentials from the literature (e.g. Carter, 1995) and applying them on a weighted basis to the present emissions mix for RFG and CNG would introduce uncertainties.

This study used a compromise approach to examine ozone forming potentials of the alternative fuels. A single generic set of incremental runs by specie was done. The increments chosen represented the difference between the RFG emissions case and the no-motor-vehicles case, except for several species for which a larger increment was necessary to produce a significant response. The results were assumed to represent the average ozone formation potential for these individual species over the range of motor vehicle emissions spanning no vehicles to the full RFG case. The emissions from the CNG case will fall within this range, and these average species-specific ozone potentials can be weighted to produce a fuel-specific ozone formation potential for either RFG or CNG. Any proposed approach would be limited by the factors

discussed above; this approach has the advantage that the specie-specific ozone formation potentials are appropriate for this set of episode conditions, domain, and emissions mix.

A series of nine simulations were conducted in which a single chemical species that is emitted by RFG vehicles was to the S1 scenario. The simulations include eight organic species, plus NO_x for comparison purposes. Table 6-7 lists the incremental species emissions (ΔQs). The emissions for FORM, ACET and ISOP were scaled upwards by factors of 10 or 100 in order to obtain a significant O_3 response. The estimated peak O_3 sensitivity and the O_3 formation potential for each pollutant depend on the degree to which the O_3 response can be linearly scaled.

The largest change in daily maximum ozone (ΔO_3) was predicted in response to motor vehicle NO_x emissions. The negative sign indicates that an increase in NO_x emissions produced a decrease in predicted peak O_3 for 28 August. The large response for NO_x reflects the large emission increment (197 tons/day). On an emissions-weighted basis ($\Delta O_3/\Delta Q$), the largest incremental O_3 response is predicted for OLE. The smallest emissions-weighted responses are predicted for PAR and for TOL, which also has a predicted negative O_3 response on 28 August.

These O_3 sensitivities are similar to those reported by Bergin et al. (1995). The peak O_3 at the surface reflects the competing effects of NO_x titration and radical scavenging and O_3 production by increased efficiency of NO_2 formation by radical chemistry. The negative sensitivity of O_3 to TOL emissions is generally thought to occur under large VOC:NO_x ratios for which O_3 formation is expected to be NO_x-limited. On 28 August, the domain average VOC:NO_x ratio ranges from 15:1 to 20:1. In this range, Bergin et al. indicates TOL would have a negative sensitivity effect.

Table 6-7. O_3 Sensitivities (ppb/ton) for Peak Maximum Daily O_3 in Los Angeles on 28 August 1997 (unless noted otherwise, the ΔQ is the difference between S1 and RFG emissions scenarios)

Species	$\Delta O3$ (ppb)	ΔQ (TPD)	$\Delta O3/\Delta Q$ ppb/ton
NO_x	-5.21	197.0	-0.026
PAR	1.29	92.0	0.014
TOL	-0.33	25.0	-0.013
XYL	0.90	26.5	0.034
FORM	1.32	7.1*	0.187
ACET	2.32	18.5**	0.125
OLE	1.20	5.5	0.217
ETH	0.48	3.7	0.130
ISOP	2.36	15.0**	0.157

* = x 10 actual
** = x 100 actual

Peak O_3 sensitivity is sometimes not a good indicator of O_3 formation potential since the meteorological component of the O_3 buildup cannot be separated from the emissions. An approach that is less dependent on the source characteristics and on the dispersion pattern is to estimate how many tons of O_3 were formed or destroyed per ton of a specific chemical emitted over the entire domain. The net O_3 production by species between daily maximums was also estimated for the entire Los Angeles modeling domain for August 28, based on the sensitivity runs described above. The resulting estimates of O_3 formation potential in terms of tons of O_3 per ton of emissions are summarized in Table 6-8.

Table 6-8 also presents VOC reactivity weights that are normalized by the sum of all the VOC sensitivities. Any VOC emission source can be weighted on the basis of reactivity using the weights presented in Table 6-8. Note that of all the VOCs, the PARs, while contributing the largest mass emissions, are assigned the smallest weighting factor. Also, fuel that is rich in TOL is likely to produce less O_3 than one with less TOL.

Table 6-8. O_3 Formation Potentials (ton-O_3/ton-Q) Over the Entire Modeling Domain in Los Angeles on 28 August 2007

Species	ΔM[a] (Tons)	ΔQ (TPD)	ΔM/ΔQ (ton/ton)	Normalized VOC Reactivity Weight
NO_x	204	197.0	1.04	NA
PAR	7.7	92.0	0.083	0.010
TOL	-7.4	25.0	-0.296	-0.038
XYL	6.3	26.5	0.238	0.030
FORM	14.2	7.1*	2.00	0.254
ALD2	27.7	18.5**	1.50	0.191
OLE	14.0	5.5	2.55	0.323
ETH	1.2	3.7	0.324	0.041
ISOP	22.2	15.0**	1.48	0.188

[a] Cumulative Mass change from hour beginning 2300 on 27 August through 2400 on 28 August.

By weighting the emissions by reactivity using Table 6-8, we can compare the O_3 formation potential for the CNG scenario with the RFG scenario. The results of such reactivity weighting are summarized in Table 6-9. An incremental increase of 6.2 tons of VOC from CNG fuel vehicles translates into a 0.14 ton reactivity weighted increment. The RFG fueled vehicle emission difference is greater. A 153 ton increase translates to a 3 ton reactivity weighted increment. On a reactivity-weighted basis, the VOC emissions increment for RFG fuel vehicles is 21 times the increment for CNG vehicles (3 versus 0.14 tons), while the VOC mass emissions (unweighted) from RFG are 25 times the CNG emissions (154 versus 6.2 tons). The small difference is attributable primarily to a larger TOL fraction in the RFG emissions.

6.6 Mass Budget Analysis

The mass flux budget provides information regarding the role of initial and boundary conditions and the influence of different sources and sinks of a given chemical. It can also indicate whether a chemical is highly reactive with a short lifetime. The overall 2-day cumulative mass exchanges for selected species into and out of the modeling domain are summarized in Table 6-10.

For O_3, the net chemical production over two days is roughly equal to the domain-wide total mass. The net increase in O_3 mass is only 7% of the total mass present at the end of the episode. The export of O_3 through the side boundaries equals about half of the chemical production of O_3 and is much larger than the deposition flux. This large export, as was shown earlier, is dominated by outflow through the eastern boundary of the modeling domain.

Table 6-9. Reactivity-Weighted Daily VOC Emissions Increment for Alternative Fuel Scenarios, Los Angeles, 2007 (units are tons/day)

Species	RFG Fueled Vehicles		CNG Fueled Vehicles	
	Emission (tons)	Reactivity weighted emission (tons)	Emissions (tons)	Reactivity weighted emission (tons)
PAR	92	0.92	4.6	0.046
OLE	5.5	1.78	0.14	0.045
ETH	3.7	0.15	0.51	0.021
TOL	25	-0.95	0.49	-0.019
XYL	27	0.80	0.37	0.011
FORM	0.71	0.18	0.09	0.023
ACET	0.19	0.04	0.04	0.008
ISOP	0.15	0.03	0.0	0.00
Total	154	2.95	6.2	0.14

Table 6-10. A Summary of Cumulative Domain-wide Mass Exchanges (Fluxes, Sources, Sinks) for Selected Chemicals Over the Two-Day Period 27-28 August 2007 (units are tons)

Species	Run	Net	Top flux	Side Flux	Deposition	Emission	Chemistry	Total Mass[a]
O3	S1	913	-3290	-5490	-2140	0	11800	13400
NO_x	S1	-103	567	823	-94	677	-2080	199
VOC	S1	-1360	777	2110	0	1040	-5290	4330
BENZ	S1	5.5	-18	10	0	16	-2	137
BENZ	RFG	15	-21.7	8.4	0	31.4	-2.3	146
FORM	S1	-107	165	330	0	6.6	-609	296

[a] The total mass is rounded to three significant figures and is the domain-wide total at midnight between 27 and 28 August.

Relatively little NO_x mass is stored in the atmosphere, resulting in low predicted NO_x concentrations in rural regions and aloft. The fluxes are several times larger than the typical total mass, suggesting that the turnover time of NO_x within the domain is significantly less than a day. The total NO_x mass is very responsive to the chemistry and fluxes through the boundaries. Over the course of the two-day episode, the total mass decreased by 50 percent.

The chemical destruction of VOC is of the same magnitude as the domain-total VOC mass. The combined fluxes of VOC through the top and lateral boundaries are approximately three times larger than the emissions, suggesting that unless the source region is very localized, the boundary conditions may affect the O_3 response to VOC emission control strategies.

BENZ is fairly nonreactive with only 1 % of the total mass of BENZ reacting over the course of the two-day episode. The BENZ emissions are of the same approximate size as the lateral and top boundary fluxes. The total mass of BENZ is over a factor of five larger than the source term. Under the case of the RFG fueled vehicles, the emission rate is several times larger than the boundary imports and exports. This difference suggests that the boundary conditions are not so large as to dominate over the response of the model to increased RFG BENZ emissions.

The FORM emissions are many times smaller than the total mass and the lateral fluxes, indicating that changing the FORM source term is unlikely to have much of an effect on human exposure to FORM throughout the modeling domain. The chemistry is rather reactive, with the rate of destruction exceeding the total rate of mass import. The net loss over two days is about a third of the total mass, and in this respect FORM behaves like the overall VOC.

7.0 Analysis of Future-Year Modeling Results for Atlanta

Three future-year UAM-IV model simulations for Atlanta were made for 2007. The 1987 base-year emissions were projected to 2007 through application of appropriate growth and control factors. Such projections become rather uncertain after a few years due to the vagaries of the economy, unforeseen shifts in demography, and the complex interplay between evolving emission control programs. The use of AFVs will result not only in changes in the on-road mobile emissions component, but also in emission changes associated with fuel processing and distribution.

Three emission inventories were prepared for the future year modeling. The first inventory contained all point and area source emissions in the Atlanta area except those associated with on-road vehicles, plus gasoline fuel distribution and marketing. In addition, it contained emissions for all diesel vehicles, both on- and off-road, and emissions for all heavy-duty gasoline-fueled motor vehicles. This emissions scenario was called S1, and when modeled, provides an indication of what fraction of the surface O_3 concentrations are due to sources other than light- and medium-duty gas vehicles. The sources comprising the S1 scenario were called "*unaffected sources*" since they were not involved in or affected by motor vehicle fuel substitution.

The second inventory consisted of emissions from all light- and medium-duty gasoline on-road motor vehicles. In addition, it included emissions from those point and area sources associated with gasoline-fuel distribution and marketing. These on-road emissions, when added to the S1 inventory emissions, produced the 2007 LRVP scenario[1]. This scenario was used to estimate the future year response of O_3 due to an inventory containing a gasoline fuel motor vehicle fleet. In a similar manner, an emissions scenario was developed that assumed all light- and medium-duty gasoline vehicles were instead dedicated to use of CNG. This inventory, when added to the S1 inventory, produced the CNG scenario inventory.

As indicated in the introduction, a major goal of this study is to quantify the degree to which the use of LRVP gasoline and CNG fuel vehicles may affect ambient concentrations of and population exposures to O_3 and toxics during a severe O_3 episode. In this section, we present and analyze the results of the three UAM simulations where the changes in model inputs reflect the effects of alternative vehicle fuels.

7.1 Surface Emissions Inventory Description

Our focus is on surface emission sources of VOCs and NO_x, the major precursors of O_3. Of secondary interest are the emissions of the toxic compounds FORM, ACET, BENZ, and BUDI. The surface emissions inventory consists of four major components: biogenics, low-level points, off-road area emissions (fixed plus stationary), and on-road mobile emissions. We summarize the VOC and NO_x emissions components for each of the three emissions inventories in Table 7-1. The daily tonnages of emissions for NO_x are expressed as NO_2 equivalents and the VOCs are expressed in terms of CH_4 equivalent mass for only the primary CBM-IV species (e.g., no BENZ or BUDI). For comparison, elevated point source emissions are also contained in Table 7-1.

---

[1]Emissions for this scenario are based on low RVP gasoline.

Table 7-1. Estimated Emissions in Atlanta Modeling Domain for 2007 Emission Scenarios

Pollutant	Source Type	S1 Unaffected Sources (tons/day)	Alternative Fuel Scenario Incremental Emissions (tons/day)	
			LRVP	CNG
VOC	Motor Vehicle	39	209	2.5
	Area	365	11	1.1
	Low Level Point	55	6.0	0.6
	Elevated Point	24	0.2	0
	Biogenics	1,010	0	0
	Total VOC[a]	1,500	230	4.2
NO_x	Motor Vehicle	122	364	55
	Area	189	0	0
	Low Level Point	0.2	0	0
	Elevated Point	380	0	0
	Biogenics	28	0	0
	Total NO_x[a]	720	360	55

[a] Totals are rounded to two or fewer significant figures and do not include CO and CH_4.

The emissions totals in Table 7-1 indicate that biogenic emissions in Atlanta constitute a major fraction of the total VOC emission budget. These biogenic emissions are used directly as obtained from the DNR. It should also be noted that (unlike the Los Angeles inventory) the Atlanta biogenic emissions include a small soil NO_x component. For all emission scenarios, the largest VOC source categories are biogenics and area sources. For NO_x, elevated point sources account for 53% of S1 scenario emissions and 49% of CNG (plus S1) scenario emissions. For the LRVP scenario, the motor vehicle source category has the largest NO_x emissions (45%). The CNG fuel vehicle emissions contribute minimal VOCs; their contribution to NO_x emissions is only 15% of the NO_x emissions from LRVP gasoline fuel vehicles.

The spatial distribution of surface emissions of NO_x and VOC for the S1 inventory is shown in Figure 7-1. The NO_x emissions pattern indicates that Atlanta is a rather compact, well defined island of NO_x emissions. The major highways appear as spokes from the central core. The largest NO_x emissions occur near each of the three airports in the region. The VOC emissions indicate the dominance of the biogenic emissions. The density of emissions in the urban core is roughly a factor of four larger than the surrounding rural areas. The peak NO_x emission rate per cell is smaller than that for VOCs (6.0 vs. 9.6 tons per day), and the total tonnage emitted per day is four times larger for VOCs than for (non-elevated) NO_x.

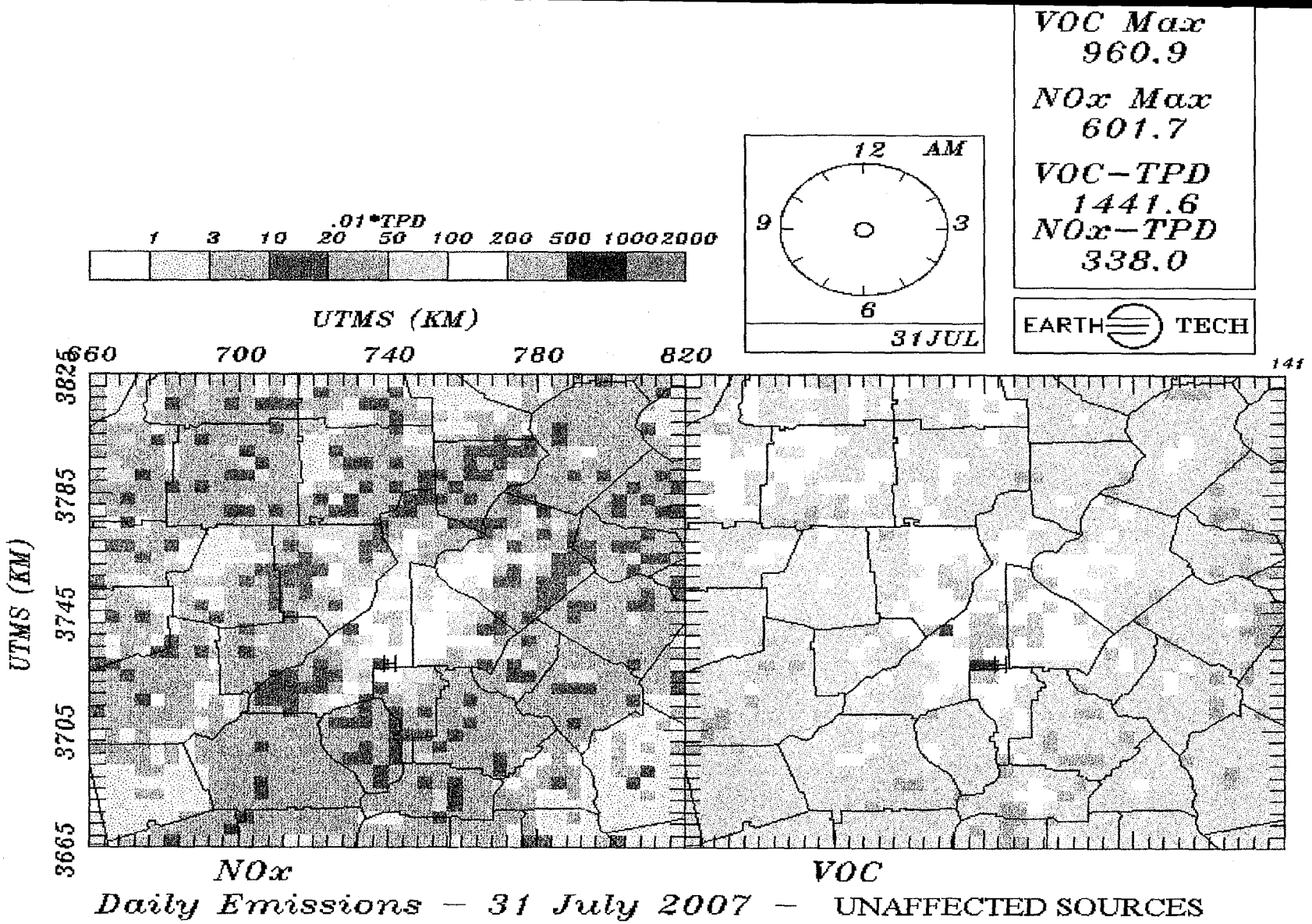

Figure 7-1. Daily Atlanta VOC and NO_x emissions density plot for 2007 with on-road light- and medium-duty vehicle emissions removed.

The diurnal pattern of domain-total NO_x and VOC by major component for the S1 inventory is shown in Figure 7-2. Diesel and gasoline (heavy truck) vehicle emissions peak around 0700 local standard time (LST) in the morning and again around 1600 LST in the evening. Biogenic VOC emissions appear to peak around 1500 LST when the highest temperatures of the day occur. Low-level point source VOCs show an activity profile that resembles a square wave signal between 0900 and 1800 LST, corresponding to the work day.

The speciation of the LRVP gasoline scenario on-road mobile emissions is presented in Table 7-2. This table shows several interesting features, including low FORM emissions. With standard gasoline, one expects on the order of 2% of VOC emissions to be FORM. For the gasoline scenario, FORM and ACET together represent only 1% of total emissions. Aromatic compounds (TOL and XYL) or the toxic compound BENZ represent, after PAR, the second largest source of organic carbon.

Figure 7-3 shows the spatial patterns of daily VOC emissions from gasoline and CNG fuel scenarios. The differences between the scenarios are dwarfed by the large biogenic VOC emissions. The highway corridors only begin to show up for the gasoline scenario. Emission differences are also evident in the Atlanta urban core and to the northwest (Marietta area). The CNG VOC emissions spatial pattern is essentially identical to Scenario S1.

Table 7-2. *Speciation of VOC Emissions Increment for* LRVP Gasoline Scenario for Atlanta, 2007

CBM-IV Species	Emissions (tons per day, as CH_4 equivalents)
PAR	130
XYL	29
TOL	34
BENZ	11
OLE	12
ETH	11
FORM	1.5
ACET	0.90
HALD	.063
BUDI	0.58

Figure 7-4 illustrates the spatial pattern of daily low-level NO_x emissions for the two fuel scenarios. The NO_x emissions peak in the downtown Atlanta area. The spatial pattern for the LRVP scenario clearly shows highway corridors bracketing the downtown urban maximum. The grid-cell maximum and domain-wide daily total emission rates show that NO_x from gasoline fuel vehicles is much greater than that for the CNG fuel scenario (8.9 TPD vs. 6.5 TPD and 700 vs. 390 TPD, respectively).

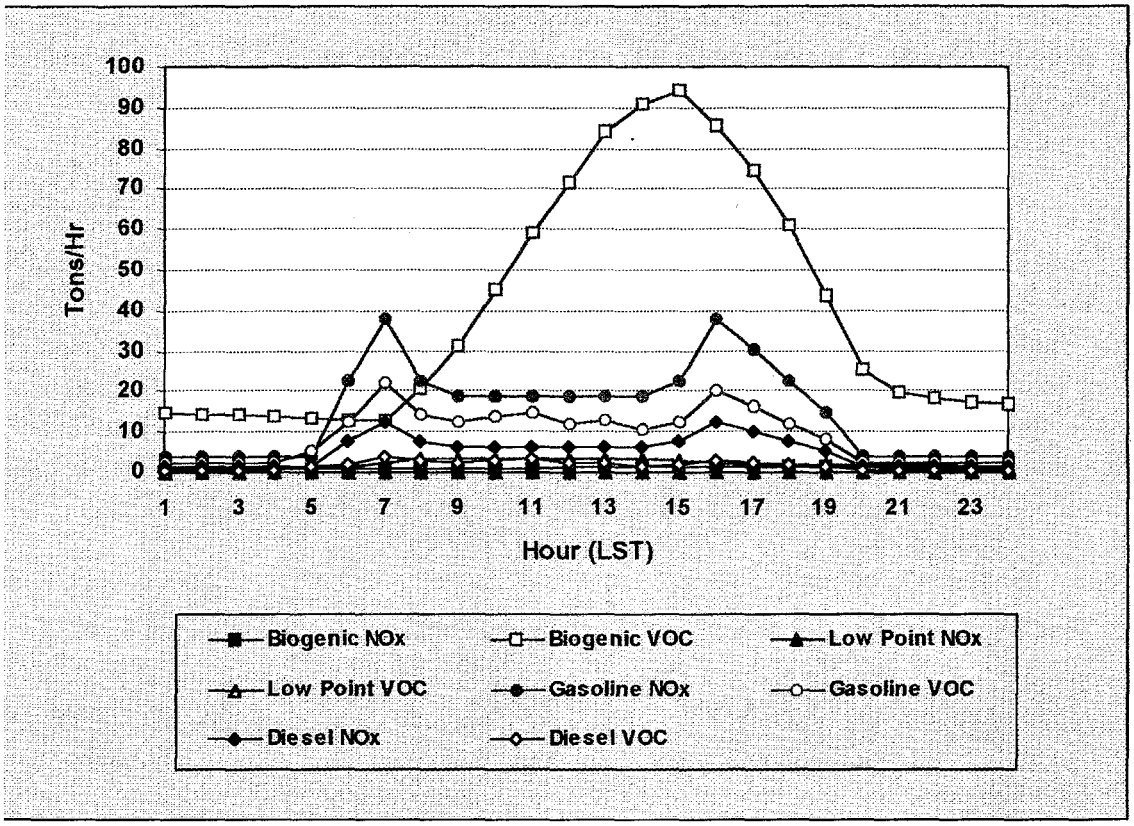

Figure 7-2. Diurnal trend in NO_x and VOC emissions for Atlanta by emission category for 2007.

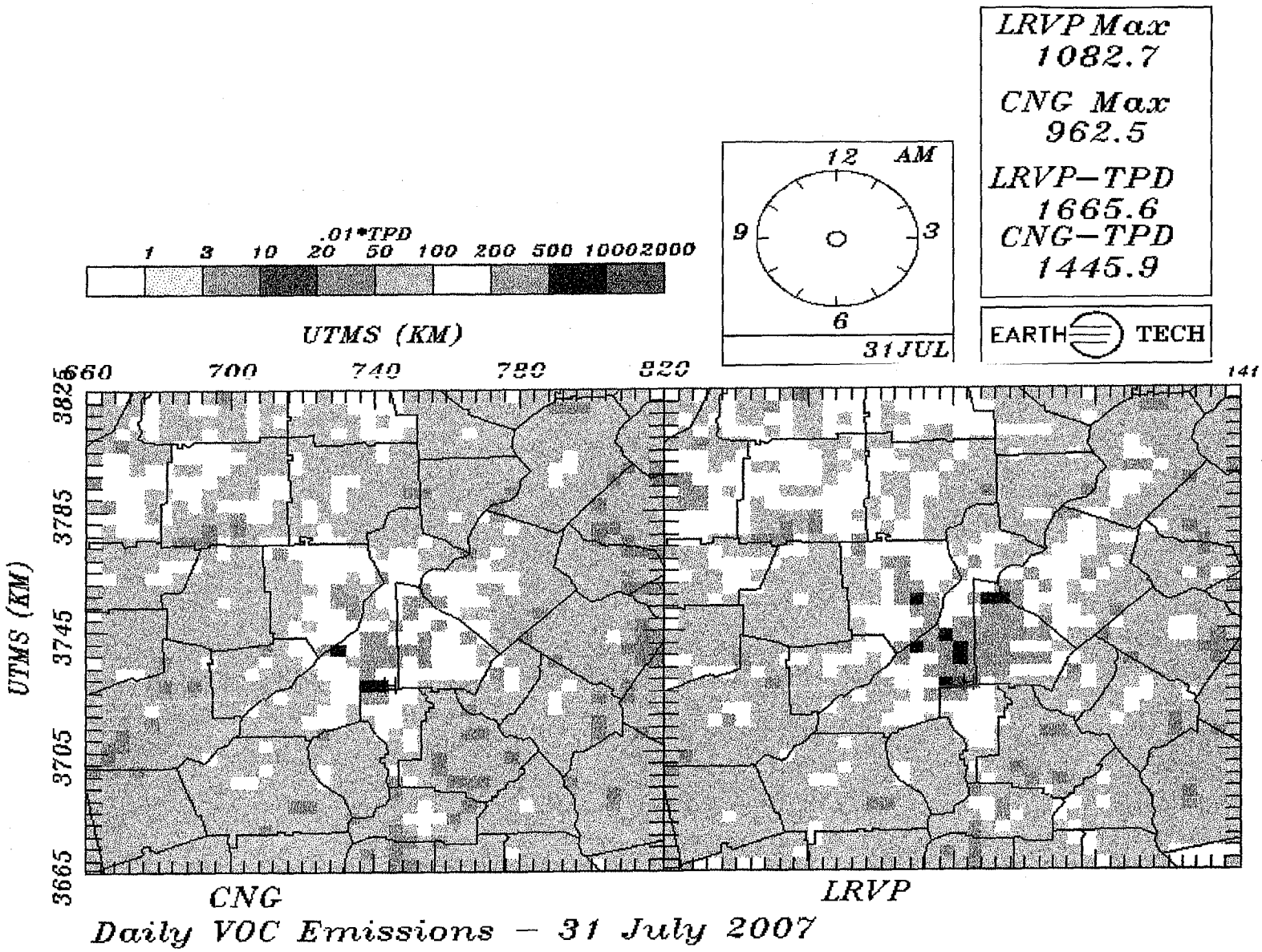

Figure 7-3. Spatial pattern of daily VOC emissions in Atlanta for 31 July for 2007 for CNG and LRVP scenarios.

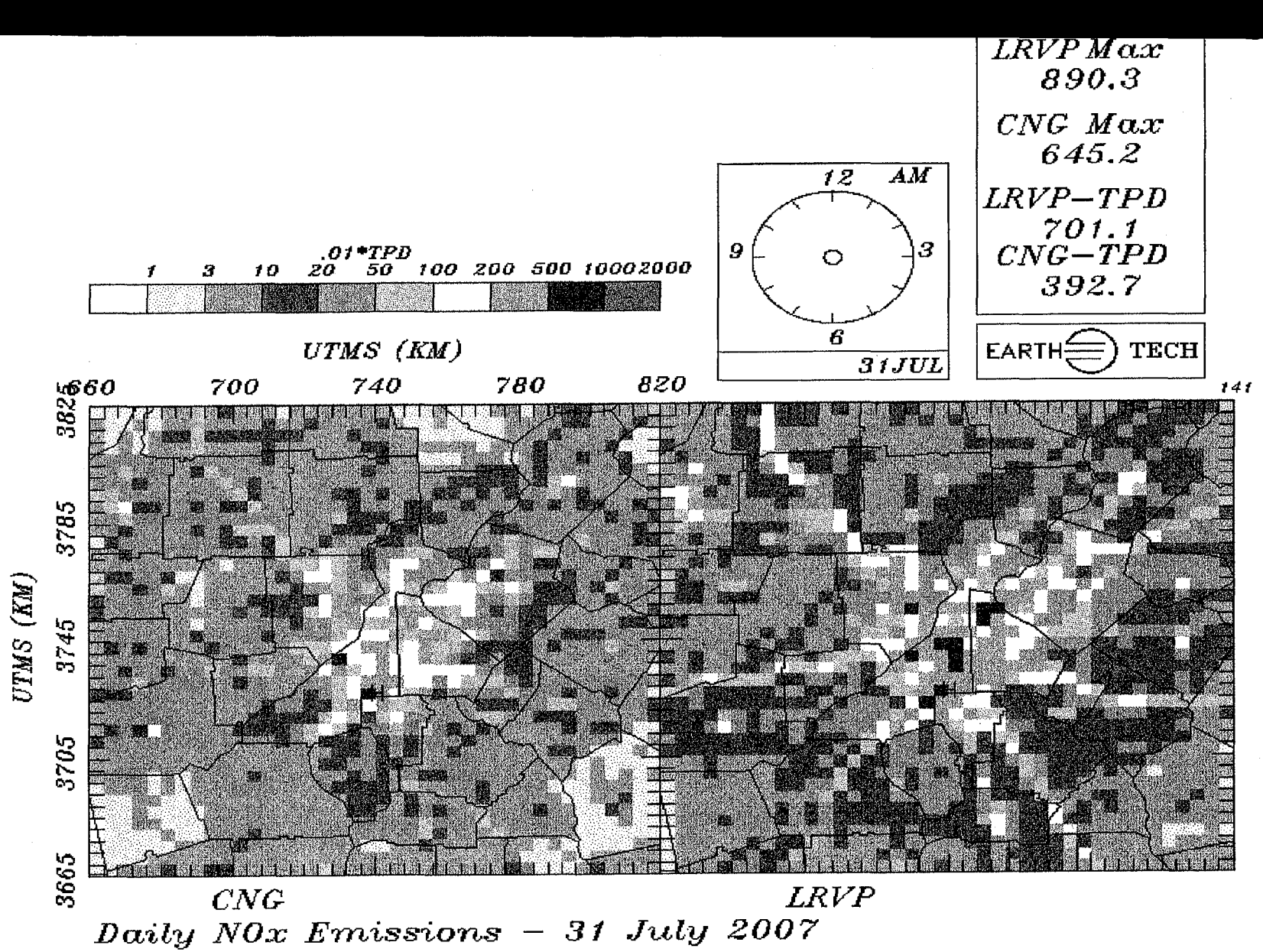

Figure 7-4. Spatial pattern of daily NO_x emissions in Atlanta for 31 July for 2007 for CNG and LRVP scenarios.

7.2 Intercomparisons of Daily Maximum Hourly O_3

The changes in the spatial pattern of peak predicted 1-hour average O_3 with emissions from LRVP gasoline fueled vehicles can be seen by comparing the daily O_3 maxima for the S1 and LRVP cases, which are displayed in Figure 7-5 for 30 July and Figure 7-6 for 31 July. On 30 July, the maximum O_3 concentration for the LRVP scenario occurs north of downtown Atlanta, while the S1 maximum occurs in the industrial region southeast of Atlanta, near the Fulton County airport. The predicted maximum O_3 increases from 156 ppb for S1 to 172 ppb for the gasoline scenario. Another notable difference is significantly lower predicted O_3 concentrations west of downtown for the S1 simulation.

On 31 July (Figure 7-6), the difference in the predicted maximum O_3 is significantly smaller, with the S1 peak value (172 ppb) slightly higher than the LRVP scenario (168 ppb). The pattern of peak predicted O_3 for the LRVP scenario contains an O_3 "hole" when compared to the S1 scenario. The predicted peak moves from southeast of downtown (Decatur-Stone Mountain area) for S1 to north of downtown (towards Swanee). The LRVP scenario shows lower O_3 in the Atlanta urban core, ringed by areas of predicted higher O_3. The O_3 increases more than 20 ppb over a wide area north of Atlanta in Cherokee County.

The predicted spatial patterns of daily peak 1-hour average surface O_3 with and without CNG fuel vehicles are given in Figures 7-7 and 7-8 for 30 and 31 July, respectively. Comparison of the two plots in Figures 7-7 indicates little discernible difference in peak O_3 for the S1 and CNG scenarios for 30 July. On 31 July (Figure 7-8), the location of peak daily O_3 coincides for both scenarios. The peak O_3 for the CNG scenario is lower than that for either the S1 or LRVP scenario on 31 July. There is again evidence of an O_3 "hole," relative to the S1 scenario. The major emissions difference between the S1 and CNG scenarios is higher NO_x emissions. We suspect that the lower predicted O_3 is caused by titration of O_3 with NO from vehicle emissions.

The maximum and domain average O_3 concentrations for each scenario are summarized in Table 7-3. The gasoline vehicle emissions contribute 16 ppb to the maximum peak O_3 concentration on 30 July, while peak O_3 decreases by 3 ppb (relative to S1) on 31 July. In contrast, CNG fuel vehicles contribute less than 3 ppb to the maximum concentration on 30 July. On 31 July, the CNG scenario produces a 6 ppb decrease in peak O_3.

Table 7-3. Daily Maximum and Domain Average Peak O_3 Concentrations for 2007 Atlanta Emission Scenarios (units are ppb)

Statistic	Scenario	30 July	31 July
Maximum daily 1-hr	S1	156	172
Maximum daily 1-hr	LRVP	172	168
Maximum daily 1-hr	CNG	159	166
Domain average 1-hr	S1	53.4	55.3
Domain average 1-hr	LRVP	56.8	57.9
Domain average 1-hr	CNG	54.1	55.9

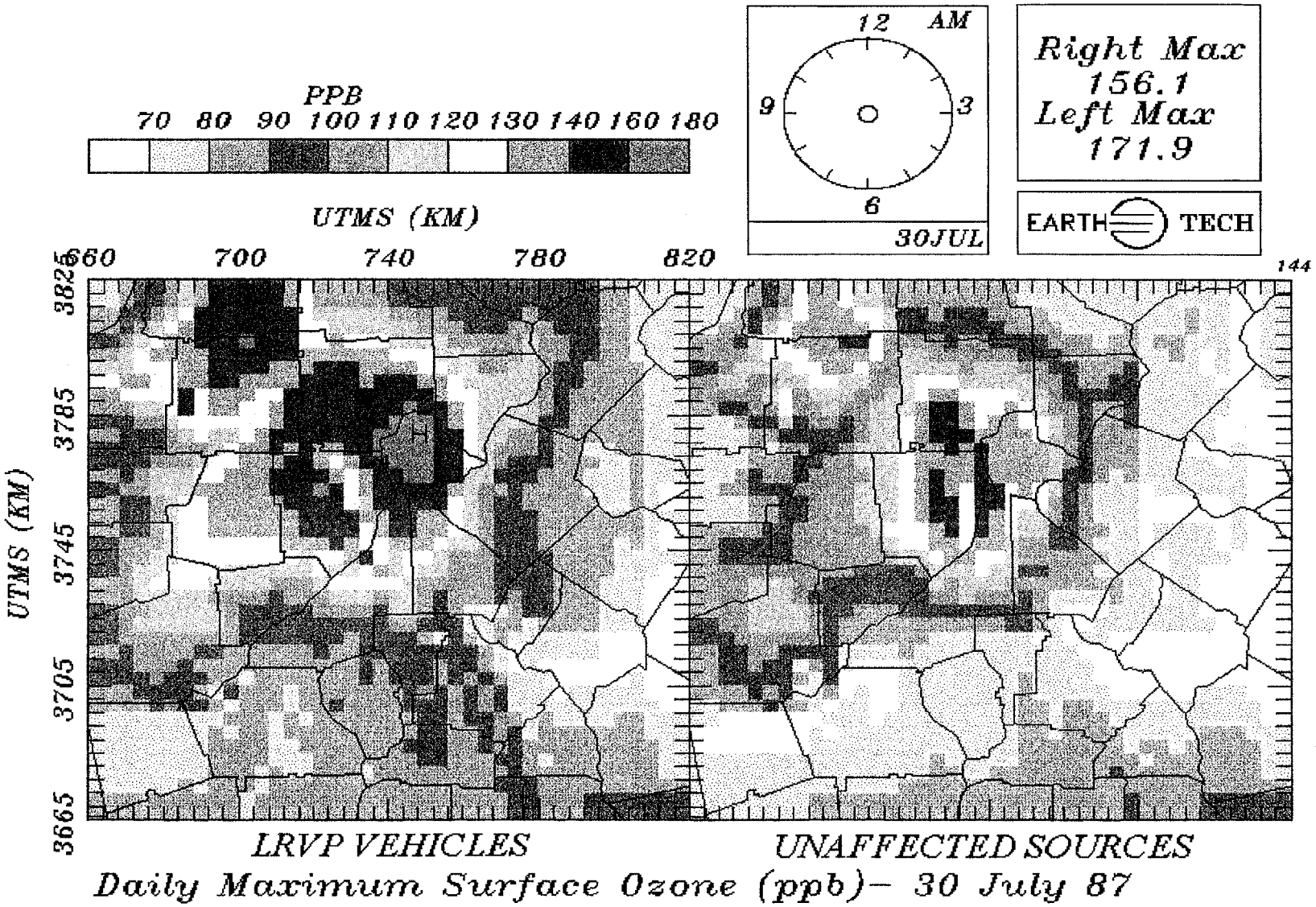

Figure 7-5. Daily maximum 1-hour O_3 concentrations with and without on-road motor vehicles for Atlanta for 2007 for 30 July LRVP scenario.

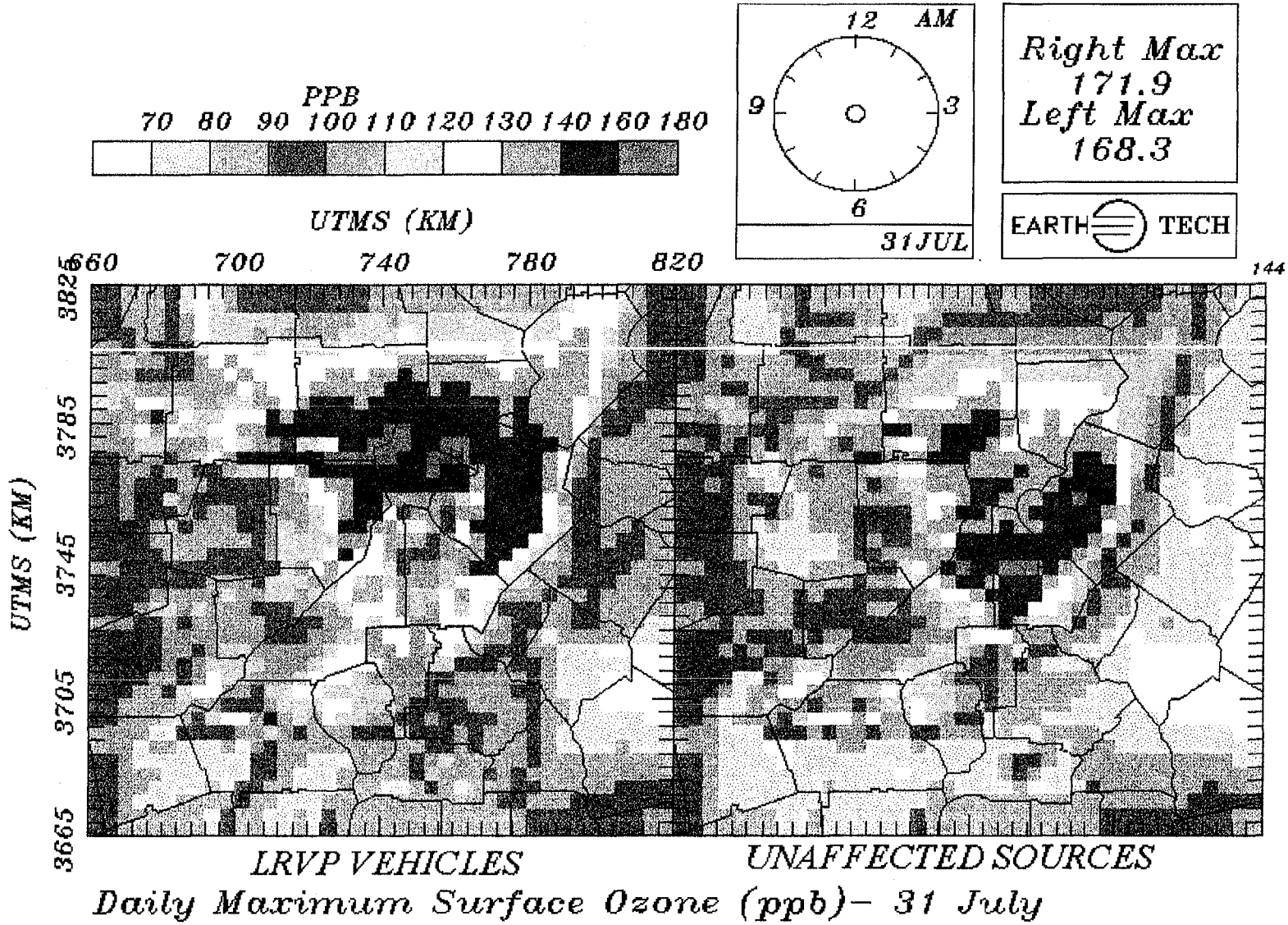

Figure 7-6. Daily maximum 1-hour O_3 concentrations with and without on-road motor vehicles for Atlanta for 2007 for 31 July for LRVP scenario.

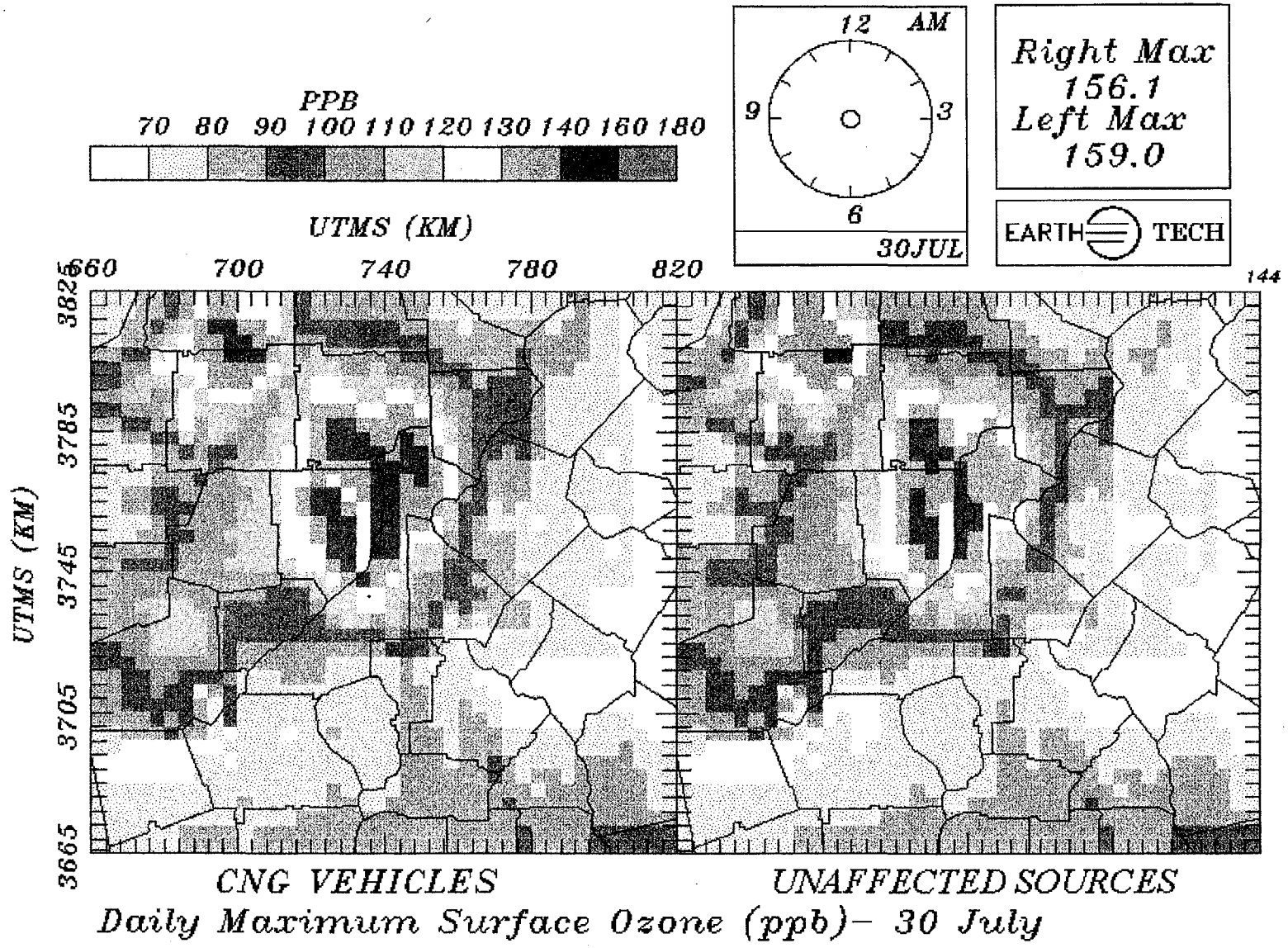

Figure 7-7. Daily maximum 1-hour O_3 concentrations with and without on-road motor vehicles for Atlanta for 2007 for 30 July for CNG scenario.

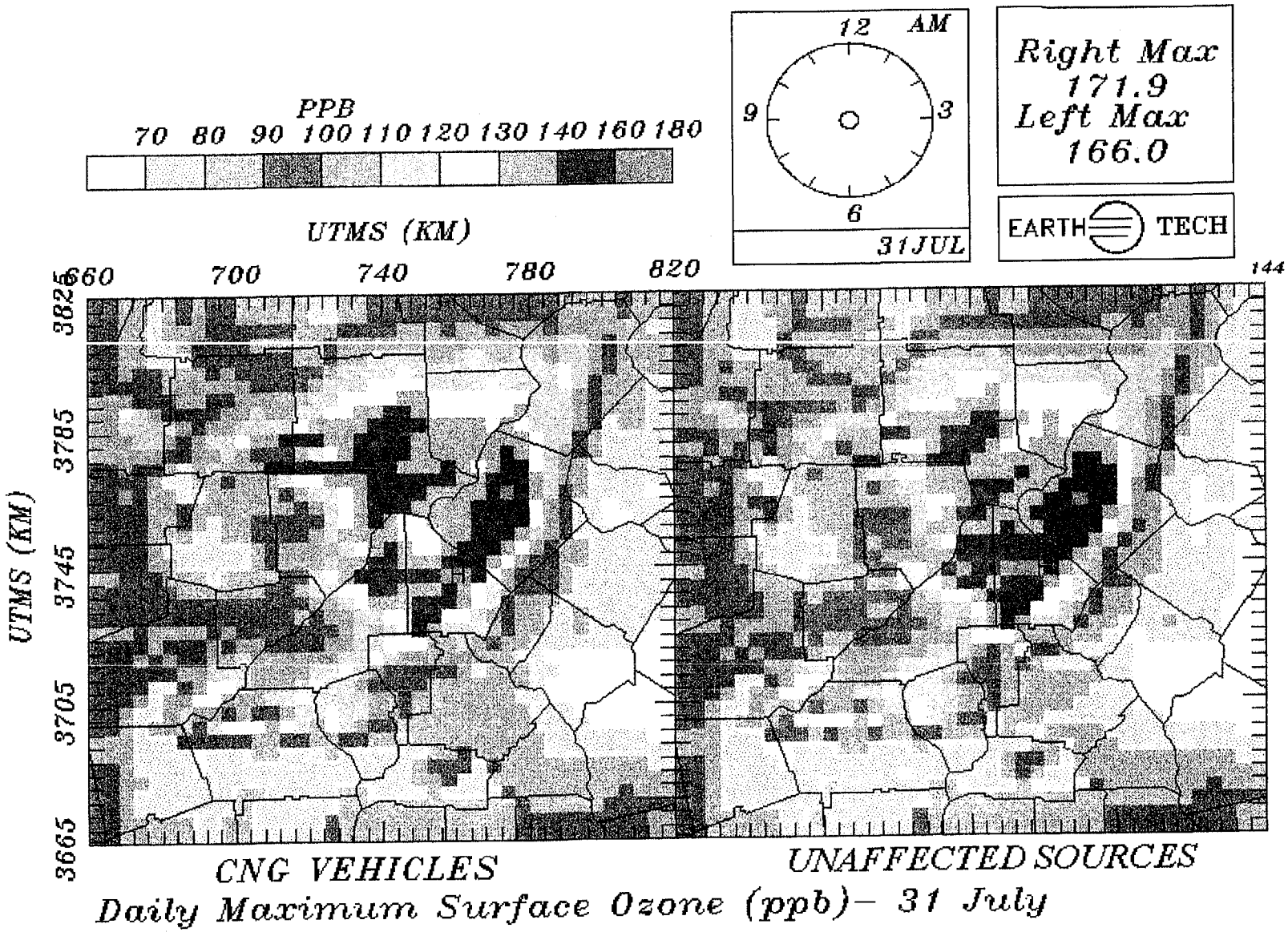

Figure 7-8. Daily maximum 1-hour O_3 concentrations with and without on-road motor vehicles for Atlanta for 2007 for 31 July for CNG scenario.

Predicted daily maximum 1-hour VOC concentrations for the LRVP and CNG scenarios are shown in Figure 7-9 for 31 July. The peak VOC concentrations occur in the vicinity of the Dekalb County airport. The maximum VOC concentration for the LRVP scenario is about 50% higher than the CNG scenario, reflecting the large difference in VOC emissions.

The daily peak 1-hour NO_x concentrations for LRVP and CNG scenarios are shown in Figure 7-10 for 31 July. The maximum predicted NO_x concentration for the LRVP scenario is 80% higher than the CNG maximum, which again illustrates the large differences in emissions. In terms of the spatial patterns of NO_x concentrations, the largest differences show up in the major highway corridors and in the urban core of Atlanta.

7.3 Intercomparisons of Daily Maximum 8-Hour Ozone

The maximum daily and domain-average 8-hour O_3 concentrations for the CNG and LRVP scenarios for both days are given in Table 7-4. The spatial pattern of daily peak 8-hour average O_3 concentrations for the CNG and LRVP scenarios are shown in Figures 7-11 and 7-12 for 30 and 31 July, respectively. For both fuel scenarios, the patterns of 8-hour average O_3 concentrations on 31 July are similar to the peak 1-hour concentrations shown in Figures 7-6 and 7-8, including the O_3 "holes". The predicted 8-hour maximum concentrations for both scenarios increase, relative to S1, unlike the predicted decreases seen for peak 1-hour concentrations. On 30 July, the maximum 8-hour O_3 concentration increases by 18 ppb, relative to S1. The domain-wide maximum 8-hour average O_3 concentrations decrease for both scenarios from 30 July to 31 July. For both days, the LRVP scenario results in higher 8-hour O_3 concentrations than does the CNG scenario.

Table 7-4. Maximum and Domain-Average Peak 8-hr Average O_3 Concentration in the Atlanta Modeling Domain (units are ppb)

Statistic	Scenario	30 July	31 July
Maximum daily 8-hr	S1	126.0	118.1
Maximum daily 8-hr	LRVP	143.6	121.7
Maximum daily 8-hr	CNG	128.7	119.7
Domain average 8-hr	S1	53.4	55.3
Domain average 8-hr	LRVP	56.7	57.9
Domain average 8-hr	CNG	54.1	55.9

The maximum predicted 8-hour O_3 concentration remains in the same location for S1 and for both fuel scenarios, in Gordon County at the northwestern edge of the modeling domain. The concentration pattern for the CNG scenario is very similar to the S1 case.

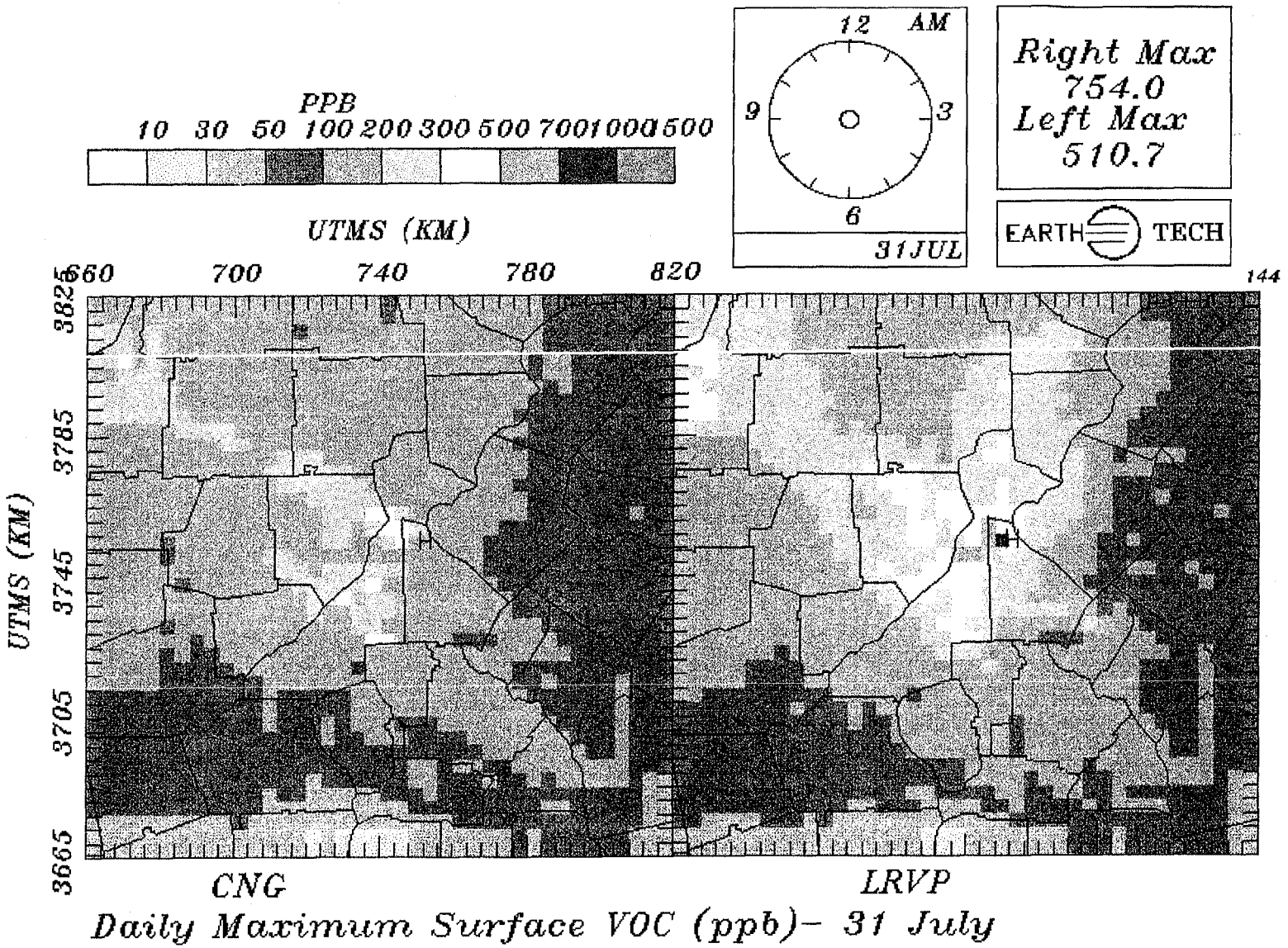

Figure 7-9. Daily maximum 1-hour surface VOC concentrations for Atlanta for 2007 for 31 July for CNG and LRVP scenarios.

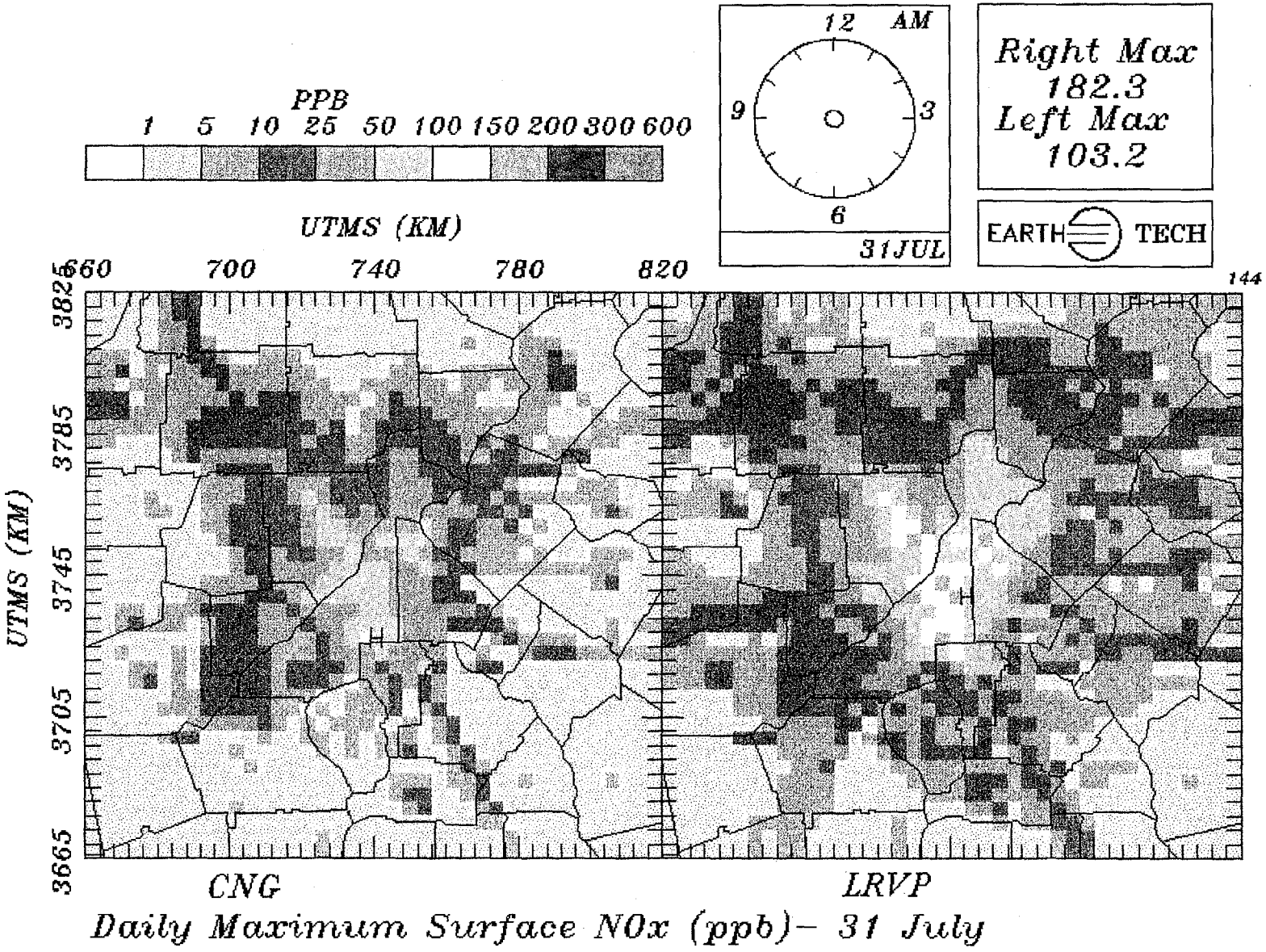

Figure 7-10. Daily maximum 1-hour surface NO_x concentrations for Atlanta for 2007 for 31 July for CNG and LRVP scenarios.

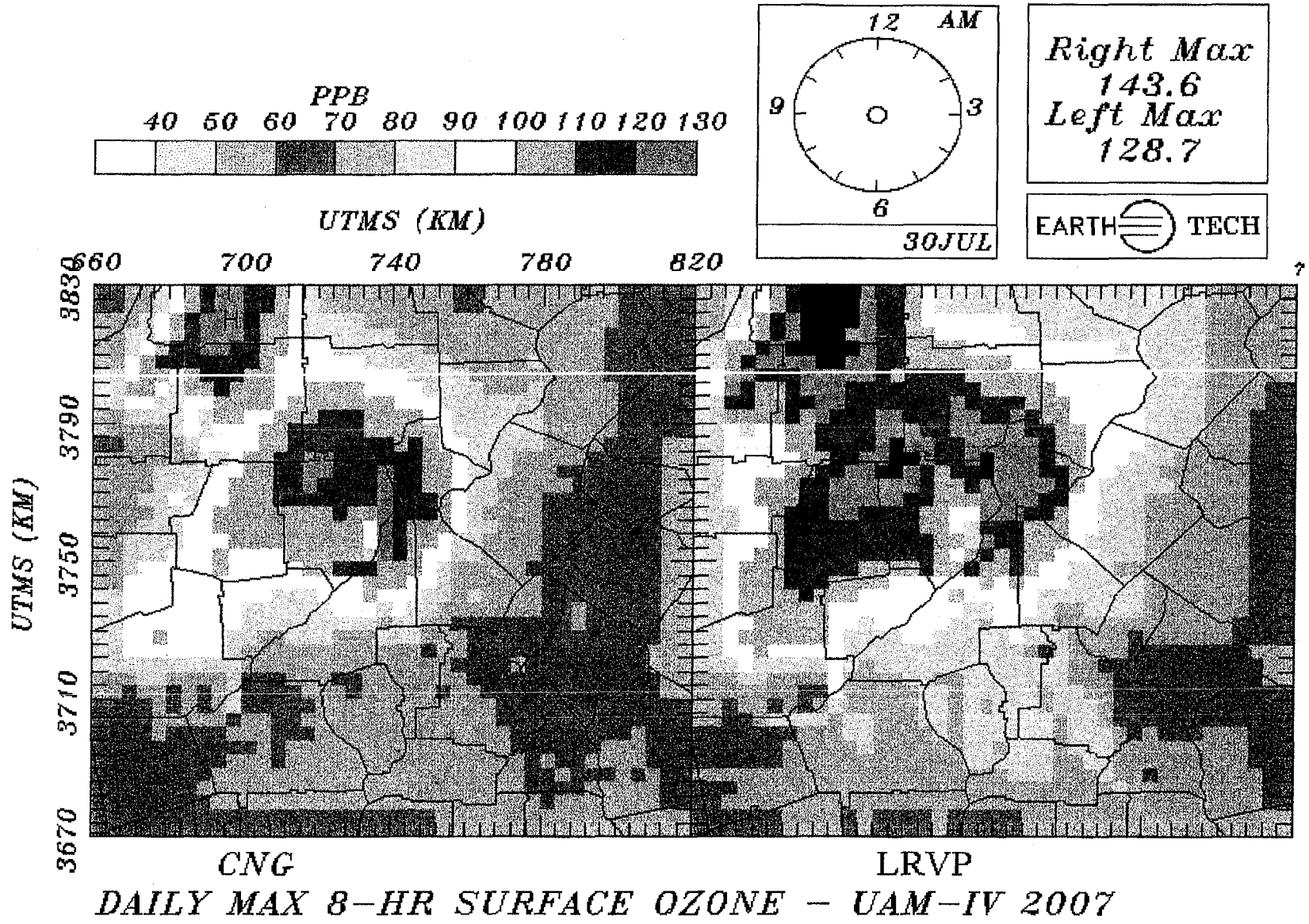

Figure 7-11. Daily maximum 8-hour surface O_3 concentrations for Atlanta for 2007 for 30 July for CNG and LRVP scenarios.

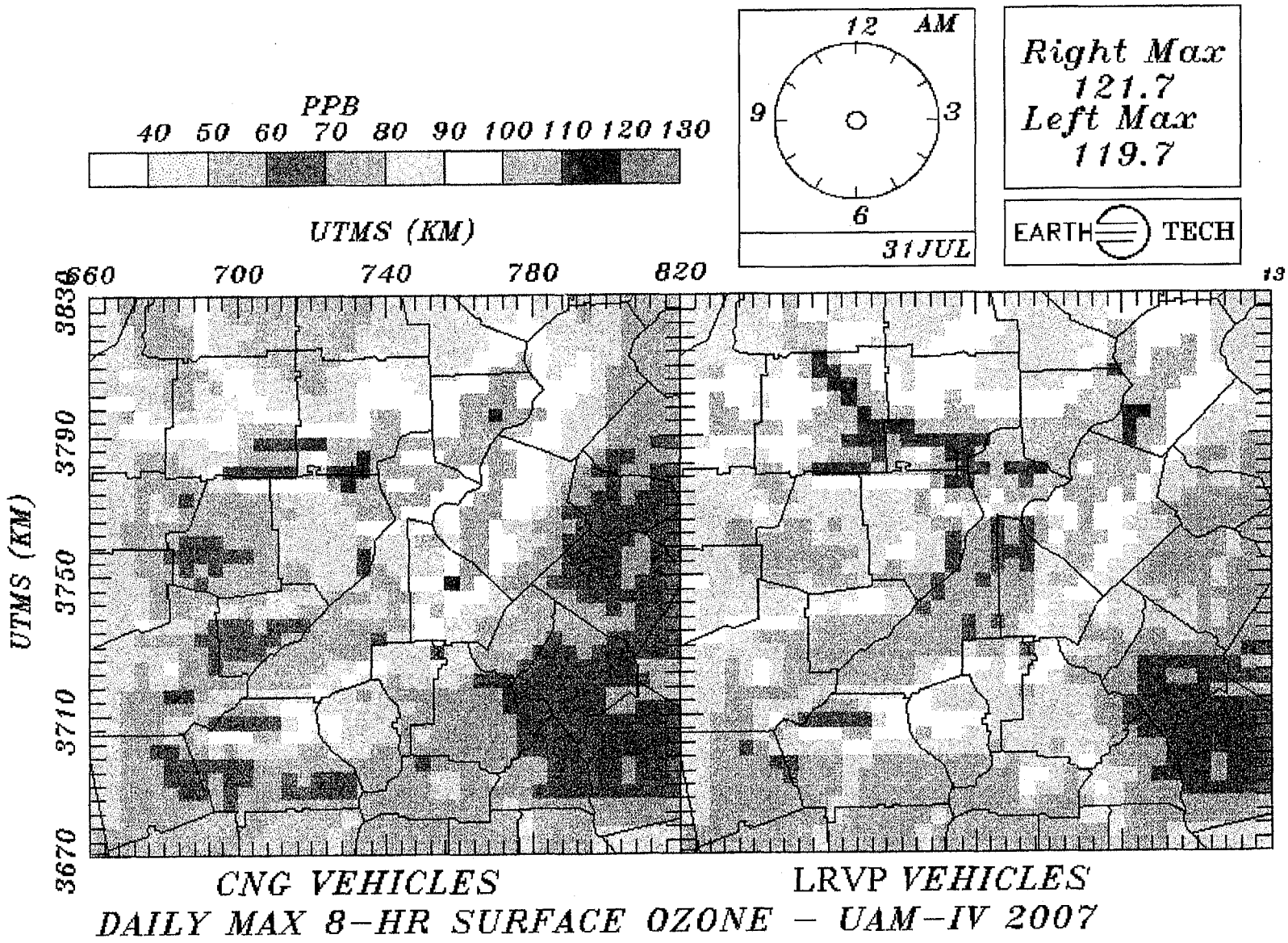

Figure 7-12. Daily maximum 8-hour surface O_3 concentrations for Atlanta for 2007 for 31 July for CNG and LRVP scenarios.

7.4 Intercomparisons of Exposures to Ozone and Toxics

Population exposure estimates were developed using a population file supplied by DNR, representing 1990 census data distributed to a 4x4 km grid. The population density for the Atlanta modeling domain is displayed in Figure 7-13. The maximum population density is located in downtown Atlanta as would be expected. The peak population density is approximately 2,200 people per square kilometer (35,000 per grid cell).

The exposure to O_3 was estimated on a daily basis as the sum over all hours of the product of the hourly predicted O_3 concentration in a cell times the population present in the grid cell. Two sets of exposure estimates were calculated, the first (No Threshold) using all hourly concentrations, and the second (Threshold 80 ppb) using only hourly concentration predictions exceeding 80 ppb. The domain-wide daily exposures to O_3 are summarized in Table 7-5. No Threshold exposures for the three scenarios for the two days are within 5% of each other. On 30 July, the LRVP scenario has the highest exposure, while on 31 July, higher exposures are calculated for the CNG and S1 scenarios. With an 80 ppb concentration threshold, exposure estimates are lower by roughly a factor of 10. The differences between scenarios are more pronounced, with the highest exposure estimates on both days for the LRVP scenario, roughly 25% higher than the S1 scenario. For each scenario, the exposure estimates for 30 July and 31 July are very similar. The 80 ppb threshold exposures for Atlanta are considerably higher than those calculated for Los Angeles, despite the lower population, which reflects predicted peak ozone concentrations above 80 ppb that cover a larger area and persist for more hours.

The spatial distribution and magnitude of No Threshold O_3 exposures are very similar between the CNG and gasoline scenarios for both modeling days. Plots of cumulative O_3 exposure for the CNG and LRVP scenarios are given for 31 July in Figure 7-14 , the day with the highest modeled O_3 exposures. Note that the units are ppm-people-hours. The peak in O_3 exposure occurs in the vicinity of downtown Atlanta, in the grid cell with the highest population density. The largest differences in O_3 exposures, while not shown in the figure, occur in central Atlanta (Fulton County proper), an area of high surface NO_x emissions.

Table 7-5. Estimated Population Exposures to Predicted O_3 Concentrations in Atlanta for 2007 (units are 10^6 people x ppm-hours)

	No Threshold		80 ppb Threshold	
Emission Scenario	30 July	31 July	30 July	31 July
S1	4.4	4.6	0.47	0.46
LRVP	4.5	4.4	0.59	0.59
CNG	4.4	4.6	0.49	0.49

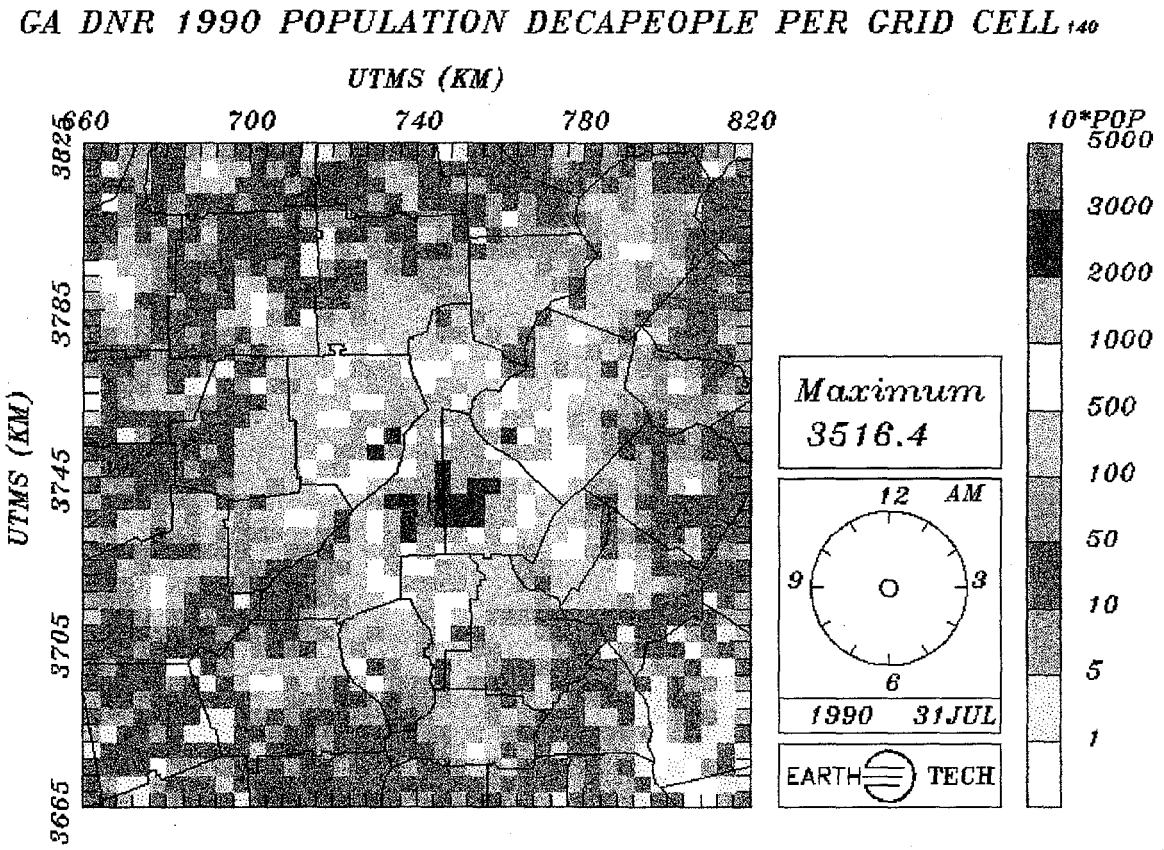

Figure 7-13. Population density in the Atlanta modeling domain for 1990.

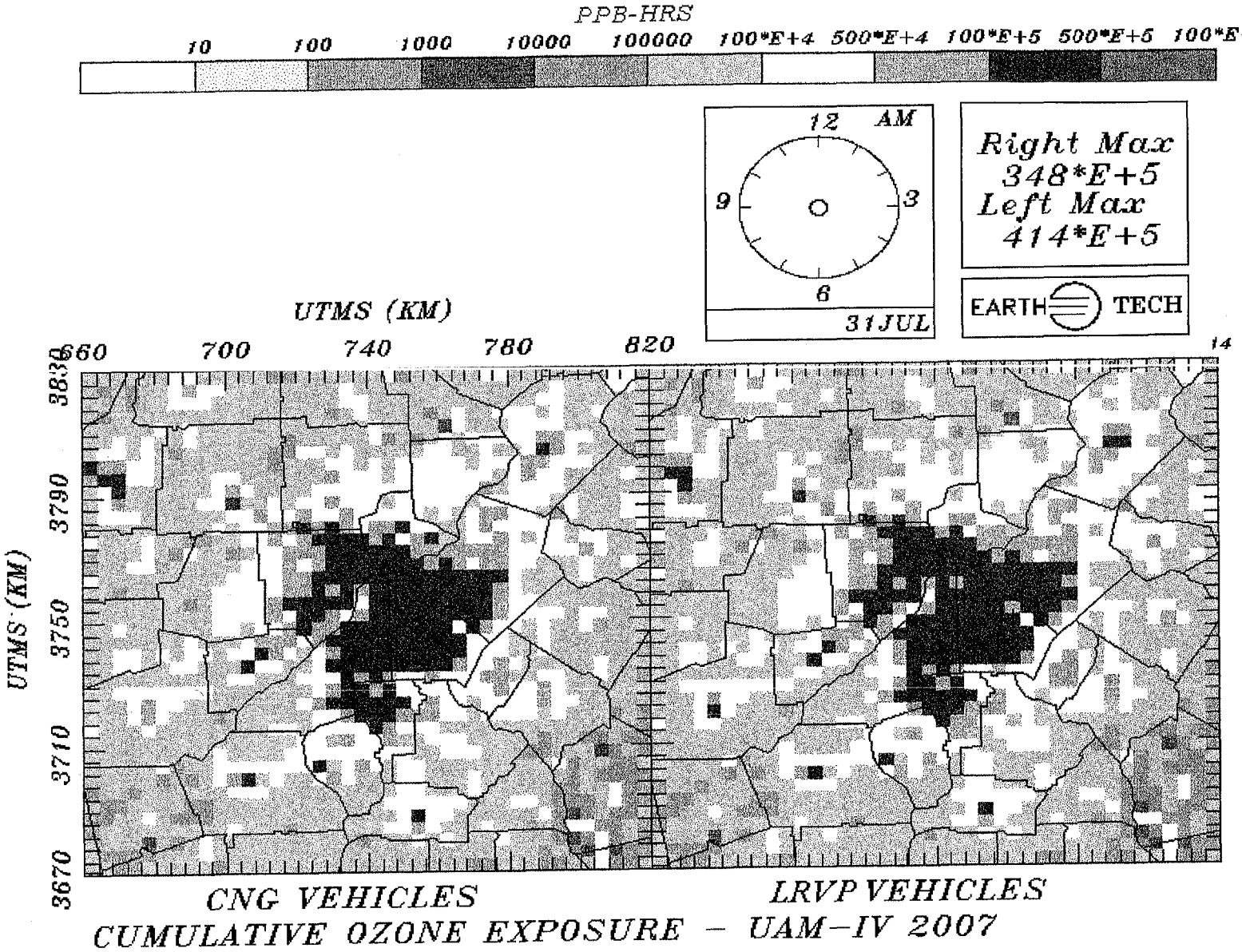

Figure 7-14. Cumulative surface O_3 exposures for Atlanta for 2007 for 31 July for CNG and LRVP scenarios.

The maximum daily 1-hour concentrations and the population exposure to the four toxic compounds (FORM, ACET, BENZ, and BUDI) are summarized in Table 7-6. Several observations can be made from this table including the following:

- Of all the toxic compounds examined, predicted concentrations and population exposures for FORM are the largest.
- Peak exposures tend to occur on 31 July for all compounds.
- The largest predicted toxic concentrations and exposures occur for the LRVP gasoline scenario.
- The CNG and S1 scenarios are most similar in terms of the maximum predicted concentrations and exposures.

The cumulative FORM exposure patterns for 31 July for the LRVP and CNG scenarios are shown in Figure 7-15. Note that the units are ppb-people-hours. The highest predicted exposure occurs in the vicinity of downtown Atlanta. The LRVP scenario exposures to FORM are most different from those of the CNG scenario in and around Atlanta. The CNG pattern of population exposure to toxic compounds is most like that of the S1 scenario (not shown).

Table 7-6. Daily Maximum 1-Hour Concentrations and Domain-wide Cumulative Populations Exposures to Each of the Four Toxic Compounds in the Atlanta Modeling Domain for 2007 (units are ppb people-hours)

Statistic	Date	Scenario	FORM	ALD2	BENZ	BUDI
Maximum daily 1-hr	30 July	S1	14.1	6.31	1.21	2.12
		LRVP	15.4	6.48	2.24	2.00
		CNG	14.2	6.32	1.24	2.08
Maximum daily 1-hr	31 July	S1	18.2	6.70	1.26	2.91
		LRVP	18.7	7.55	3.20	3.00
		CNG	18.2	6.75	1.05	2.91
Cumulative exposure	30 July	S1	0.36	0.13	0.0190	0.0032
		LRVP	1.39	0.14	0.034	0.0040
		CNG	0.36	0.13	0.019	0.0032
Cumulative exposure	31 July	S1	0.33	0.13	0.0194	0.0035
		LRVP	0.36	0.14	0.036	0.0049
		CNG	0.33	0.13	0.0196	0.0035

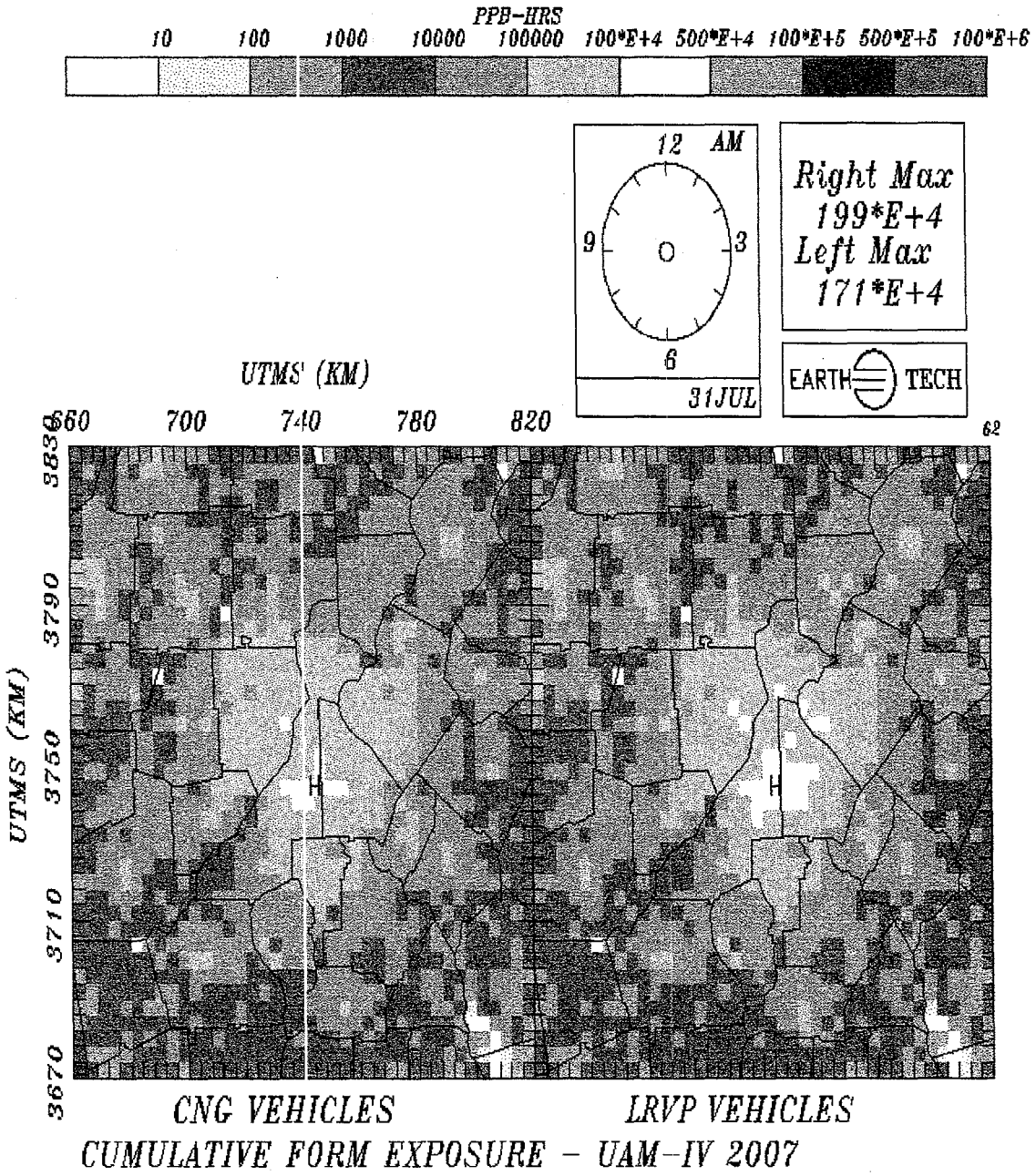

Figure 7-15. Cumulative surface FORM exposures for Atlanta for 2007 for 31 July for CNG and LRVP scenarios.

7.5 Relative Ozone Formation Potential Analysis

In order to place the VOC emissions for the CNG and LRVP scenarios on an equal footing, the VOC totals can be weighted by their ability to form O_3, expressed as the total amount (moles) of O_3 formed or destroyed per ton of each VOC species emitted. In Atlanta, the urban core is surrounded by rural areas where biogenic emissions are quite large, resulting is a large spatial variation in VOC:NO_x ratio. The spatial variation is demonstrated dramatically by Figure 7-13 which shows the daily average VOC:NO_x concentration ratios

In order to place the VOC emissions for the CNG and LRVP scenarios on an equal footing, the VOC totals can be weighted by their ability to form O_3, expressed as the total amount (moles) of O_3 formed or destroyed per ton of each VOC species emitted. In Atlanta, the urban core is surrounded by rural areas where biogenic emissions are quite large, resulting is a large spatial variation in VOC:NO_x ratio. The spatial variation is demonstrated dramatically by Figure 7-13 which shows the daily average VOC:NO_x concentration ratios predicted by the UAM-IV for the CNG and LRVP scenarios. The gasoline scenario shows a dramatic change in the VOC:NO_x ratio compared with the CNG case, with highway corridors showing up with significantly reduced ratios (e.g., 5-10 is common). The result suggests that (1) air moving from the urban core to the outskirts of Atlanta will experience large changes in VOC:NO_x ratios (over an order of magnitude), and (2) gasoline-fueled vehicle emissions lead to a situation where the urban core is definitely **not** in a NO_x limited state.

For this study, one would like to be able to calculate the ozone formation potential (ozone formed per unit emission) that would result from use of a given alternative fuel. Multiple model runs in which small emissions increments are applied independently to each CB-4 species that is emitted by use of a given fuel are made, and the resulting formation potentials are summed to yield the composite ozone formation potential of the fuel. However, there is a conflict between using a small enough emissions increment to maintain linearity in the resulting chemical calculations and using a large enough increment to produce a statistically detectable change in ozone concentration.

For this study, a method of establishing a statistically significant yet linearity-preserving emission increment for each specie was not available. The scope of the study did not allow development of either direct differentiation versions (e.g., ADIFOR - Bischof, 1994) or direct decoupled method versions (e.g., Yang et al., 1997) of UAM-IV to yield incremental emissions sensitivities. Also, this study involves a specific episode with specific space- and time-varying meteorological conditions and overall emissions, so using generic specie ozone forming potentials from the literature and applying them on a weighted basis to the present emissions mix for LRVP and CNG would introduce uncertainties.

This study used a compromise approach to examine ozone forming potentials of the alternative fuels. A single generic set of incremental runs by specie was done. The increments chosen represented the difference between the LRVP emissions case and the no-motor-vehicles case, except for several species for which a larger increment was necessary to produce a significant response, and the results were assumed to represent the average ozone formation potential for these individual species over the range of motor vehicle emissions spanning no vehicles to the full LRVP case. The emissions from the CNG case will fall within this range, and these average species-specific ozone potentials can be weighted to produce a fuel-specific ozone formation potential for either RFG or CNG. Any proposed approach would be limited by the factors discussed above; this approach has the advantage that the specie-specific ozone formation potentials are appropriate for this set of episode conditions, domain, and emissions mix.

A series of nine simulations was conducted in which an emissions increment for a single CB4 chemical species was added to the S1 emissions. Table 7-7 lists these incremental species emissions (ΔQs.) The emission increments for most species correspond to the LRVP gasoline scenario motor vehicle emissions. For selected species (FORM, ACET, and ISOP), emissions were scaled by factors of 10 or 300 in order to produce a numerically significant O_3 response. The estimated peak O_3 sensitivity and the O_3 formation potential for each pollutant is therefore dependent on the degree to which the O_3 response can be linearly scaled.

The O_3 sensitivity with the largest absolute magnitude is that for NO_x. The negative sign indicates that NO_x in Atlanta, on average, is more effective in destroying O_3 through titration than in promoting ozone formation. OLE and FORM are the two compounds most efficient at forming O_3 on a per ton basis, while PAR and TOL, which account for the largest fractions of VOC emissions, contribute the least to ozone production on a per ton basis.

Table 7-7. O_3 Sensitivities (ppb/ton) Based on Maximum 1-Hour Average O_3 Concentrations in Atlanta on 31 July (unless noted otherwise, the ΔQ is the difference between S1 and LRVP emissions scenarios)

Species	ΔO3 (ppb)	ΔQ (TPD)	ΔO3/ΔQ ppb/ton
NOx	-14.4	363	-0.040
PAR	5.40	132	0.041
TOL	0.65	34.0	0.019
XYL	3.06	29.0	0.106
FORM	6.31	14.7*	0.429
ACET	2.31	9.0**	0.257
OLE	4.89	11.6	0.422
ETH	3.09	11.0	0.281
ISOP	2.34	19.0**	0.123

* = 10 x actual
** = 300 x actual

These O_3 sensitivities are typical and are similar to those reported by Bergin et al (1995). The peak O_3 at the surface is formed through the competing processes of O_3 destruction through NO_x titration and radical scavenging and O_3 production resulting from NO_2 formation by radical chemistry. Bergin et al found that O_3 sensitivity for TOL is a function of the prevailing VOC:NO_x emissions ratio, with negative sensitivity for VOC:NO_x ratios above 14. Our calculations for 31 July show a small positive O_3 sensitivity for TOL. Figure 7-16 demonstrates that the average VOC:NO_x ratio over Atlanta is of order 5-10, a range where Bergin et al indicate that positive O_3 sensitivity for TOL is expected. (As noted earlier, however, large spatial variations in VOC:NO_x ratio occur across the domain.)

Peak O_3 sensitivity is not always a good indicator of O_3 formation potential, since the meteorological component of the O_3 buildup cannot easily be separated from the emissions. For example, the domain maximum prediction will not respond equally to emissions that occur in different parts of the domain. An approach that is less dependent on source characteristics and dispersion patterns is to estimate how many tons of O_3 were formed or destroyed per ton of a specific chemical emitted, across the entire domain, using the same series of simulations described above. Domain-wide net O_3 production was therefore estimated for 31 July. The resulting O_3 formation potentials, stated as tons of O_3 per ton of emissions, are summarized in Table 7-8.

Table 7-8. O_3 Formation Potentials (ton-O_3/ton-Q) Over Atlanta Modeling Domain for 31 July Episode Day

Species	ΔM[a] tons	ΔQ (TPD)	ΔM/ΔQ ton/ton	Reactivity weight
NOx	383	363	1.05	NA
PAR	4.0	132	0.030	0.021
TOL	-32.0	34.0	-0.941	-0.669
XYL	-5.0	29.0	-0.172	-0.122
FORM	15.0	14.7	1.020	0.725
ACET	0.0	9.0	0.0	0.0
OLE	16.0	11.6	1.38	0.980
ETH	1.0	11.0	0.091	0.065
ISOP	0.0	18.0	0.0	0.0

[a] Cumulative Mass change for hour beginning 2300 on 30 July thru 2400 on 31 July.

Table 7-8 also presents VOC reactivity weights that are calculated by dividing the individual sensitivities by the sum of all the VOC sensitivities. Any fuel can be weighted on the basis of reactivity using the weights presented in Table 7-8. From these results, we see that the ozone formation potentials for TOL and XYL are negative, in contrast to the ozone sensitivities in Table 7-7.

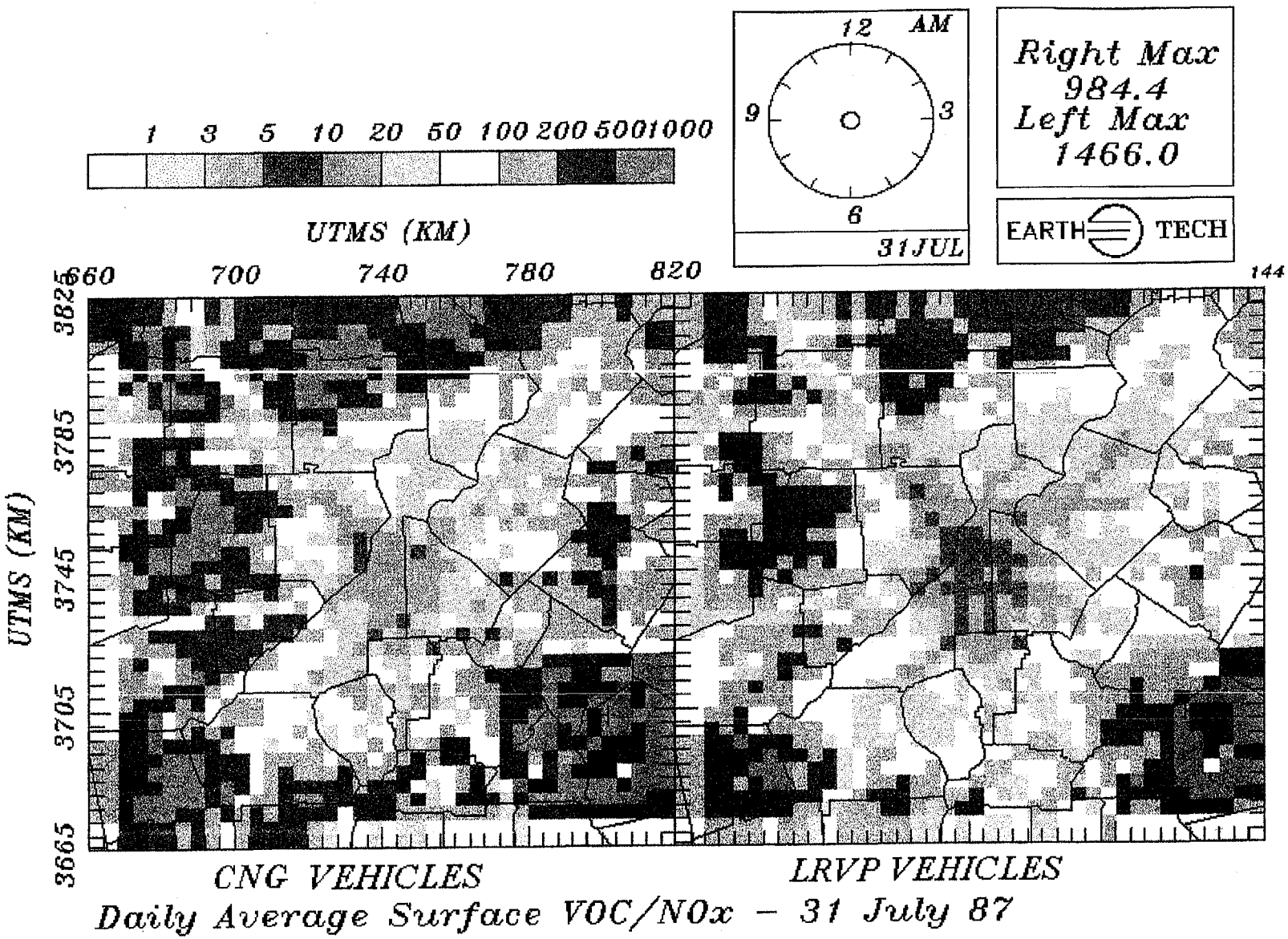

Figure 7-16. Estimated daily average VOC:NO_x concentration ratios for Atlanta for 2007 for 31 July for CNG and LRVP scenarios.

Table 7-9. A Summary of Actual and Reactivity-Weighted Daily VOC Emissions from Alternatively Fueled vehicles by Species for 31 July 2007 in the Atlanta Modeling Domain (units are tons/day)

	LRVP Fuel Vehicles		CNG Fuel Vehicles	
Species	Emissions	Reactivity Weighted Emissions	Emissions	Reactivity Weighted Emissions
PAR	130	2.73	2.82	0.06
OLE	12	11.76	0.99	0.48
ETH	11	0.72	0.39	0.03
TOL	34	-22.75	0.27	-0.18
XYL	29	-3.54	0.25	-0.03
FORM	1.5	1.09	0.07	0.05
ACET	0.90	0.0	0.04	0.0
ISOP	0.0	0.0	0.0	0.0
Total*	218.4	-10.0	4.33	0.41

* Remainder of emissions do not change and were not modeled with a sensitivity simulation.

It is uncertain how an X% increase in VOC emissions from CNG-fueled vehicles will increase O_3 formation relative to an X% increase in VOC emissions from gasoline-fueled vehicles. By weighting the emissions by reactivity, we can compare on an equal footing the O_3 formation potential of changes in VOC emissions for different fuel scenarios. Such a reactivity weighting was performed, with the results summarized in Table 7-9. The LRVP gasoline fueled vehicle emission increment produces a *negative* reactivity-weighted increment. The CNG vehicle emissions increment, while smaller than the VOC increment from gasoline fuel vehicles by more a factor of 70, produces a small positive reactivity-weighted increment. These results are somewhat deceptive, since they reflect the domain-wide VOC contribution to potential ozone formation. Actual modeling results, which reflect the combined effect of NO_x and VOC emissions increments, show a mixed impact of emissions from LRVP gasoline fuel vehicles on predicted peak ozone for 31 July. The maximum daily 1-hour ozone concentration predicted for the LRVP scenario decreased by 4 ppb relative to the S1 scenario maximum, but the domain average 1-hr concentration increased by 2.6 ppb for 31 July.

7.6 Mass Budget Analysis

The mass flux budget provides information regarding the role of initial and boundary conditions and the influence of different sources and sinks of a given chemical. It can also indicate whether a chemical is highly reactive with a short lifetime. The overall 2-day cumulative mass exchanges for selected species into and out of the modeling domain are summarized in Table 7-10.

Table 7-10. Cumulative Domain-wide Mass Exchanges (Fluxes, Sources, Sinks) for Selected Chemical Species Over the Two-Day Period 30-31 July 2007 (units are tons)

Specie	Scenario	Net	Top Flux	Side Flux	Deposition	Emission	Chemistry	Total Mass
O3	S1	507	2290	-3770	-2010	0	4000	7370
NOx	S1	-21	73	297	-114	860	-1250	143
VOC	S1	-97	253	-853	0	2020	-1520	948
BENZ	S1	-1.4	5.7	-24.7	0	16.5	-1	25
BENZ	LRVP	-0.5	5.3	-43	0	37	-1	31
FORM	S1	-16	24	-65	0	7.5	18	89

Note: The total mass is rounded to three significant figures and is the domain-wide total at midnight between 30 and 31 July.

For O_3, the net chemical production over two days is about half of the domain-wide total mass. The net increase in the O_3 mass is on the order of 5% of the total mass. The lateral export of O_3 through the sides nearly equals the chemical production of O_3 and is nearly twice the deposition flux. This large export is primarily outflow through the northern boundary of the modeling domain.

Relatively little NO_x mass is stored in the atmosphere, resulting in very low predicted NO_x concentrations in rural regions and aloft. The modeled NO_x fluxes are several times larger than the total mass, suggesting that the turnover time of NO_x within the domain is significantly less than a day. The total NO_x mass is very responsive to the chemistry and fluxes through the boundaries. However, over the course of the two-day episode, the total mass decreased by only 15 percent.

The chemical destruction of VOC is 60% larger than the domain-total VOC mass. The fluxes of VOC through the top and lateral boundaries are considerably smaller than the emissions, suggesting that the boundary conditions do not affect the O_3 response to VOC emission changes.

The FORM emissions are many times smaller than the total mass and the lateral fluxes, indicating that changing the FORM source term is unlikely to have much of an effect on human exposure to FORM throughout the modeling domain. The net loss over two days is about 18% of the total mass.

BENZ reacts very slowly, with 3-4% of the total mass reacting over the course of the two-day episode. For both the S1 and Gasoline scenarios, BENZ emissions are of the same approximate size as the combined lateral and top boundary fluxes. The total mass of BENZ is also about the same size as the source term. These results indicate that most of what is being emitted is later exported out the northern boundary.

8.0 References

ARB (1994). EMFAC7F model, Version 1.1. California Air Resources Board, Technical Support Division, Mobile Source Emission Inventory Branch, Sacramento, CA.

Atkinson, R. (1990). "Gas-phase Tropospheric Chemistry of Organic Compounds: A Review." Atmospheric Environment 24A, 1-41.

Atkinson, R. et al. (1994). "Formation Yields of Epoxides and O(3P) Atoms from the Gas-phase Reactions of O3 with a Series of Alkenes." International Journals of Chemical Kinetics, Vol. 26, 945-950.

Bergin, M.S.; Russell, A.G.; and Milford, J.B. (1995). *Quantification of Individual VOC Reactivity Using a Chemically Detailed, Three-Dimensional Photochemical Model*, Environ. Sci. Technol. 29:3029-3037.

Bischof, C., A. Carle, P. Khademi, A. Mauer, and P. Hovland (1994). ADIFOR 2.0 User's Guide. Argonne National Laboratory report ANL/MCS-TM-192.

Carter, W.P.L. and Atkinson, R. (1989). "Computer Modeling Study of Incremental Hydrocarbon Reactivity." Environ. Sci. Technol. (23) pp 864-880.

Carter, W.P.L. (1990). "A Detailed Mechanism for the Gas-Phase Atmospheric Reactions of Organic Compounds." Atmos. Environ. (24A:3); pp. 481-518.

Carter, W.P.L. (1994). "Development of Ozone Reactivity Scales for Volatile Organic Compounds," *J. Air and Waste Manage. Assoc.*, 44: 881-899.

Carter, W.P.L. (1995). "Atmospheric Process Evaluation of Mobile Source Emissions", Environ. Sci. Technol.

Chang, Y.T. and Rudy, S.J. (1990). "Ozone-Forming Potential of Organic Emissions from Alternatively-Fueled Vehicles." Atmos. Environ. (24A:9); pp. 2421-2430.

Department of Natural Resources (November 1994). *The 1994 State Implementation Plan for the Atlanta Ozone Nonattainment Area.* Prepared by the Air Protection Branch. Atlanta, GA: Georgia Dept. of Natural Resources, Environmental Protection Division.

Emigh, R.A., and J.G. Wilkinson (1995). *The Emissions Modeling System (EMS-95) User's Guide.*

Gery, M.W., G.Z.Whitten, J.P. Killus and M.C. Dodge (1989). *A Photo Chemical Mechanism for Urban and Regional-scale Computer Modeling,* J. Geophys. Res. 94: 12925-56.

Harley, R.A., and G.R. Cass (1994). *Modeling the Concentrations of Gas-Phase Toxic Organic Air Pollutants: Direct Emissions and Atmospheric Formation,* Environ. Sci. Technol., 28, 88-98.

Kelly, N.A. and Groblicki, P.J. (1993). "Real-World Emissions from a Modern Production Vehicle Driven in Los Angeles," *Journal of the Air and Waste Management Association*, 43:1351.

Killus, J.P. (1996). *Development and Testing of a Toxics Version of the Carbon Bond 4 Mechanism.* Technical memorandum to Radian Co, Sacramento, CA 95827.

Ligocki, M.P. and Whitten, G.Z. (1992). "Modeling of Air Toxics with the Urban Airshed Model (UAM)" Presented at the 85th Annual Meeting and Exhibition, Air and Waste Management Association, Kansas City, MO. 92-84.12.

Moortgat, G.; Veryet, B; and Lesclaux, R. (1989). "Absorption Spectrum and Kinetics of Reactions of the Acetylperoxy Radical." J. Phys. Chem., Vol. 93, pp. 2362-2368.

Morris, R.E. and Myers, T.C. (June 1990). *User's Guide For the Urban Airshed Model, Volume I: User's Manual for UAM (CB-IV).* EPA-450/4-90-007A. Work performed by Systems Applications, Inc., San Rafael, CA. Research Triangle Park, NC: U.S. Environmental Protection Agency, Office of Air Quality Planning and Standards.

Pollack, A.K., J.P. Cohen, J.L. Fieber, R.E. Morris, and G. Yarwood (1993). *Methodology for Modeling the Air Quality Impacts of Changing the Composition of Duels Used in Light-Duty Gasoline Vehicles,* Auto/Oil Air Quality Improvement Research Program, Phase I, Final Report, Systems Applications International, San Rafael, California.

Reichhart, T. (1995). "A New Formula for Fighting Urban Smog." Environ. Sci. Technol. (29:1); pp. 36A-41A.

Russell, A.G., L.A. McNair, M.T. Odman, and N. Kumar (1991). *Organic Compound Reactivities and the Use of Alternative Fuels,* Draft Final Report to the California Air Resource Board.

SCAQMD (1994). *1994 Air Quality Management Plan: Meeting the Clean Air Challenge.* South Coast Air Quality Management District, Diamond Bar, CA.

U.S. DOE (1994). *Emissions of Greenhouse Gases in the United States 1987-1992.* DOE/EIA-0573, Department of Energy, Energy Information Administration, Office of Energy Markets and End Use, Washington, DC.

U.S. EPA (1993). MOBILE5a Emission Factor Model, Version Date March 23, 1993. United States Environmental Protection Agency, Office of Mobile Sources, Ann Arbor, MI.

U.S. EPA (1995). "State Workbook for Estimating Greenhouse Gas Emissions, Second Edition." EPA-230-B-95-001, U.S. Environmental Protection Agency, Office of Planning and Evaluation.

Yang, Yueh-Jiun et al. (1997). Fast Sensitivity Analysis of Three-Dimensional Photochemical Models, 22nd NATO/CCMS International Technical Meeting on Air Pollution Modeling and its Application.